UNIVERSIDAD COMPLUTENSE DE MADRID
FACULTAD DE MEDICINA

TESIS DOCTORAL

KV1.5 and KV7 channels as pharmacological targets in pulmonary arterial hypertension

Canales KV1.5 y KV7 como dianas farmacológicas en la hipertensión arterial pulmonar

MEMORIA PARA OPTAR AL GRADO DE DOCTOR

PRESENTADA POR

Marta Villegas Esguevillas

DIRIGIDA POR

Ángel Luis Cogolludo Torralba
Belén Climent Flórez

Madrid

UNIVERSIDAD COMPLUTENSE DE MADRID

FACULTAD DE MEDICINA

TESIS DOCTORAL

K_V1.5 and K_V7 channels as pharmacological targets in pulmonary arterial hypertension

Canales K_V1.5 y K_V7 como dianas farmacológicas en la hipertensión arterial pulmonar.

MEMORIA PARA OPTAR AL GRADO DE DOCTOR

PRESENTADA POR

Marta Villegas Esguevillas

DIRECTORES

Dr. Ángel Luis Cogolludo Torralba
Dra. Belén Climent Flórez

UNIVERSIDAD COMPLUTENSE DE MADRID

FACULTAD DE MEDICINA

TESIS DOCTORAL

$K_V1.5$ and K_V7 channels as pharmacological targets in pulmonary arterial hypertension

Canales $K_V1.5$ y K_V7 como dianas farmacológicas en la hipertensión arterial pulmonar.

MEMORIA PARA OPTAR AL GRADO DE DOCTOR

PRESENTADA POR

Marta Villegas Esguevillas

DIRECTORES

Dr. Ángel Luis Cogolludo Torralba
Dra. Belén Climent Flórez

PROGRAMA DOCTORADO EN INVESTIGACIÓN BIOMEDICA

El trabajo descrito en la presente Tesis Doctoral ha sido llevado a cabo en el laboratorio de farmacología y fisiopatología vascular en el Departamento de Farmacología y Toxicología de la Facultad de Medicina y ha sido financiada por los siguientes proyectos de investigación:

- PID2020-117939RB-I00: *Canales K_V como dianas farmacológicas en la hipertensión arterial pulmonar y la disfunción eréctil (Kv_PAHED)*. Ministerio de Ciencia e Innovación.

La doctoranda Marta Villegas Esguevillas ha sido beneficiaria:

- Programa de Financiación de Universidad Complutense de Madrid-Banco Santander para contratos predoctorales de personal investigador en formación. Convocatoria 2020. CT82/20-CT83/20.
- Programa Estatal de Promoción del Talento y su Empleabilidad en I+D+i. programa de Formación del Profesorado Universitario (FPU). Convocatoria 2021. FPU21/06289.
- Beca de Movilidad Ciberes para la realización de la estancia corta en el extranjero. Convocatoria 2024.

MENCIÓN DE DOCTORADO INTERNACIONAL

La presente tesis doctoral de Dña. Marta Villegas Esguevillas titulada "Canales $K_V1.5$ y K_V7 como dianas farmacológicas en la hipertensión arterial pulmonar", realizada en el Departamento de Farmacología y Toxicología, de la Facultad de Medicina de la Universidad Complutense de Madrid, cumple los requisitos exigidos por la Universidad Complutense de Madrid para obtener la mención de Doctor Internacional (R.D. 99/2011):

1. La doctoranda matriculada en el programa de doctorado en Investigación Biomédica ha realizado una estancia predoctoral en una institución internacional, durante al menos 3 meses:
    - Nombre de la institución: Università degli Studi di Napoli Federico II. Dipartimento di Neuroscience, Reproductive Sciences and Dentistry. Nápoles (Italia)
    - Supervisor: Dr. Vincenzo Barrese
    - Duración de la estancia: 90 días (septiembre-diciembre 2024)
2. La tesis doctoral ha sido evaluada por dos doctores pertenecientes instituciones internacionales.
3. Un miembro del tribunal evaluador de la tesis doctoral pertenece a un centro de investigación extranjero.
4. La tesis doctoral ha sido redactada en inglés, y al menos, una parte de la defensa será presentada en una de las lenguas habituales para la comunicación científica, distinta a cualquiera de las lenguas oficiales en España.

AGRADECIMIENTOS

Llevar a cabo esta Tesis Doctoral ha sido un viaje largo, lleno de trabajo, esfuerzo y retos que, poco a poco, se han ido superando. Sin embargo, nada de esto habría sido posible sin el entorno tan especial que me ha acompañado durante estos años.

En primer lugar, quiero expresar mi más sincero agradecimiento a mis directores de tesis, el Dr. Ángel Cogolludo Torralba, Catedrático del Departamento de Farmacología y Toxicología de la Facultad de Medicina (UCM), y la Dra. Belén Climent Flórez, Profesora Titular del Departamento de Fisiología de la Facultad de Farmacia (UCM). **Ángel**, gracias por tu apoyo constante, tu paciencia, tu confianza y tu rigor científico. Gracias por estar siempre presente y por guiarme con equilibrio entre exigencia y cercanía. **Belén**, gracias por tu pasión contagiosa en cada ámbito de la vida, tu energía incansable y por creer siempre en mí, incluso cuando ni yo misma lo hacía. Tú veías en mí lo que yo no era capaz de ver. Gracias por inspirarme, por motivarme y por hacerme crecer en muchos aspectos.

Al Dr. Francisco Pérez Vizcaíno, director del Departamento de Farmacología y Toxicología de la Facultad de Medicina (UCM), gracias por tu compromiso con la ciencia y por transmitir siempre esa pasión que contagia. Gracias por ser un ejemplo de cómo se puede liderar desde la bondad.

A todos mis compañeros y compañeras de laboratorio que me han acompañado durante esta etapa: gracias por compartir conmigo el día a día, las frustraciones, los logros y las risas. Gracias por hacer del trabajo un lugar donde siempre encontré apoyo, complicidad y buenos momentos.

Me gustaría también agradecer al Dr. Vincenzo Barrese y a Camilla, porque además de acogerme científicamente, me hicieron sentir muy bien recibida, haciendo de Nápoles una segunda casa.

A todos mis amigos y amigas, por estar, por escuchar, por acompañar incluso sin entender del todo de qué iba esto.

A Pablo, por lo que fuimos, lo que somos y lo que seremos. Gracias por quererme como me quieres, cuidarme como lo haces y soportarme como me soportas. Este

camino no ha sido fácil, pero ahora vienen etapas mejores. Por mil viajes en moto más.

A mi familia, tanto los Villeguitas como los Esguevillas, os quiero con todo mi corazón. Mami y Papi, gracias por el amor y el cariño que siento nada más entrar por la puerta de casa. Sois mi hogar, mi refugio incondicional. Nuri, mi hermana, mi mejor amiga, gracias por ser como eres, por tu corazón tan bonito y por estar siempre. Y a Buddy, nuestro hermano de cuatro patas, porque los abrazos peludos también curan.

INDEX

K_V1.5 and K_V7 channels as pharmacological targets in pulmonary arterial hypertension

INDEX

K_V1.5 and K_V7 channels as pharmacological targets in pulmonary arterial hypertension

ABBREVIATIONS

5-HT	Serotonin
ACh	Acetylcholine
ATP	Adenosine triphosphate
AUC	Area under the curve
BMP	Bone morphogenetic proteins
BMPRII	Bone morphogenetic protein receptor type II
BSA	Bovine serum albumin
$[Ca^{+2}]_{cyt}$	Cytosolic calcium concentration
$[Ca^{+2}]_{ext}$	Extracellular calcium concentration
Ca^{+2}-CaM	Calcium-calmodulin complex
cAMP	Cyclic adenosine monophosphate
CAV	Caveolin-1
CSA	Cross-sectional area
cGMP	Cyclic guanosine monophospate
CREB	cAMP response element-binding protein
DAPI	4',6'-Diamidino-2-phenylindole
DMSO	Dimethyl sulfoxide
DMEM	Dulbecco's modified eagle medium
DNA	Deoxyribonucleic acid
DPO-1	Diphenylphosphine oxide
EC50	Half maximal effective concentration
ENG	Endoglin
eNOS	Endothelial nitric oxide synthase
Em	Membrane potential
ER	Endoplasmic reticulum
ET-1	Endothelin-1
FBS	Fetal bovine serum
HIV	Human immunodeficiency virus
Hpx/Su	Model of chronic hypoxia combined Su5416
IL	Interleukin
K^+	Potassium
K_{2P}	Dual pore domain potassium channels
K_{ATP}	ATP-sensitive potassium channels
K_{Ca}	Calcium-activated potassium channels
KCNE	K^+ channel subfamily E
K_{IR}	inward rectified potassium channels
K_V	Voltage-gated potassium channels
MLCK	Myosin light chain kinase
MAM	Mitochondria-associated endoplasmic reticulum membranes
MLCP	Myosin light chain phosphatase
mPAP	Mean pulmonary arterial pressure

NF-kβ	Nuclear factor k-light-chain-enhancer of β cell
NO	Nitric oxide
PA	Pulmonary arteries
PAECs	Pulmonary artery endothelial cells
PAH	Pulmonary arterial hypertension
PASMCs	Pulmonary artery smooth muscle cells
PBS	Phosphate saline buffer
PCH	Pulmonary capillary haemangiomatosis
PDE5	Phosphodiesterase 5
PGI2	Prostacyclin
PH	Pulmonary hypertension
Phe	Phenylephrine
PIP_2	Phosphatidylinositol 4,5-bisphosphate
PKA	Protein kinase A
PKC	Protein kinase C
PVR	Pulmonary vascular resistance
PVOD	Pulmonary veno-occlusive disease
ROS	Reactive oxygen species
RV	Right ventricle
S1R	Sigma-1 receptor
sGC	Soluble guanylyl cyclase
sPAP	Systolic pulmonary arterial pressure
TASK	Two pore acid-sensitive K^+ channels
TGF- β	Transforming growth factor- β
TM	Transmembrane
TXA_2	Thromboxane A2
VGCC	Voltage-gated calcium channel
WHO	World health organization

ABSTRACT

INTRODUCTION

Pulmonary arterial hypertension (PAH) is a rare, progressive, and potentially life-threatening vascular disease characterized by sustained vasoconstriction, vascular remodelling, *in situ* thrombosis, and inflammation. This condition leads to a progressive increase in pulmonary vascular resistance, which elevates right ventricular afterload, ultimately causing right ventricular hypertrophy, heart failure, and death. Despite therapeutic advances that have improved the quality and life expectancy of patients, PAH remains a disease with a high mortality rate.

One of the key pathophysiological mechanisms of PAH is ionic remodelling, primarily characterized by decreased expression and/or activity of potassium (K^+) channels, particularly $K_V1.5$ and TASK-1, which are essential for the regulation of vascular tone and cell proliferation. Among these, voltage-dependent potassium (K_V) channels play a critical role in pulmonary vascular homeostasis. Their functional dysregulation contributes to PAH pathogenesis by promoting vasoconstriction, smooth muscle proliferation, and resistance to apoptosis. However other channels such as K_V7 appear to retain their functionality, making them attractive candidates for pharmacological activation.

Therefore, $K_V1.5$ and K_V7 channels have been identified as relevant pharmacological targets in PAH. In this context, a newly identified K_V7 channel agonist, URO-K10, shows great efficacy in activating these channels. In addition, recent studies have shown that activation of the sigma-1 receptor (S1R) can modulate the activity of various ion channels, including $K_V1.5$, offering new opportunities for their functional restoration in PAH. This could be achieved through the use of selective S1R agonists (PRE084) or commercially available drugs with S1R agonist properties, such as fluoxetine and dimemorfan.

HYPOTHESIS AND OBJECTIVES

The central hypothesis of this Doctoral Thesis is whether targeted modulation of specific K_V channels represents an effective therapeutic strategy to reverse or slow

the ionic remodelling characteristic of PAH. Consequently, this approach will improve pulmonary vascular function and delay disease progression.

To test this hypothesis, the following specific objectives were proposed:

1. To evaluate the pulmonary vasodilatory and antiproliferative effects of the novel K_V7 channel activator, URO-K10.
2. To assess the effects of the S1R agonist, PRE084, on K_V1.5 channel activity and its impact on pulmonary, cardiovascular function, and vascular remodelling in an in vivo PAH model.
3. To analyse the potential of clinically approved S1R agonist drugs, such as fluoxetine and dextromethorphan, to enhance K_V1.5 activity in PAH.

MATERIALS AND METHODS

Two experimental rat models of PAH were used: the monocrotaline (MCT)-induced model and the model of chronic hypoxia combined with VEGF receptor inhibition (Hpx/Su), along with their respective controls. Human pulmonary artery (PA) samples and pulmonary artery smooth muscle cells (PASMCs) from healthy individuals undergoing thoracic surgery were also used.

Methodologies included hemodynamic and echocardiographic studies, vascular reactivity analysis via wire myography, patch-clamp recordings of K_V currents, BrdU proliferation assays, Western blotting, immunocytochemistry, histological analyses of heart and lung tissues, and metabolomics using nuclear magnetic resonance spectroscopy.

RESULTS

This Doctoral Thesis demonstrated that URO-K10 is a potent K_V7 channel activator with superior efficacy compared to classical agonists such as retigabine and flupirtine. URO-K10 significantly increased K^+ currents in PASMCs from rat and human PA. Its vasodilatory and electrophysiological effects were abolished by the

K_V7-specific inhibitor XE991, confirming a K_V7-dependent action. Unlike traditional activators, URO-K10 remained effective in the absence of the regulatory subunit KCNE4, indicating an independent mechanism. Additionally, it exhibited antiproliferative effects on human PASMCs. Notably, its vasodilatory efficacy was enhanced under PAH-mimicking ionic remodelling conditions, both *in vitro* and in MCT-induced PAH rat models.

In a second study, the S1R agonist PRE084 was evaluated in the Hpx/Su in vivo PAH model. PRE084 increased $K_V1.5$ activity in PASMCs, reduced hypercontraction, and improved endothelium-dependent relaxation in PA. Beyond improving vascular remodelling, PRE084 exerted cardioprotective effects by reducing right ventricular dysfunction, hypertrophy, and fibrosis, decreasing right ventricular systolic pressure, and showing a tendency to reduce pulmonary arterial pressure. These effects were likely mediated by $K_V1.5$ activation, modulation of the pAKT signalling pathway, and restoration of inositol levels.

Finally, the repurposing potential of fluoxetine and dimemorfan, both S1R agonists, was investigated. Both increased $K_V1.5$ currents in PASMCs from control and PAH (Hpx/Su) rats. These effects were abolished by the S1R antagonist BD1047, confirming receptor involvement. Additionally, both compounds reduced phenylephrine-induced vasoconstriction.

CONCLUSIONS

1. URO-K10 is a K_V7 channel activator, with vasodilatory effects much more effective and potent than retigabine and flupirtine, and it also exerts antiproliferative effects.
2. The action of URO-K10 is independent of the KCNE4 subunit.
3. URO-K10 demonstrates greater vasodilatory efficacy under the pathophysiological conditions of PAH.
4. Activation of the S1R receptor by PRE084 improves vascular and cardiac function in PAH models, and importantly, is able to reduce right ventricular

systolic blood pressure and tends to reduce pulmonary artery pressure. All these effects are related to an increase in K_V1.5 activity in the pulmonary arteries and a restoration of normal levels of pAKT and inositol in the right ventricle.

5. The commercially available drugs fluoxetine and dimemorfan functionally improve K_V1.5 channels through S1R, which encourages further studies to evaluate their possible repositioning in pathologies that involve dysfunction of these channels, such as PAH.

Taken together, these findings indicate that activation of K_V channel and S1R modulation represent promising therapeutic strategies. Both approaches may help to halt the progression of PAH.

RESUMEN

INTRODUCCIÓN

La hipertensión arterial pulmonar (HAP) es una enfermedad vascular rara, progresiva y potencialmente mortal, caracterizada por una vasoconstricción sostenida, un remodelado vascular, trombosis *in situ* e inflamación. Este trastorno conlleva un incremento progresivo en la resistencia vascular pulmonar, lo que eleva la poscarga del ventrículo derecho, desencadenando hipertrofia ventricular, insuficiencia cardiaca y, finalmente, la muerte. A pesar de los avances terapéuticos que han mejorado la calidad y esperanza de vida de los pacientes, la HAP sigue siendo una patología con una elevada tasa de mortalidad.

Uno de los mecanismos fisiopatológicos clave de la HAP es el remodelado iónico, caracterizado principalmente por la disminución de la expresión y/o actividad de canales de potasio (K^+), particularmente los canales $K_V1.5$ y TASK-1, esenciales en la regulación del tono vascular y la proliferación celular. Dentro de esta familia, los canales de potasio dependientes de voltaje (K_V) desempeñan un papel esencial en la homeostasis vascular pulmonar. Su desregulación funcional contribuye a la patogénesis de la HAP al promover la vasoconstricción, la proliferación del músculo liso y la resistencia a la apoptosis. Sin embargo, otros canales como los K_V7 parecen conservar su funcionabilidad, lo que los convierte en candidatos atractivos para la activación farmacológica.

Por tanto, los canales de $K_V1.5$ y K_V7 han sido identificados como posibles dianas farmacológicas relevantes en la HAP. En este contexto, se ha identificado un nuevo agonista de canales Kv7, el URO-K10, el cual muestra una gran eficacia en la activación de dichos canales. Además, estudios recientes han señalado que la activación del receptor sigma-1 (S1R) puede modular la actividad de diversos canales iónicos, incluido el canal $K_V1.5$, abriendo nuevas posibilidades para su restauración funcional en la HAP. Esto podría llevarse a cabo mediante el empleo de agonistas selectivos del S1R (PRE084) o fármacos comercializados con propiedades agonistas del S1R como la fluoxetina y el dimemorfan.

HIPÓTESIS Y OBJETIVOS

Por lo tanto, la hipótesis central de esta Tesis Doctoral es que la modulación dirigida de canales K_V específicos representan una estrategia terapéutica efectiva para revertir o frenar el remodelado iónico característico de la HAP, contribuyendo así a mejorar la función vascular pulmonar y reducir la progresión de la enfermedad.

Para demostrar esta hipótesis inicial, se proponen los siguientes objetivos específicos:

1) Evaluar los efectos vasodilatadores y antiproliferativos pulmonares del nuevo activador de los canales K_V7, URO-K10.

2) Estudiar el efecto del agonista de S1R, PRE084, sobre la actividad de los canales K_V1.5 y su impacto en la función pulmonar, cardiovascular y en el remodelado vascular en un modelo experimental in vivo de HAP.

3) Analizar el potencial de fármacos comercializados con actividad agonista sobre S1R, como la fluoxetina y el dimemorfán, para mejorar la actividad atenuada del canal K_V1.5 en la HAP.

MATERIALES Y MÉTODOS

Para ello, en este estudio se utilizaron dos modelos experimentales de HAP en rata: el modelo inducido por monocrotalina (MCT) y el modelo combinado de exposición a hipoxia crónica y al inhibidor del receptor VEGF SU5416 (Hpx/Su) y sus correspondientes controles. Además, se emplearon muestras de arterias pulmonares (AP) y células del músculo liso de arterias pulmonares (CMLAP) provenientes de humanos sanos, obtenidas tras cirugía torácica.

Las metodologías incluyeron estudios hemodinámicos y ecocardiográficos, análisis de reactividad vascular en miografía, registro de corrientes de canales K_V mediante patch-clamp, ensayos de proliferación celular (BrdU), análisis de expresión proteica por Western blot e inmunocitoquímica, así como estudios histológicos de corazón y pulmón y metabolómica.

RESULTADOS

Los hallazgos de esta tesis doctoral revelaron que el compuesto URO-K10 es un activador de canales K_V7 con una eficacia superior a la de los activadores clásicos como retigabina y flupirtina. El URO-K10 incrementó significativamente las corrientes de K^+ en CMLAP en AP de rata y humanas. Además, sus efectos fueron abolidos por el inhibidor selectivo de K_V7, XE991, confirmando que su acción es vía activación K_V7. Además, el nuevo fármaco mantuvo su eficacia en ausencia de la subunidad reguladora KCNE4, lo que indica un mecanismo de acción independiente de esta subunidad. También mostró efectos antiproliferativos sobre CMLAP humanas, lo que refuerza su utilidad terapéutica más allá de la vasodilatación. De forma destacada, su eficacia vasodilatadora fue aún mayor bajo condiciones que simulan el remodelado iónico característico de la HAP, tanto *in vitro* como en el modelo de rata de HP inducida por monocrotalina.

En un segundo estudio, se evaluó el efecto del agonista del S1R, PRE084, en el modelo in vivo Hpx/Su de HAP. Se observó que el PRE084 aumentó la actividad de los canales $K_V1.5$ en células CMLAP, atenuó la hipercontracción de las AP y mejoró la relajación dependiente de endotelio. Cabe destacar que además de mejorar el remodelado vascular pulmonar, el PRE084 ejerció efectos cardioprotectores significativos, al atenuar la disfunción del ventrículo derecho, reducir la hipertrofia y la fibrosis, disminuir la presión sistólica ventricular derecha y mostrar una tendencia a reducir la presión arterial pulmonar. Estos beneficios parecen estar mediados, al menos en parte, por la activación de $K_V1.5$, modulación de la vía de señalización pAkt y la restauración de los niveles de inositol.

Finalmente, se examinó el potencial de reposicionamiento de fluoxetina y dimemorfan, fármacos con actividad agonista sobre S1R, en la HAP. Ambos aumentaron las corrientes de $K_V1.5$ en CMLAP provenientes de ratas control y de ratas del modelo de HAP de Hpx/Su. La inhibición de S1R con BD1047 bloqueó estos efectos, confirmando la implicación directa del receptor. Además, ambos atenuaron la respuesta vasoconstrictora inducida por fenilefrina.

CONCLUSIONES

Teniendo en cuenta el trabajo desarrollado a lo largo de esta Tesis Doctoral y los objetivos planteados, se pueden extraer las siguientes conclusiones:

1. El URO-K10 es un activador de los canales K_V7, con efectos vasodilatadores mucho más eficaces y potentes que la retigabina y la flupirtina y que ejerce efectos antiproliferativos.
2. La acción del URO-K10 es independiente de la subunidad KCNE4.
3. El URO-K10 muestra una mayor eficacia vasodilatadora bajo condiciones fisiopatológicas de HAP.
4. La activación del receptor S1R mediante PRE084 mejora la función vascular y cardíaca en modelos de HAP, y de forma importante, es capaz de reducir la presión sistólica del ventrículo derecho y tiende a reducir la presión arterial pulmonar. Todos estos efectos se relacionan con un aumento en la actividad de K_V1.5 en las arterias pulmonares y con una restauración de los niveles normales de pAKT e inositol en el ventrículo derecho.
5. Los fármacos comercializados fluoxetina y dimemorfan mejoran funcionalmente los canales K_V1.5 a través de S1R, lo que sugiere su posible reposicionamiento en patologías que cursan con una disfunción de dichos canales como la HAP.

En conjunto, los resultados sitúan a la activación de canales K_V y del receptor S1R como posibles estrategias terapéuticas prometedoras para frenar el avance de la HAP.

INTRODUCTION

1. Potassium (K^+) channels

1.1. Generalities

Without ion channels, life, as we know it, would not be possible. These transmembrane proteins are key to the development of fundamental physiological functions such as breathing, movement, cognition, and cardiac rhythm maintenance. Ion channels are essential for rapid intercellular communication, allowing the selective passage of ions through the cell membrane. Their function depends on electrochemical gradients maintained by homeostatic mechanisms, which allow small changes in ion concentration to generate rapid variations in membrane potential, crucial in cell signalling (Hille et al., 1999).

In particular, potassium (K^+) channels constitute the largest and most diverse family of ion channels in the human genome, with more than 70 coding genes identified. These proteins are present in practically all cell types and are involved in fundamental processes such as regulation of membrane potential, repolarisation after action potentials, cell volume homeostasis, hormone secretion, cell proliferation and apoptosis. In excitable tissues such as the brain, heart and smooth muscle, their role is particularly relevant, although they also play key roles in non-excitable tissues, such as the immune system (González et al., 2012).

1.2. Structural and functional classification of K^+ channels

From a structural and molecular perspective, K^+ channels are grouped into four major families according to the number of transmembrane domains per subunit and their activation mechanism (Roden & George, 1997).

a) Inwardly rectifying channels (K_{ir}). Tetrameric channels in which their monomers represent the simplest structural form with two transmembrane segments (2TM) and a P-loop selectivity filter. These channels mainly facilitate the influx of K^+ into the cell and are regulated by intracellular signals.

b) Two-pore domain K^+ channels (K_{2P}). These dimeric channels possess four transmembrane domains (4TM) and two P regions per subunit, forming functional dimers. They conduct 'leak' currents that stabilize resting

membrane potential and regulate cellular excitability in a voltage-independent manner.

c) Voltage-gated K^+ channels (K_V). These tetrameric channels are characterized by six transmembrane segments (6TM) (S1-S6) per subunit, with a voltage-sensing domain (S1-S4) and a pore-forming domain (S5-P-S6). They assemble as functional tetramers, are sensitive to voltage changes and constitute the most abundant K^+ channel subfamily (Wulff et al., 2009).

d) Calcium-activated K^+ channels (K_{Ca}). These tetrameric channels are activated mainly by increases in intracellular Ca^{2+} concentrations. Although they share the 6TM architecture with K_V channels, their activation depends on Ca^{2+}-binding sensors such as calmodulin or specific regulatory domains.

1.3. Voltage-gated potassium (K_V) channels

Voltage-gated K^+ channels (K_V) represent the largest and most functionally diverse family of K^+ channels. They are encoded by at least 40 different genes, grouped into 12 subfamilies (K_V1 to K_V12). Each functional channel is composed of a tetramer of α-subunits, which can assemble as either homotetramers or heterotetramers (Coetzee et al., 1999; Wulff et al., 2009). Each α-subunit comprises six transmembrane segments (S1–S6) (Ackerman & Clapham, 1997; D. M. Kim & Nimigean, 2016): the S1–S4 segments form the voltage-sensing domain, in which the S4 segment contains positively charged residues (mainly arginines) that detect changes in membrane potential, while the S5–P–S6 segments forms the central pore domain. The S6 helix functions as the gating element, controlling the opening and closing of the ion-conducting pathway.

Due to their accessibility, both the N- and C-terminal domains are key sites for post-translational modulation through interactions with auxiliary proteins and signalling molecules. These include β-subunits, K^+ channel subfamily E (KCNEs) regulatory subunits, phosphatidylinositol 4,5-bisphosphate (PIP_2), and kinases such as PKC and PKA, which collectively modulate channel behaviour (England et al., 1995; Huang et al., 2023; Mondejar-Parreño et al., 2020; Sewing et al., 1996). Functionally, activation of the voltage sensor triggers a conformational change that is

transmitted to the pore via the S4–S5 linker, resulting in displacement of the S6 segment and subsequent channel opening (Jensen et al., 2012). Moreover, K_V channel activity is finely regulated at multiple levels, including transcriptional expression, post-translational modifications, trafficking to the membrane, membrane insertion, recycling and degradation. These layers of control allow K_V channels to respond dynamically to physiological stimuli and pathological conditions.

1.4. K^+ channels in the pulmonary vasculature

Numerous K^+ channels are expressed in the circulatory system, though their distribution and functional roles differ between the pulmonary and systemic vasculature. In pulmonary artery smooth muscle cells (PASMCs), K_V channels, particularly subtypes $K_V1.2$, $K_V1.5$, $K_V2.1$, $K_V7.4$, and $K_V7.5$, are key regulators of the resting membrane potential and vascular tone. In addition, other K^+ channels such as TASK-1 (K_{2P} channel) and ATP-sensitive K^+ channels (K_{ATP}), composed of $K_{ir}6.1$ and SUR2 subunits, are also significantly expressed in the pulmonary circulation (Mondéjar-Parreño et al., 2021).

In addition to PASMCs, pulmonary artery endothelial cells (PAECs) also express a wide range of K^+ channels, including $K_V1.5$, $K_V2.1$, $K_V2.2$, K_{ATP}, TASK-1, TASK-2, $K_{Ca}2.3$ and $K_{Ca}3.1$(Mondéjar-Parreño et al., 2021). Moreover, K_V channels are expressed in other vascular-associated cell types. For example, in immune cells such as macrophages and T lymphocytes, $K_V1.3$ channels regulate cellular activation, proliferation and cytokine secretion. Their activity influences immune responses and has been implicated in vascular inflammation and remodelling (Chandy & Norton, 2017).

1.4.1. Role of K^+ channels in the pulmonary vasoconstriction, cell survival, apoptosis and proliferation

In PASMCs, intracellular K^+ concentration is tightly regulated to maintain vascular tone and essential cellular functions (Burg et al., 2008). Under physiological conditions, extracellular K^+ ranges between 3-5 mmol L^{-1}, whereas intracellular concentrations reach approximately 140 mmol L^{-1}. This electrochemical gradient drives the outward movement of K^+ ions, leading to membrane hyperpolarization

(Nelson & Quayle, 1995). In *ex vivo* conditions, the resting membrane potential of PASMCs ranges from -65 mV and -40 mV (Boucherat et al., 2015; Lambert, Capuano, et al., 2018), and plays a key role in modulating Ca^{2+} influx, which in turn regulates contractility, apoptosis, and proliferation (Burg et al., 2008; Okada et al., 2001).

Activation of K^+ channels induce K^+ efflux, causing membrane hyperpolarization and decreased opening of voltage-gated Ca^{2+} channels (VGCCs). The resulting reduction in cytosolic Ca^{2+} concentration promotes relaxation and vasodilation. In contrast, K^+ channel inhibition causes membrane depolarization, VGCC activation, leading thus, to increase intracellular Ca^{2+} and vasoconstriction (Cogolludo, Moreno, et al., 2006; Cole & Welsh, 2011). PASMCs contraction starts when Ca^{2+} binds to calmodulin, activating myosin light chain kinase (MLCK), which phosphorylates the 20-kDa regulatory light chain of myosin, thereby increasing myosin ATPase activity and initiating cross-bridge cycling and contraction. Relaxation occurs when myosin light chain phosphatase (MLCP) removes the phosphate group from myosin (Webb, 2003).

In addition to contractility, K^+ channels modulate apoptosis, proliferation, and cell cycle progression. During apoptosis, cell shrinkage is a hallmark event. This reduction in cell volume during apoptosis is mediated by the coordinated efflux of K^+ and Cl^-, which generates an osmotic gradient that causes water to exit the cell via aquaporins (Burg et al., 2008; Maeno et al., 2000). Notably, increased expression of the human *KCNA5* gene, which encodes the K_V1.5 channel, augments K_V currents and promotes apoptosis (Brevnova et al., 2004). Intracellular K^+ levels also influence caspase and nuclease activity: low K^+ concentrations favour apoptosis, while elevated levels exert anti-apoptotic effects (Burg et al., 2008; Vera-Zambrano, Lago-Docampo, et al., 2023). Furthermore, K^+ channels contribute to cell proliferation by modulating intracellular Ca^{2+}, which regulates transcription factors like CREB and NF-κB and promotes cell cycle progression (Burg et al., 2008; Dolmetsch et al., 1997). In PASMCs, depolarization-induced Ca^{2+} influx facilitates G_0/ G_1 transition, DNA synthesis, and mitosis. Inhibition of K^+ channels is linked to PASMCs proliferation, supporting the idea that depolarization-induced increases in intracellular Ca^{2+} facilitate cell cycle progression (Burg et al., 2008; Dolmetsch et al., 1997). Therefore, a proper balance between proliferation and apoptosis is crucial for PASMCs

homeostasis, as its dysregulation contributes to pulmonary vascular remodelling, an important feature of pulmonary vascular diseases (Burg et al., 2008; Okada et al., 2001) (Figure 1).

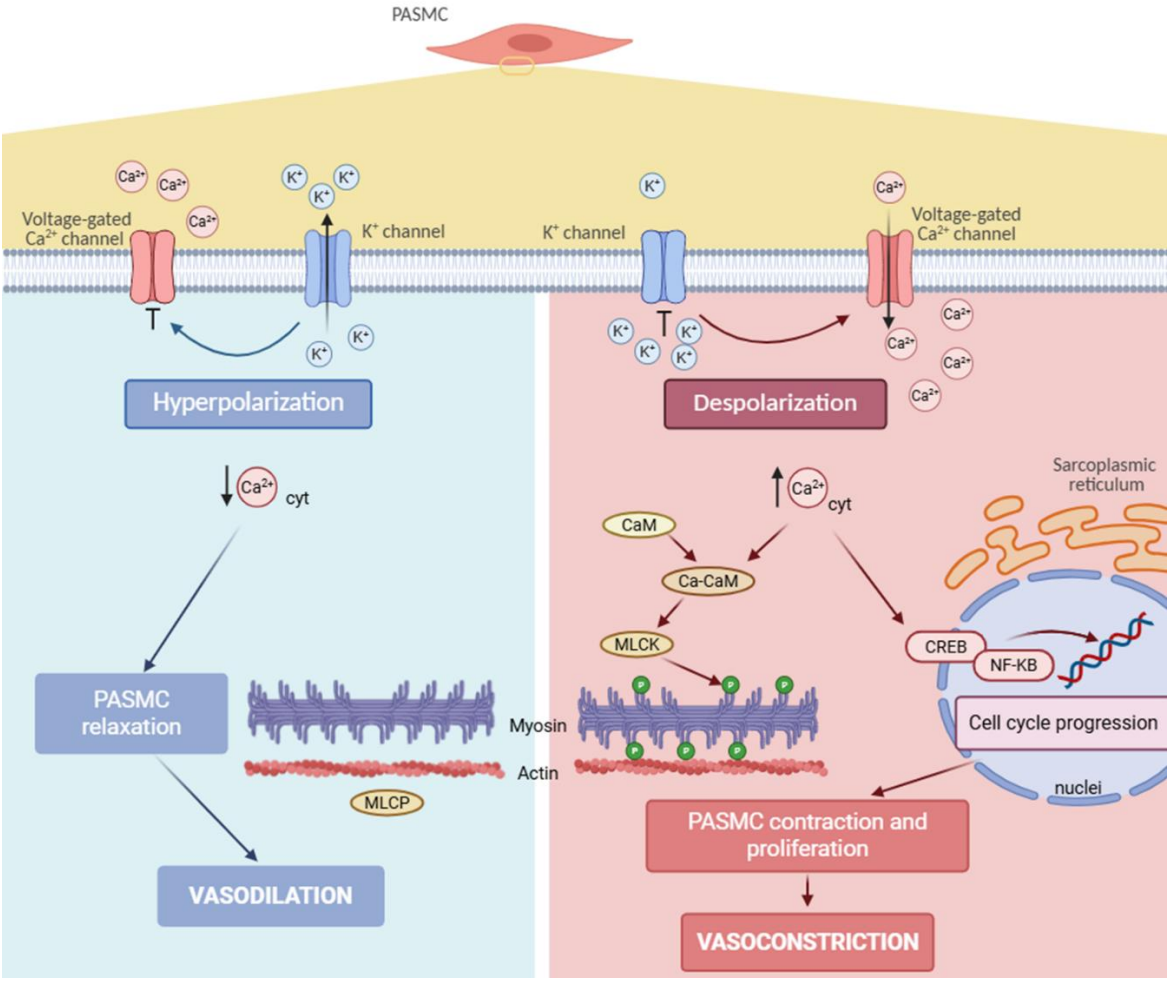

***Figure 1*. *Role of K⁺ channels in the regulation of vascular tone and PASMCs proliferation*.** This cartoon illustrates the role of K^+ channels in PASMCs. Left panel (blue) shows that the activation of K^+ channel leads to K^+ efflux and membrane hyperpolarization, which reduces the opening probability of voltage-gated Ca^{2+} channels, resulting in decreased cytosolic Ca^{2+} levels. This favours PASMCs relaxation and vasodilation. Right panel (red): reduced K^+ channel activity causes - membrane depolarization, increasing voltage-gated Ca^{+2} channel activity and intracellular Ca^{+2} influx. Cytosolic Ca^{+2} binds to calmodulin (CaM) and forms the Calcium-Calmodulin complex (Ca-CaM), activating myosin light chain kinase (MLCK), which phosphorylates the light chain of myosin and initiating cross-bridge cycling and contraction. In parallel, the elevated cytosolic Ca^{2+}regulates transcription factors like CREB and NF-κB and promotes cell cycle progression. These processes contribute to pulmonary vasoconstriction and proliferation. Created with BioRender.

1.4.2. K_V1.5 and K_V7 channels in the pulmonary vasculature

Among the K_V channels expressed in the pulmonary vasculature, K_V1.5 and K_V7 have proven to be key regulators of membrane potential in PASMCs and, consequently, of pulmonary vascular tone. K_V1.5 is the predominant K_V channel in the distal regions of the pulmonary arteries, where its activation under physiological conditions contributes to the maintenance of low vascular tone and ensures optimal ventilation-perfusion matching in the lungs (Remillard et al., 2007). Several studies have shown that K_V1.5 inhibition is involved in pulmonary vasoconstriction induced by various relevant stimuli, including serotonin, thromboxane A_2, hypoxia, and reactive oxygen species (ROS) (Cogolludo et al., 2003, 2008, 2019; Cogolludo, Frazziano, et al., 2006; Cogolludo, Moreno, et al., 2006). At the molecular level, K_V1.5 is subject to complex post-translational regulation, including phosphorylation, sumoylation, and acylation, which modulate both its subcellular localization and gating properties (Benson et al., 2007; Kwak et al., 1999; L. Zhang et al., 2007). In addition, K_V1.5 membrane trafficking may be regulated by several mechanisms including dynein-dependent or caveolae-dependent mechanisms, which determine its surface expression and, consequently, its functional availability (Choi et al., 2005; Cogolludo, Moreno, et al., 2006). Recent evidence also suggests that the Sigma-1 receptor (S1R) participates in the modulation of K_V1.5 channel activity, acting as a molecular chaperone that influences its trafficking and functional expression at the plasma membrane (discussed below). Another critical step for K_V1.5 to reach the plasma membrane and become fully functional involves a glyxosylation on its loop between the S1 and S2 transmembrane domains (N. V Shen et al., 1993). This modification is essential for proper protein maturation, and as a result, K_V1.5 can be detected in both immature (non-glycosylated) and mature (glycosylated) forms, typically visible as two distinct bands in Western blot analyses (Vera-Zambrano, Lago-Docampo, et al., 2023).

K_V7 channels have emerged as essential regulators of membrane potential in PASMCs. Unlike K_V1.5, K_V7 channels, particularly K_V7.4 and K_V 7.5, generate slowly activating, non-inactivating K^+ currents that promote sustained membrane hyperpolarization and prolonged vascular relaxation (Barrese et al., 2018; Haick &

Byron, 2016; Mackie & Byron, 2008). K_V7 channel activity, cell localization, channel trafficking, and drug sensitivity can be modulated by KCNEs regulatory subunits (Abbott, 2020; Barrese et al., 2018). Recent studies have confirmed their involvement in nitric oxide (NO)-induced vasodilation and in pulmonary vascular dysfunction associated with tobacco exposure (Mondéjar-Parreño et al., 2019; Mondejar-Parreño et al., 2020; Sevilla-Montero et al., 2021).

Together, $K_V1.5$ and K_V7 channels form part of the physiological machinery that maintains pulmonary vascular homeostasis, ensuring a balance between contraction and relaxation of PASMCs in response to fluctuating mechanical and chemical stimuli in the pulmonary circulation.

2. The pulmonary circulation

The respiratory system is a complex and dynamic network of organs and tissues whose primary function is to facilitate gas exchange. It comprises the airways, lungs, pulmonary vasculature, and respiratory muscles, all of which work in concert to ensure effective oxygenation and carbon dioxide removal.

The pulmonary circulation operates as a low-pressure, high flow system, forming a closed circuit between the right heart and the lungs. Unlike the systemic circulation, which delivers oxygenated blood to the entire body, the pulmonary circuit is specialized for gas exchange and is structurally and functionally adapted to maintain low vascular resistance. The mean pulmonary arterial pressure (mPAP) under physiological conditions is approximately 14 mmHg, which is 7 - 8 times lower than that in the systemic circulation. This low-pressure environment is essential to protect the delicate alveolar-capillary interface and to ensure efficient diffusion of respiratory gases (Burg et al., 2008; Kovacs et al., 2009).

Pulmonary arteries (PA) are composed of three histological layers: the intima, consisting of a single layer of endothelial cells in direct contact with the blood; the media, composed primarily of PASMCs and elastic fibres, responsible for maintaining vascular tone; and the adventitia, which includes fibroblasts and connective tissue

that confer mechanical support and protection (Figure 2). Compared to systemic arteries, PA possess thinner walls and a smaller medial layer, reflecting their adaptation to accommodate high volumes of blood at low pressure without compromising gas exchange (Townsley, 2012).

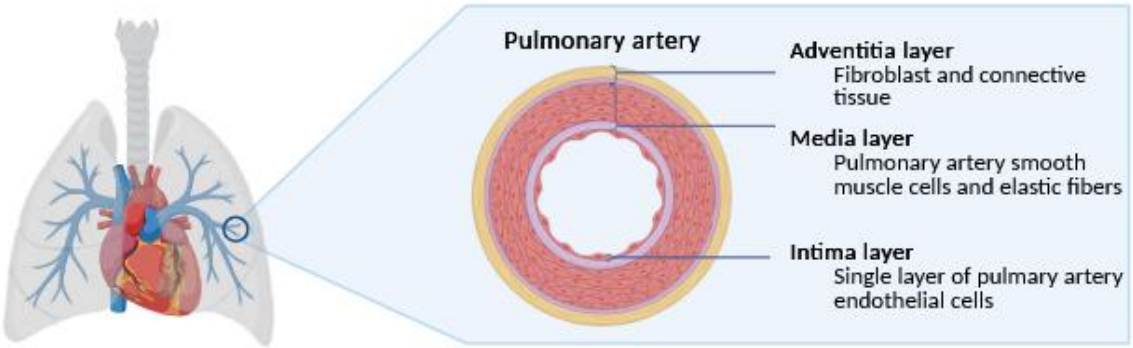

Figure 2. Anatomy of pulmonary artery. Pulmonary arteries consist of three layers: intima (endothelium), media (smooth muscle and elastic fibres) and adventitia (fibroblasts and connective tissue)**.** Created with BioRender.

Vascular tone in the pulmonary circulation is tightly regulated by a balance of vasoactive substances (e.g., nitric oxide, prostacyclin, endothelin-1), oxygen tension, and mechanosensitive pathways, such as the shear stress generated by the frictional force of blood flow. This precise control ensures the dynamic matching of perfusion to ventilation, a process known as ventilation–perfusion coupling, which is critical for optimal pulmonary function. Nonetheless, alterations in these finely regulated physiological mechanisms can contribute to the development of pulmonary vascular diseases, such as pulmonary hypertension, which will be addressed in the following section.

3. Pulmonary hypertension

3.1. Definition and classification

Pulmonary hypertension (PH) is a hemodynamic disorder characterised by a persistent increase in mPAP above 20 mmHg, as measured by right heart catheterization, along with a pulmonary vascular resistance (PVR) equal to or greater than three Wood units (Kovacs et al., 2024; Simonneau et al., 2019). PH includes a heterogeneous group of diseases that, despite sharing similar clinical manifestations, hemodynamic profiles, histological features and therapeutic approaches, differ in their underlying pathophysiology and prognosis (Kovacs et al., 2024; Simonneau et al., 2019). The most accepted classification, endorsed by the European Society of Cardiology and the European Respiratory Society (ESC/ERS), categorizes PH into five groups according to aetiology and pathophysiological mechanisms. This classification was most recently updated during the 6th World Symposium on Pulmonary Hypertension held in Nice in 2018 (Simonneau et al., 2019). Table 1 presents a simplified overview of this classification, with a particular emphasis on Group 1: Pulmonary arterial hypertension (PAH).

1. Pulmonary arterial hypertension (PAH)
    - I. Idiopathic
    - II. Hereditable
    - III. Associated with drugs and toxins
    - IV. Associated with
        - i. Connective tissue disease
        - ii. HIV infection
        - iii. Portal hypertension
        - iv. Congenital heart disease
        - v. Schitosomiasis
    - V. PAH with features of venous/capillary (PVOD/PCH) involvement
    - VI. Persistent PH of newborn
2. PH associated with left heart disease
3. PH due to lung diseases and/or hypoxia
4. PH due to pulmonary artery obstructions
5. PH with unclear and/or multifactorial mechanisms

Table 1. Clinical classification of PH. Taken from Kovacs et al., 2024.

This Doctoral Thesis focuses on PAH, which represents a unique form of PH characterized by progressive remodelling of the pulmonary arterioles, leading to increased resistance, right ventricular overload, and eventual heart failure.

3.2. Diagnosis and epidemiology

PAH is a rare and progressive disease that, despite advances in treatment, remains associated with high mortality. Recent data indicate that the five-year transplant-free survival rate is approximately 57%, highlighting the severity of the condition and the critical need for early diagnosis and timely intervention (Hendriks et al., 2022).

Early diagnosis of PAH is particularly challenging due to its nonspecific clinical presentation, including exertional dyspnea, fatigue, dry cough, and general malaise. These symptoms are frequently misattributed to more prevalent cardiovascular or respiratory disorders, leading to delayed recognition and late-stage referrals, limiting the window for early intervention and disease-modifying therapies (Delcroix & Howard, 2015)

A definitive diagnosis requires right heart catheterization, which allows for precise hemodynamic measurements such as mPAP and calculation of PVR. Non-invasive techniques such as transthoracic echocardiography, are frequently used as first-line screening tools. They offer valuable information on right ventricular dimensions and function estimated pulmonary pressures. Prognostic evaluation is based on multiple clinical and functional parameters, including the functional classification systems of the New York Heart Association (NYHA) and the World Health Organization (WHO), which categorize the severity of symptoms during physical activity via the six-minute walk test (6MWT), gas exchange assessments such as diffusing capacity for carbon monoxide (DLCO), and cardiac biomarkers including B-type natriuretic peptide (BNP) and N-terminal pro-BNP (NT-proBNP) (Galiè et al., 2016).

From an epidemiological perspective, PAH is a low-prevalence disease, with an estimated annual incidence of 5 to 10 cases per million people in Europe (Hendriks et al., 2022). Once considered a disease primarily affecting young adults, recent registry data indicate an increasing number of elderly patients at diagnosis, many of whom present with multiple comorbidities (Lau et al., 2017). Additionally, a notable

feature of PAH is its sex-related prevalence, as it affects women more frequently — particularly in idiopathic and heritable forms— men typically present with more severe hemodynamic compromise and worse long-term outcomes (Bousseau et al., 2023). These differences suggest sex-specific variations in pulmonary vascular biology, possibly mediated by hormonal, genetic, or epigenetic factors, and represent an emerging area of research.

3.3. Aetiology

PAH is a complex and multifactorial disease influenced by genetic predisposition, epigenetic modifications, and environmental triggers (Guignabert et al., 2024; Humbert et al., 2019). While traditionally considered idiopathic in many cases, advances in molecular biology and genomics over the past two decades have substantially expanded our understanding of the etiological landscape of PAH, revealing a spectrum of underlying mechanisms that can predispose to or trigger the development of this condition in susceptible individuals.

A major breakthrough in the field was the identification of mutations in the BMPR2 gene, which encodes the type 2 receptor of bone morphogenetic proteins (BMPs), a member of the transforming growth factor-β (TGF-β) superfamily. This receptor plays a central role in regulating vascular cell growth, differentiation, and apoptosis. BMPR2 mutations are present in approximately 70–80% of heritable PAH (hPAH) cases and in 10–20% of idiopathic PAH (iPAH), making it the most prevalent known genetic defect associated with the disease. Subsequent studies have identified other mutations in genes related to the same signalling pathway, including ACVRL1/ALK1 (activin receptor-like kinase 1), ENG (endoglin), CAV1 (caveolin-1), SMAD9 (SMAD family member 9) and TBX4 (T-box transcription factor 4) (Austin & Loyd, 2014; Morrell et al., 2019).

In addition to these mutations, growing evidence supports the role of ion channelopathies in the aetiology of PAH. Among these, loss-of-function mutations in the *KCNK3* gene, which encodes TASK-1 channel, have been reported in both heritable and idiopathic forms of the disease. These mutations lead to diminished potassium current, membrane depolarization, and increased calcium influx, thereby

promoting pulmonary vasoconstriction and smooth muscle proliferation (Ma et al., 2013). Similarly, mutations in the *KCNA5* gene, responsible for encoding the K_V1.5 channel, have been described in PAH patients and are associated with reduced channel expression and function, further reinforcing the emerging concept of PAH as a channelopathy in certain subsets of patients (Remillard et al., 2007; Vera-Zambrano, Lago-Docampo, et al., 2023).

Although genetic alterations provide important insights into susceptibility to PAH, they do not fully account for the clinical heterogeneity observed. This has led to growing interest in epigenetic mechanisms—such as DNA methylation, histone modifications, and microRNAs—which regulate vascular homeostasis and have been implicated in both experimental model and patients with PAH. In parallel, environmental and exogenous factors play a significant etiological role, including appetite-suppressant drugs (e.g., fenfluramine derivatives), chronic hypoxia, viral infections (such as HIV), connective tissue diseases, portal hypertension, and congenital heart defects, all of which are recognized contributors to specific PAH subtypes (Galiè et al., 2016; Orcholski et al., 2018).

3.4. Pathophysiology

The pathophysiology of PAH is complex and is characterized by persistent vasoconstriction and pulmonary vascular remodelling. This remodelling involves the proliferation and hypertrophy of PASMCs, progressive neointimal proliferation of endothelial cells, adventitial fibrosis, in *situ* thrombosis, inflammation, and, in advantage stages, the formation of complex plexiform lesions (Humbert et al., 2019). These structural changes lead to progressive luminal narrowing and obliteration of the vascular bed, thereby increasing pulmonary vascular resistance and pulmonary artery pressure, ultimately resulting in right ventricular hypertrophy. When compensatory mechanisms fail, the condition progresses to right ventricular failure and, eventually, death (Humbert et al., 2019; Simonneau et al., 2019). The pathogenesis of PAH is multifactorial and involves, among others, the interplay of endothelial dysfunction, chronic inflammation and ion channel dysregulation (Figure 3).

Endothelial dysfunction—induced by factors such as genetic mutations, hypoxia, mechanical stress, and chronic inflammation—leads to an imbalance in the production of vasoactive mediators and is recognized as an initiating and perpetuating factor in the PAH. There is an upregulation of vasoconstrictors and pro-thrombotic factors including endothelin-1 (ET-1), serotonin (5-HT), thromboxane A2 (TXA_2) and angiotensin II (Ang II), coupled with a reduction in vasodilatory and antithrombotic mediators like NO and prostacyclin (PGI_2) (Budhiraja et al., 2004; Humbert et al., 2019). Additionally, multiple growth factors such as platelet-derived growth factor (PDGF), fibroblast growth factor 1 (FGF-1) and epidermal growth factor (EGF), along with anti-apoptotic protein like Bcl-2, drive vascular cell proliferation and resistance to apoptosis (Chen et al., 2022; Tajsic & Morrell, 2010).

Inflammation further contributes to disease progression. PAH lungs often exhibit perivascular infiltration of immune cells—including T and B lymphocytes, macrophages, dendritic cells, and mast cells—alongside elevated levels of pro-inflammatory cytokines, such as IL-6, IL-1β, and TNF-α, establishing a pro-remodelling environment (Rabinovitch et al., 2014; Soon et al., 2010).

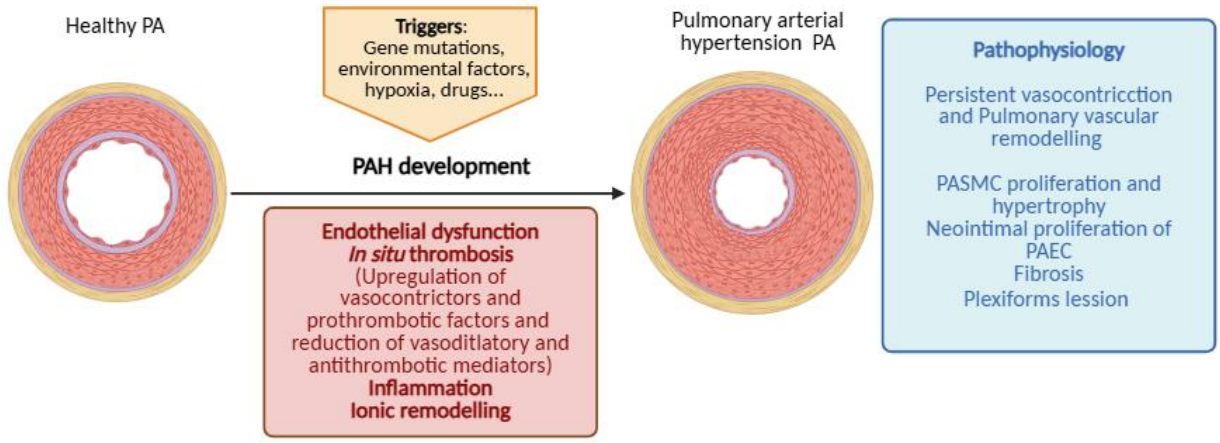

Figure 3. Molecular imbalance and cellular alterations involved in the pathophysiology of PAH. The main alterations in PAH involve endothelial dysfunction and *in situ* thrombosis driven by an increase in vasoconstrictor and prothrombotic factors such as endothelin-1 (ET-1), serotonin (5-HT), thromboxane A2 (TXA_2), angiotensin II (Ang II), along with a reduction in vasodilatory mediators such as nitric oxide (NO) and prostacyclin (PGI_2). In addition, inflammation is promoted by elevated levels of pro-inflammatory cytokines (e.g., IL-6), and ionic remodelling is characterized by a downregulation of $K_V1.5$ and TASK-1 channel. Consequently, the pathophysiology is marked by persistent vasoconstriction and pulmonary

vascular remodelling, which involves PASMCs proliferation and hypertrophy, neointimal proliferation of PAECs, fibrosis and plexiform lesions. Created with BioRender.

Numerous studies have demonstrated that one of the earliest pathogenic mechanisms in PAH is the *ionic remodelling*, which involves alterations in the expression and function of ion channels in PASMCs. In particular, dysfunction of potassium channels—including TASK-1 (*KCNK3*), K_{ATP}, and K_V1.5 (*KCNA5*)—has been identified as a hallmark feature of PAH (Boucherat et al., 2015; Ma et al., 2013; Mondéjar-Parreño et al., 2021; Perez-Vizcaino et al., 2021) (Figure 4). This downregulation or loss of activity of K+ channels leads to membrane depolarization, resulting in increased intracellular calcium concentration ($[Ca^{2+}]_{int}$) via VGCC. This calcium influx promotes key pathological processes such as vasoconstriction, hyperproliferation of PASMCs and apoptosis resistance (Boucherat et al., 2015; Burg et al., 2008; Cogolludo et al., 2007; Lambert, Capuano, et al., 2018; Mondéjar-Parreño et al., 2021; Wang et al., 2005; J. X.-J. Yuan et al., 1998). On the other hand, K_V7 channel activity seems to be preserved in experimental models of pulmonary hypertension (Mondéjar-Parreño et al., 2020; Morecroft et al., 2009).

Figure 4. Ion channel remodelling of PASMCs in PAH. *This* ionic remodelling involves the downregulation of ion channel expression or function, such as K_V1.5 and TASK-1 channels in PASMCs. However, K_V7 channels seem to be preserved. These changes turn the membrane potential more depolarized and, consequently, stimulate contraction and hypertrophy and the transition to a proliferative phenotype of PASMCs. Created with BioRender.

3.5. Pharmacological treatment

Over the past decades, a better understanding of the pathophysiology of PAH has led to the development of effective therapies that target intracellular calcium regulation and endothelial dysfunction through three main pathways: enhancing NO and PGI_2 signalling and inhibiting the effects of ET-1 (Montani et al., 2014).

Nitric oxide-mediated vasodilation occurs when NO, synthesized by endothelial nitric oxide synthases (eNOS), diffuses into the smooth muscle, where it activates soluble guanylyl cyclase (sGC). This fact increases cyclic guanosine monophosphate (cGMP) concentration, leading to a reduction in intracellular calcium and pulmonary artery vasodilation. However, cGMP levels decline due to degradation by phosphodiesterase 5 (PDE5). Therefore, two current therapeutic strategies act at this molecular level and include: stimulation of sGC with drugs such as riociguat, and inhibition of PDE5 with drugs like sildenafil and tadalafil. Other approved therapies for PAH include those related to PGI_2, such as synthetic PGI_2 (epoprostenol), PGI_2 analogs (treprostinil and iloprost), and the PGI_2 receptor agonist (selexipag). Finally, therapies that block the ET-1 signaling pathway have also been approved, including bosentan, macitentan, and ambrisentan. The use of combination therapy with at least two drugs that target different dysregulated pathways is currently highly recommended. However, despite combination treatments, therapy resistance is common, and lung transplantation is often required (Galiè et al., 2019; Lau et al., 2017; Montani et al., 2014; Sitbon et al., 2015).

Despite the availability of these therapies and the implementation of combination strategies targeting multiple pathways, PAH remains a progressive and incurable disease. A significant proportion of patients exhibit incomplete or absent responses to current medications (Dhoble et al., 2022). Furthermore, none of the currently approved therapies directly addresses the ionic remodelling that characterizes PAH. Given the fundamental role of potassium channel dysfunction in the pathogenesis of the disease, modulation of these channels may represent a promising avenue for the therapeutic intervention. This approach is currently under investigation and constitutes the central focus of the experimental research described in the present Doctoral Thesis.

3.6. Targeting K_V channels in PAH

As outlined in previous chapters, K_V channels are essential regulators of pulmonary vascular tone, influencing not only smooth muscle contractility but also key cellular processes such as proliferation, differentiation, and apoptosis. In this context, the pharmacological modulation of K_V channels has emerged as a promising therapeutic strategy in PAH attempting to reverse the ionic remodelling. Interestingly, activators of *KCNK3* (Antigny et al., 2016) and K_{ATP} channels (Zhu et al., 2015) have been shown to attenuate pulmonary hypertension in several experimental models. As previously mentioned, K_V1.5 channels play a predominant role in the total K_V current present in PASMCs, while K_V7 channels are relatively preserved in PAH. Therefore, the present Doctoral Thesis focuses specifically on counteracting ionic remodelling by attempting to pharmacologically activate K_V7 channels, as well as on the restoration of K_V1.5 channel activity, including its upstream regulatory mechanisms, particularly the sigma-1 receptor (S1R).

3.6.1. K_V7 channels: a preserved target in PAH

In contrast to other potassium channels whose expression or function is markedly suppressed in PAH, K_V7 family channels—particularly K_V7.4 and K_V7.5—appear to remain functionally preserved, and their pharmacological activation could prove beneficial in compensating for the dysfunction of other K^+ channels, positioning them as attractive pharmacological targets (Mondéjar-Parreño et al., 2020; Morecroft et al., 2009; Sedivy et al., 2015). Noteworthy, preclinical studies have shown that pharmacological activation of these channels elicits beneficial effects on the pulmonary vasculature. Among the first compounds evaluated were flupirtine and retigabine, classical K_V7 channel openers. Flupirtine has been reported to reduce increased right ventricular pressure and right ventricular hypertrophy in two independent murine models of pulmonary hypertension (Morecroft et al., 2009; Sedivy et al., 2015). Consistent with these findings, recent studies from our lab have reported that retigabine-induced pulmonary vasodilation is enhanced in the hypoxia + SU5416-induced PAH model, and this effect has been attributed to the upregulation of the regulatory subunit KCNE4, which enhances both the functional activity and membrane stability of K_V7.4 channels (Mondéjar-Parreño et al., 2020). In addition to

their direct vasodilatory effects, K_V7 channel activation has been shown to modulate part of the vascular responses to currently approved PAH therapies targeting the NO–cGMP pathway, such as sildenafil and riociguat (Mondéjar-Parreño et al., 2019). This supports the hypothesis that K_V7 modulation could be integrated into multimodal therapeutic strategies aimed at improving efficacy and overcoming treatment resistance in non-responders.

However, the effectiveness of classical K_V7 channel activators in the pulmonary circulation appears limited (Mondéjar-Parreño et al., 2020). Therefore, recent efforts have focused on the development of next-generation K_V7 activators. In this context, the newly synthesized compound URO-K10 has emerged as a potent K_V7 channel activator, with EC_{50} values in the submicromolar range, and the ability to activate $K_V7.4$ and $K_V7.5$ channels independently of KCNE4 expression (Lee et al., 2020; Seefeld et al., 2018).

Taken together, these findings support the therapeutic potential of K_V7 channel activators as innovative pharmacological tools to restore pulmonary vascular function. Their preserved activity in disease conditions, responsiveness to selective openers, and interaction with endogenous vasodilatory pathways place K_V7 channels at the forefront of therapeutic research in PAH.

3.6.2. $K_V1.5$ in PAH: modulation by the sigma-1 receptor

Therapeutic efforts aimed at restoring $K_V1.5$ function have shown promising results. Strategies such as gene therapy using *KCNA5*-encoding plasmids (Pozeg et al., 2003) were shown to attenuate PH induced by chronic hypoxia exposure. In addition, targeting specific microRNAs (e.g., miR-1, miR-29a) have also shown useful to enhance $K_V1.5$ channel activity in PAH (Babicheva et al., 2020; Mondejar-Parreño et al., 2019). However, we still lack suitable and feasible pharmacological strategies aimed at increasing/recovering $K_V1.5$ channel function.

In this context, the sigma-1 receptor (S1R) has emerged as a possible novel modulator of $K_V1.5$. The sigma-1 receptor is a 25 kDa ligand-regulated chaperone protein is primarily localized at mitochondria-associated endoplasmic reticulum membranes (MAMs) (Almaamari et al., 2025; Hayashi & Su, 2007; Weng et al., 2017). It exhibits a

trimeric structure, with each protomer containing a single transmembrane helix, the N-terminal domain facing the endoplasmic reticulum (ER) lumen, and the C-terminal domain associated with the cytosolic surface of the MAM (Schmidt et al., 2016; Schmidt & Kruse, 2019). Under basal conditions, S1R forms a complex with the immunoglobulin-binding protein BiP (Schmidt & Kruse, 2019). Upon ligand binding, this complex dissociates, and S1R translocates to other subcellular compartments—such as the ER membrane, mitochondrial membrane, plasma membrane, or nuclear envelope—where it regulates the activity of various associated proteins, including ion channels, receptors, and kinases. Multiple studies have demonstrated that S1R physically interacts with and modulates the activity of inositol 1,4,5-trisphosphate receptors, as well as ion channels such as voltage-gated potassium channels like K_V1.2, K_V1.3, K_V1.4, and interestingly K_V1.5; voltage-gated calcium channels (e.g., Ca_v2.2), and sodium channels like Na_v1.5. Additionally, S1R has been shown to interact with a wide range of G protein-coupled receptors and other intracellular signalling proteins (Aydar et al., 2002; Hayashi & Su, 2001; Kinoshita et al., 2012; Kourrich et al., 2013; Schmidt & Kruse, 2019; Tchedre et al., 2008; Vera-Zambrano, Baena-Nuevo, et al., 2023; K. Zhang et al., 2017).

Activation of S1R—whether by endogenous ligands or pharmacological agonists—has been shown to exert diverse functional roles in both physiological and pathological processes. While initially studied in neurological disorders, including neurodegeneration, stroke, and substance addiction (Malar et al., 2023), S1R has more recently gained attention in the cardiovascular field. In experimental models of myocardial infarction, S1R have been shown to improve cardiac function (Gao et al., 2018; Ito et al., 2013), as well as by attenuating cardiac hypertrophy in experimental models of cardiac pressure overload (Bhuiyan et al., 2010; Bhuiyan & Fukunaga, 2009; Tagashira et al., 2010). Additionally, S1R activation has been shown to attenuate myocardial injury caused by sepsis by reducing apoptosis and mitochondrial oxidative damage (Li et al., 2024). More recently, some studies have demonstrated that administration of a S1R agonist, PRE084, protects against methamphetamine-induced hypertension, vascular remodelling, and fibrosis, whereas blockade of S1R with BD1047 worsens these pathological changes (Xu et al., 2024). Concordantly, S1R

knockout mice exhibit contractile dysfunction, increased fibrosis, exacerbated vascular remodelling, and elevated blood pressure following methamphetamine exposure (Abdullah et al., 2018). The cardioprotective functions of S1R have been linked to its ability to modulate several key cellular pathways, including apoptosis, endothelial integrity, fibrotic signalling, hypertrophic growth, angiogenesis, inflammation and mitochondrial dynamics (Munguia-Galaviz et al., 2023).

Additionally, it has been reported that clinically approved drugs such as the antitussive dimemorfan (Y. Shen et al., 2008), the antidepressants fluoxetine and fluvoxamine (Hashimoto, 2015; Ishima et al., 2014), and the anti-dementia agent donepezil (Hashimoto, 2013), share S1R agonistic properties, and interestingly, have shown beneficial effects in experimental models of PAH (Qiu et al., 2021; Sun et al., 2022; Zhai et al., 2009). However, these effects have not been related to a possible activation of $K_V1.5$ channels. In this context, recent studies from our group have shown that S1R not only interacts directly with $K_V1.5$ channels, but also its activation by the selective agonist PRE084 enhances $K_V1.5$ activity in PASMCs, leading to reduced pulmonary vasoconstriction and cell proliferation (Vera-Zambrano, Baena-Nuevo, et al., 2023). However, whether this interaction is sufficient to restore $K_V1.5$ functionality in the specific context of PAH remains to be determined.

Taken together, these findings support the therapeutic potential of restoring $K_V1.5$ activity, either through direct modulation or via S1R regulation. Since PAH pathogenesis involves not only endothelial dysfunction and inflammation, but also profound ionic remodelling, targeting potassium channels such as $K_V1.5$ and K_V7 could represent an effective strategy to reverse the aberrant vascular phenotype. Understanding the molecular basis of these alterations is therefore critical for designing new pharmacological interventions. Based on this rationale, the present investigation was designed, and its hypothesis and objectives are outlined in the following section.

HYPOTHESIS AND OBJECTIVES

General hypothesis: Members of the K_V channel family play essential roles in the physiological regulation of pulmonary vascular tone and remodelling. Their functional dysregulation contributes to the pathogenesis of PAH by promoting vasoconstriction, smooth muscle proliferation and resistance to apoptosis. Therefore, targeted modulation of specific K_V channels may offer attractive therapeutic approaches for the treatment of PAH.

To demonstrate this initial hypothesis, the following **specifics objectives** are proposed:

1. To evaluate the pulmonary vasodilator and antiproliferative effects of the novel K_V7 channel activator URO-K10.
2. To analyse the potential of the S1R agonist PRE084 to rescue attenuated $K_V1.5$ activity and improve impaired pulmonary and cardiovascular function and remodelling in an *in vivo* experimental PAH model.
3. To analyse the potential of approved drugs with S1R agonistic properties, fluoxetine and dimemorfan, to improve the attenuated $K_V1.5$ channel activity in PAH.

MATERIALS AND METHODS

I. Ethics statement

The animals were cared for according to the Directive 2010/63/EU of the European Parliament on the protection of animals used for scientific purposes. All experimental procedures involving animals were approved by the Institutional Ethical Committee of the Universidad Complutense de Madrid (Spain), the regional Committee for Laboratory Animals Welfare (Comunidad de Madrid, Ref. number PROEX-301/16 and PROEX-171.4/24) and the Institutional Animal Care and Use Committee of Seoul National University (approval number: SNU-190408–3).

II. Human samples

Lung samples, which were discarded by pathologist after thoracic surgery, were obtained from the Hospital Universitario de Getafe (Madrid, Spain) and used with the approval of the hospital's Human Research Ethics Committee (Ref. A04/16) following informed consent. Human PA and pulmonary artery smooth muscle cells (PASMCs) were isolated from these lung samples obtained from 16 non-PAH patients (6 men, 8 women, mean age 70.0 ± 2 years) undergoing lobectomy during resection of lung carcinoma.

III. Animal models

Control male Wistar and Sprague-Dawley rats (age: 6–8-week-old; weight 200 ± 50 gr) were obtained from Envigo (Barcelona, Spain) and Koateg (South Korea), respectively. Animals were kept in an enriched environment under standard conditions of temperature at 24 ºC and 12:12 h light/dark cycle with free access to food and water, at the Institutions animal care facilities. The animal experiments were designed to have equal group sizes using randomized and blinded analyses. In some cases, however, group sizes were unequal due to unexpected loss of animals or samples during procedures.

To develop the monocrotaline-induced PH model (MCT-PH), monocrotaline (Sigma, USA) was dissolved in 2 mL of 1 mol L^{-1} HCl, the pH was adjusted to 7.4 using NaOH and the resulting solution was diluted to distilled water to a final volume of 17 mL. Sprague-Dawley rats were randomly assigned into MCT-PH and control groups and

treated with a single intraperitoneal injection of monocrotaline (60 mg kg^{-1}) or saline, respectively. After 21 days, all the animals were weighed and sacrificed.

Regarding the PH model involving the combined exposure to SU5416 plus hypoxia (Hpx/Su), male Wistar rats weighing approximately 180 g were subcutaneously injected with a single dose of the vascular endothelial growth factor (VEGF) receptor 2 inhibitor SU5416 (20 mg kg^{-1}) or vehicle. Following the injection, SU5416-treated animals were placed in glass chambers and exposed to a hypoxic environment (10% O_2) for three weeks. Control rats (normoxic group) were housed in the same room under standard ambient oxygen levels. Oxygen concentrations within the hypoxia chambers were continuously monitored using an oxygen sensor (DrDAQ Oxygen Sensor; Pico Technology, UK). To maintain proper environmental conditions, carbon dioxide and water vapor produced by the animals were absorbed using soda lime and silica gel, respectively. Chambers were briefly opened every two days to perform routine animal care. Following the 3-week hypoxia exposure, animals were returned to normoxic conditions for one week. Subsequently, osmotic mini-pumps (RWD Life Science, USA) were implanted; some were filled with PRE084 and supplied at a concentration of 7.5 mg kg^{-1} per day, while others contained vehicle solution (DMSO and distilled water). The animals were maintained for an additional three weeks before being sacrificed.

IV. Echocardiographic measurements

Animals were lightly anesthetized (inhalation of 5% isoflurane in oxygen for induction, and 1.5%–2% for maintenance), and the skin was shaved. Animals were positioned in a left lateral decubitus position and kept in normothermia during the experiments with a heating pad with thermic control through a rectal probe. Transthoracic echocardiography was performed using the VIVID q system (GE Healthcare, Germany) equipped with a 13-MHz probe (12S-RS, GE) (Adão et al., 2025). Images and clips were recorded and analysed off-line. At least three stable cardiac cycles were averaged for subsequent assessment of pulmonary artery, right ventricle (RV), left ventricle (LV), and right atria (RA) structure and function, including, but not limited to, pulmonary artery acceleration time normalized for ejection time (PAAT/PAET) for pulmonary hypertension determination, RV area (RVA), and RA area (RAA), tricuspid

annular plane systolic excursion (TAPSE) and tissue (s') Doppler for RV structure and function, LV internal diameter (LVID), LV wall thickness (LVWT), and LV ejection fraction (LVEF) for the LV.

V. Hemodynamic measurements

After echocardiographic evaluation, the rats were anaesthetized, checked according to the toe-pinch reflex, and intubated via a 14-gauge catheter and ventilated (VentElite, Harvard Apparatus, UK) with 100% O_2, with tidal volume and respiratory rate adjusted to animal weight. Then, animals were placed on their right side and a left thoracotomy was performed (Adão et al., 2018), so that a first catheter with a high-fidelity pressure sensor (SPR-869, Millar Instruments, USA) could be introduced into the RV through the apex; and a second catheter (SPR-847, Millar Instruments, USA) through the LV apex which was then advanced into the ascending aorta. Pressure signals were continuously acquired using MPVS Ultra (Millar Instruments, USA), digitally recorded with a PowerLab 16/30 system (ADinstruments, ANZ), and subsequently analysed off-line using LabChart 8 Pro software (ADinstruments, ANZ). After hemodynamic measurements, rats were euthanized by anaesthetic overdose and subsequent exsanguination. Afterwards, the heart and lungs collected in bloc for subsequent histological, functional and molecular analysis.

VI. Assessment of right ventricle hypertrophy

At the end of the recordings, whole hearts were excised and weighed and, consecutively, RV and LV plus septum (LV + S) were carefully dissected, separated, and measured individually. Fulton index [RV/(LV+S)] was calculated to assess RV hypertrophy.

VII. Tissue collection and cell isolation

Rat lung and mesenteric vascular beds and human lung samples were dissected in Krebs solution which contained the following (in mmol L^{-1}): 119 NaCl, 4.7 KCl, 1.2 KH_2PO_4, 1.2 $MgSO_4$, 2 $CaCl_2$, 11 sodium bicarbonate and 11 glucose; pH 7.4 and it was filtered through a filter of 0.2 µm pore. Freshly isolated rat and human PASMCs were obtained by enzymatic digestion, as described previously (Cogolludo et al.,

2008). Briefly, PA were dissected in Ca^{2+}-free physiological salt solution (Ca^{2+}-free PSS) composed of (in mmol L^{-1}): 130 NaCl, 5 KCl, 1.2 $MgCl_2$, 10 glucose, and 10 HEPES (adjusting to pH 7.3 with NaOH). For isolation of PASMCs, PA were cut longitudinally and incubated in Ca^{2+}-free PSS containing (in mg mL^{-1}): 1.5 papain (Worthington, USA), 0.8 dithiothreitol (#D0632, Sigma-Aldrich) and 0.7 albumin (#A0281, Sigma-Aldrich) for 10-15 min. By vigorous agitation with a smooth, wide-tipped pipette, the tissue was dissociated and PASMCs were isolated and stored at 4 °C.

VIII. Rat and human pulmonary arteries culture

Rat and human PA were incubated during 24 h in the absence (Ctrl) or in the presence of PRE084 (20 µmol L^{-1}), dimemorfan (5 µmol L^{-1}), fluoxetine (0.3 µmol L^{-1}) or the S1R antagonist BD1047 (10 µmol L^{-1}) in DMEM supplemented with 1 % non-essential amino acids and 1 % antibiotics. Samples were placed in an incubator maintaining a temperature of 37 ºC, 99 % humidity and 5 % CO_2.

IX. Molecular interference with morpholino

The morpholino oligonucleotides used to knock down KCNE4 in isolated PA work through a steric blocking mechanism that specially interference with the mRNA, thereby preventing the transcription of the target gene. So, to inhibit the KCNE4 expression, morpholinos were designed to bind the 5' untranslated regions and the first 25 bases of coding sequence as previously reported (T. A. Jepps et al., 2015) (Figure 5). Control morpholino has five bases altered from the targeted sequence, which offers increased assurance that the effects observed are not the result of off-target modulation (Summerton, 1999, 2007). Control oligonucleotides or morpholinos (Gene Tools Inc., Philomath, USA) were mixed with Opti-MEM supplemented with 1% antibiotic and allowed to stand for 15 min at room temperature (RT). Subsequently, these mixtures were incubated with Lipofectamine RNAiMAX (Life Technologies Corp) for another 15 min at RT before being applied to the PA for 40 h incubation at 37 °C. This incubation period was chosen to provide sufficient time to repress target gene expression without severely affecting AP functionality (Mondejar-Parreño et al., 2019; Vera-Zambrano, Baena-Nuevo, et al.,

2023) as incubations longer than 48 h can markedly alter pulmonary vascular reactivity and sensitivity to potassium channel modulators (Manoury et al., 2009).

Figure 5. Schematic illustration of how morpholino acts to silence KCNE4. Morpholinos were designed to bind to the 5' untranslated regions and the first 25 bases of the coding sequence to prevent ribosome binding and transcription. Created with BioRender.

X. Experimental procedures for vascular reactivity studies

Rat PA and MA and human PA were cut into rings of 1.8-2 mm in length and mounted in a wire myograph (model 610 M, Danish Myo Technology, Aarhus, Denmark) with Krebs solution at 37 ºC and continuously bubbled with aerobic gas (CO_2: 5%, N_2: 74%, O_2: 21%) for the PA and carbogen gas (O_2: 95%, CO_2: 5%) (Air Products - Carbides) for the MA. Arteries were stretched to give an equivalent transmural pressure of 30mmHg for PA or 100mmHg for MA, as previous studies described (Cogolludo et al., 2008; Ozaki et al., 1998). The wire myograph was connected to the digital system PowerLab (ADInstruments, ANZ), to record vessel tension (Figure 6). Arteries were initially stimulated by increasing the K^+ concentration in the buffer to 80 mmol L^{-1}, replacing Na^+, then washed three times and allowed to recover before subsequent stimulation.

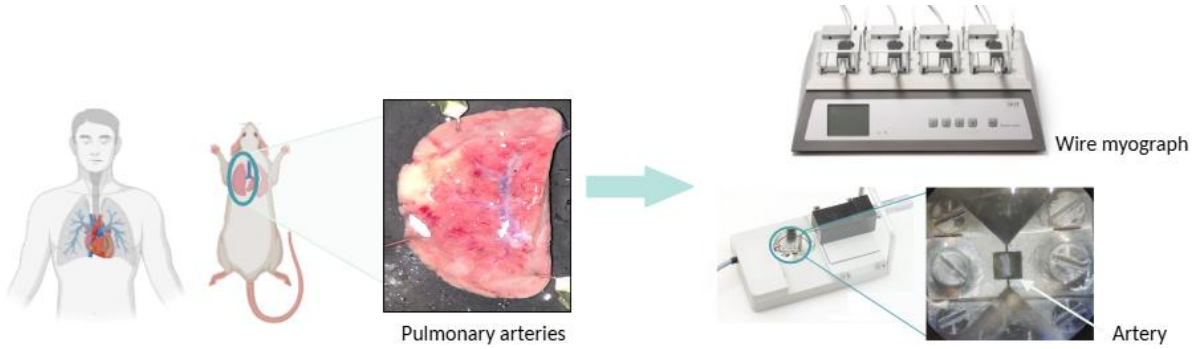

Figure 6. Vascular reactivity. Left panel shows a tree from a rat or human lung section. Right panel shows some the wire myograph and the chamber with the jaws and a mounted PA ring. Created with BioRender.

The effects of URO-K10 (0.0001–3 μmol L^{-1}), retigabine (0.01–30 μmol L^{-1}) and flupirtine (0.01–30 μmol L^{-1}) were assessed in arteries precontracted with the thromboxane A_2 analogue U46619 (PA at 0.1 μmol L^{-1} and MA at 0.3 μmol L^{-1}) or serotonin (10 μmol L^{-1}). The effects of these drugs were also evaluated in PA in which KCNE4 was silenced with morpholino. In some experiments, the effects of URO-K10 were tested in arteries pre-incubated for 15 min with the K_V7 channel inhibitor XE991 (3 or 10 μmol L^{-1}) or with the combination of the K_V1.5 channel inhibitor diphenylphosphine oxide-1 (DPO-1, 1 μmol L^{-1}) and the TASK-1 channel inhibitor ML365 (1 μmol L^{-1}).

To study the effects of S1R agonists - PRE084, fluoxetine and dimemorfan - on vascular reactivity, the contractile response induced by serotonin (5-HT, 30 nmol L^{-1}- 30 μmol L^{-1}) and phenylephrine (Phe, 1 nmol L^{-1} - 10 μmol L^{-1}) was examined in PA. The contraction to Phe was also tested after 15 min incubation with DPO-1 (1 μmol L^{-1}). Afterwards, dose-response relaxation curves were performed for acetylcholine (1 nmol L^{-1}- 100 μmol L^{-1}) and riociguat (1 nmol L^{-1}- 10 μmol L^{-1}).

The individual cumulative concentration-response curves of the different drugs were fitted to a logistic equation in which vasodilator responses are expressed as the percentage reversal of the previous constriction with either U46619 or serotonin in each artery and vasoconstrictor response as a percentage of KCl. In addition, the maximal relaxant response (Emax) was expressed as percentage inhibition of vasoconstrictor-induced contraction and the agonist potency was reported as pD2= -log EC50. When the maximal relaxant response could not be reached, the drug concentration producing 30% relaxation was estimated from the fitted curve and expressed as (-log IC30 or pIC30).

XI. Electrophysiological studies

The electrophysiological experiments used in this Doctoral Thesis were performed using the whole-cell configuration of the patch-clamp technique with a patch clamp amplifier (Axopatch 200B, Molecular Devices, USA) and a Digidata 1322 A (Axon Instruments, USA) as previously described (Cogolludo, Moreno, et al., 2006;

Mondéjar-Parreño et al., 2019; Vera-Zambrano, Baena-Nuevo, et al., 2023). pClamp 10 software (Molecular Devices) was used for both data acquisition and analysis. Micropipettes were created from borosilicate glass capillaries (GD-1, Narishige, UK) with a programmable horizontal pipette puller and polisher (Zeitz DMZ Puller, AutoMate Scientific). For the whole cell recording, freshly isolated PASMCs were superfused with an external Ca^{2+}-free PSS (see above). Pipettes were filled with a solution of the following composition (in mmol L^{-1}): 130 KCl, 10 HEPES, 1.2 $MgCl_2$, 5 Na_2ATP, 10 EGTA with 100 nmol L^{-1} free Ca^{2+}, and pH 7.2. The average pipette resistance ranged from 4-7 MΩ and Gigaohm seal formation was achieved by suction and subsequently membrane patch was ruptured with a brief additional suction (Figure 7).

Throughout the Doctoral Thesis, K_V currents were evoked after application of 200 ms depolarizing pulses from + 60 mV to - 80 mV in decreasing steps of 10 mV (I-V protocol) or by ramped depolarizing pulses of -100 to + 40 mV for 3 s, starting from an initial potential of - 80 mV. To analyse the electrophysiological effects of the new K_V7 channel agonist, URO-K10, (0.3 or 1 µmol L^{-1}) were tested until the steady state was reached (usually between 7 and 10 min). In some experiments we checked the effect of URO-K10 in PASMCs after 10 min exposure to DPO-1 (1 µmol L^{-1}) plus ML365 (1 µmol L^{-1}). These two protocols were also performed after incubation with XE991 (10 µmol L^{-1}) for approximately 20 min. On the other hand, to analyse the electrophysiological effects of S1R agonists, K_V currents were measured with the I-V protocol before and after incubating cells for 5-10 min with the $K_V1.5$ channel inhibitor DPO-1 (1 µmol L^{-1}). Currents were normalized for cell capacitance (pA pF^{-1}) and membrane potential was recorded in current-clamp mode. Only cells with leak current less than 50 pA and series resistance between 5–30 MΩ were analysed, so these parameters were monitored throughout the experiment.

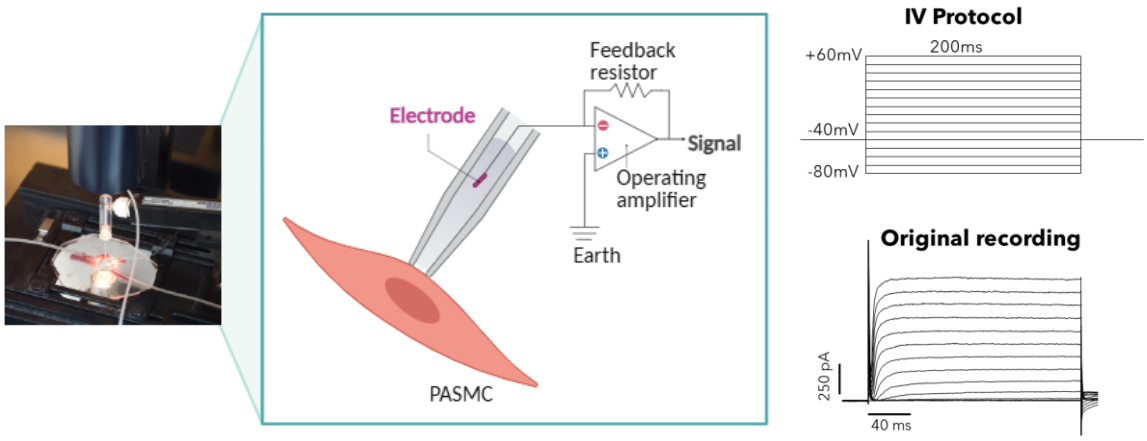

Figure 7. Whole cell patch clamp configuration. The whole cell patch-clamp configuration is achieved by bringing the pipette into close proximity with the cell membrane and applying a gentle suction to form a high-resistance seal. Next, by applying another brief but stronger suction, the cell membrane is ruptured allowing the pipette access to the cytoplasm. The right side of the figure displays a schematic illustration of the current-voltage (I-V) protocol, along with an original recording of this protocol obtained in a PASMC. Created with BioRender.

XII. Human PASMC proliferation

Human pulmonary artery smooth muscle cell proliferation was measured using a colorimetric immunoassay based on the incorporation of the thymidine analog, 5-bromo-2-deoxyuridine (BrdU), during DNA synthesis (Figure 8). Human PASMCs were grown in a flask with supplemented smooth muscle cell growth medium (C22062; PromoCell, Heidelberg, Germany) and kept in an incubator at 37 °C, 99% humidity and 5% CO_2, until sufficient number were obtained. Human PASMCs previously seeded in 96-well plate (5.000 cells/well) were first growth-arrested by incubation in medium containing 0.1% FBS for 24 h and following were stimulated to proliferate by exposure to smooth muscle cell growth medium supplemented with 5% FBS for an additional 24 h. To characterize the possible antiproliferative effect of URO-K10, human PASMCs were treated with different concentrations: 0.01, 0.1 and 1 µmol L^{-1} in 5% FBS medium. In another set of experiments and to elucidate the mechanism of action of the drug URO-K10, we tested the effects of URO-K10 in the presence of the K_V7 channel inhibitor XE991 (10 µmol L^{-1}) in medium containing 5% FBS. During the last 6 h of the 24 h treatment, BrdU was added to the cells at a final concentration of 10 µmol L^{-1}. After removing the medium, cells were fixed with Fix Denat for 30 min, the

membrane was permeabilized and the DNA was denatured to enhance accessibility of the Anti-BrdU-POD antibody (mouse monoclonal, clone BMG 6H8, Fab fragment, conjugated with peroxidase). After 90 min incubation, each well was washed three times with washing solution (1× PBS) prior to adding 100 µl/well of substrate solution (tetramethylbenzidine, TMB) for no more than 30 min at room temperature in darkness. Finally, to stop the reaction we added 25 µl of 1 mol L^{-1} H_2SO_4 in each well and the absorbance was measured using a spectrophotometric plate reader (EZ Read 400 Microplate Reader, Biochrom) at dual wavelength 450 – 690 nm (Morales-Cano et al., 2014). The absorbance values, which reflect the amount of BrdU incorporated, served as an indirect measure of cell proliferation. All proliferation assays were performed in triplicate for each sample and results were expressed as the percentage of proliferation induced by FBS 5%.

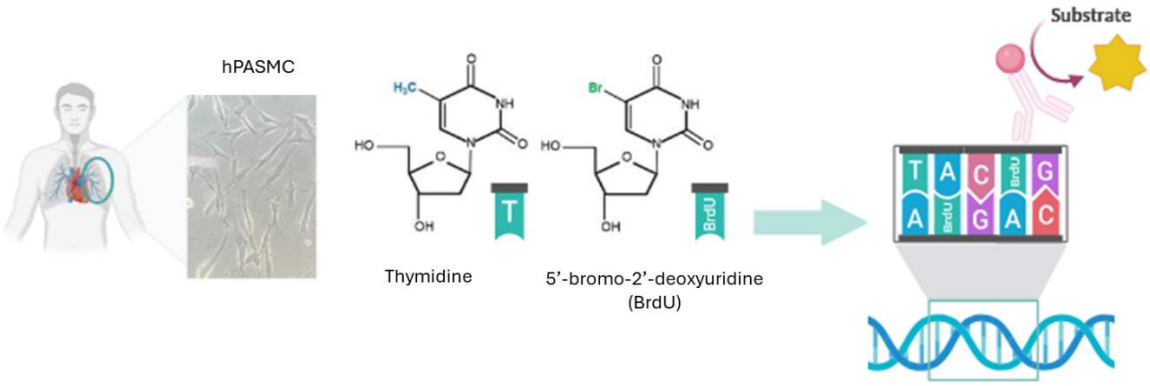

Figure 8. Human PASMC proliferation was measured using the 5-bromo-2-deoxyuridine (BrdU) assay. BrdU incorporation into DNA, replacing thymidine, was detected in PASMCs using a colorimetric immunoassay, and absorbance was used as an indirect measure of cell proliferation. Created with BioRender.

XIII. Western blot assay

PA were dissected from rat lungs and frozen in liquid nitrogen and preserved at - 80 °C. Samples were homogenized in RIPA buffer (Thermo Scientific, USA) with protease and phosphatase inhibitors (Roche, Switzerland). After 30 min incubation on ice and two short homogenization pulses in the homogenizer, the lysates were centrifuged for 10 min at 10,000 rpm at 4 °C as previously described (Climent et al., 2020). Protein concentration was determined using a colorimetric assay based on the Lowry

method, with the DC Protein Assay Kit (Bio-Rad, USA). Equal amounts of proteins (20-25 µg for PA and 50 µg for RV) were run on sodium dodecyl sulphatepolyacrylamide electrophoresis (SDS-PAGE) followed by a transference to a polyvinylidence difluoride (PVDF) membrane (Bio-Rad, USA). Membranes were blocked by incubating for one hour in 5% non-fat milk TBST (0.5 mol L^{-1} Tris pH 7.5; 1.5 mol L^{-1} NaCl; 0.1% Tween© 20) or 5% BSA TBST and then incubated overnight at 4 °C with the primary antibodies listed in Table 2. Membranes were subsequently incubated with the appropriate secondary goat anti-mouse and anti-rabbit antibodies conjugated with horseradish peroxidase at room temperature for one hour (Santa Cruz Biotech, USA, 1:10.000 dilution). Antibody binding was detected by an ECL system (Amersham PharmaciaBiotech, Amersham, UK). Blots were imaged using an Odissey Fc System (Li-COR Biosciences, USA) and quantified using Image J Lite 4.0 software. Relative protein expression levels were quantified by normalizing the intensity of each band to that of vinculin for PA or to total protein bands for RV, which were used as loading controls. In RV western blot, total protein bands were reversibly stained with Fast Green FCF and imaged using the Amersham ImageQuant 800 system (GE Healthcare Life Sciences) for quantification purposes.

Antibody	Type and Host	Dilution	Reference
Anti-K_V7.5	Polyclonal rabbit	1:200	#APC-155 Alomone
Anti-K_V7.4	Polyclonal rabbit	1:200	#Sc-50417 Santa Cruz Bio
Anti-KCNE4	Polyclonal rabbit	1:200	#HPA011420 Atlas Antibodies
Anti- K_V1.5	Polyclonal rabbit	1:360	#APC-004 Alomone
Anti-S1R	Monoclonal mouse	1:500	#sc-137075 Santa Cruz Bio
Anti-p-eNOS (S^{1177})	Monoclonal mouse	1:1000	#612392 BD Laboratories
Anti-eNOS	Monoclonal mouse	1:1000	#610296 BD Laboratories
Anti-p-Akt (Ser^{473})	Polyclonal rabbit	1:1000	#9271 Cell Signaling
Anti-Akt	Polyclonal rabbit	1:1000	#9272 Cell Signaling
Anti-Bcl-2	Monoclonal mouse	1:500	#sc23960 Santa Cruz Bio
Anti-vinculin	Monoclonal mouse	1:500	#Sc-25336 Santa Cruz Bio

Table 2. Primary antibodies for Western Blot

XIV. Immunocytochemistry

Enzymatically isolated PASMCs from PA were fixed in polylysine coated glass coverslips with 4% paraformaldehyde/PBS for 30 min at room temperature. Cells were incubated for 20 min with the membrane marker wheat germ agglutinin (WGA) (dilution 1:200; W11261; Life technologies) and blocked with PBS containing 5% FBS for 1 h as described previously (Morales-Cano et al., 2016). The coverslips were subsequently incubated with the primary rabbit anti-K_V1.5 (dilution 1:100; APC-004; Alomone Labs) antibody overnight and exposed afterwards to secondary antibody goat anti-rabbit Alexa Fluor 568 (dilution 1:500; A11036; Invitrogen) for 1 h. The samples were incubated with 4',6-diamidino-2-phenylindole (DAPI) for 10 min to stain the nuclei. Image analysis was performed using a Confocal laser scanning fluorescence microscope (Figure 9).

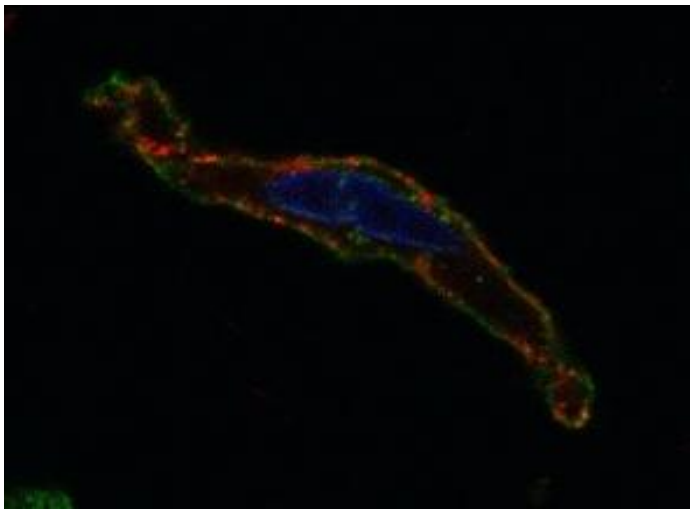

Figure 9. Representative immunofluorescence image of a rat PASMC stained with the membrane marker wheat germ agglutinin (WGA) (green), a primary rabbit anti-K_V1.5 antibody (red) and DAPI (blue).

XV. Histological analysis of lung and cardiac tissues

For lung histology, the right lung was perfused at a constant pressure (20–25 cmH_2O) with 4% paraformaldehyde via the right bronchus and subsequently embedded in paraffin. All sections were cut at 5 µm thickness, stained with hematoxylin-eosin

technique, and examined by light microscopy. Elastin was visualized by its green autofluorescence. For quantification of pulmonary vascular remodelling, PA with an external diameter between 25 and 250 µm were blindly analysed. They were categorized as muscular, partially muscular or non-muscular, based on previously described morphological criteria (Morales-Cano et al., 2014). Muscular PA were defined by the presence of both internal and external elastic laminae and more than one layer of smooth muscle cells. Partially muscular PA exhibited some features of muscularization but not throughout the entire vessel. Non-muscular PA do not present external elastin lamina and contained only one or few layers of smooth muscle cells. Only vessels with a well-preserved circular morphology were included, excluding those with tangential cuts, collapsed lumens, or poor fixation. Between 15 and 20 small vessels from at least three different lung sections were randomly selected per animal. Medial wall thickness was calculated as the difference between the diameters of the external and internal elastic laminae and quantified as the average of four measurements per vessel. Cross-sectional area (CSA) and lumen area were also measured, and results were expressed as (lumen area / cross-sectional area) x 100%. To assess the degree of vascular occlusion, the following index was applied: (total vessel area – lumen area) / total vessel area x 100. All images were analysed using ImageJ software (v1.8.0), employing the 'Raised Hand Drawing Tool'.

On the other hand, RV samples were also fixed, embedded in paraffin, and stained with hematoxin and eosin, and cardiomyocyte CSA was used as an indicator of cardiac hypertrophy. In adition, to assess cardiac fibrosis, sirius red quantifications were performed in QuPath (v.0.4.4) (Bankhead et al., 2017) using the Train Pixel Classifier tool, which generates Artificial Neural Networks classifiers capable of identifying positively stained regions.

XVI. Metabolomic analysis in RV samples

RV samples were examined in ICTS Bioimagen Complutense using magic-angle spin nuclear magnetic resonance high-resolution spectroscopy (HR-MAS) at 4 °C to minimize tissue degradation. ^{1}H-NMR spectroscopy was performed at ICTS Complutense Bioimaging at 500.13 MHz using an 11.7 T Bruker AVIII500 HD spectrometer. Samples were placed on a 50 µl zirconium oxide rotor and rotated at

5000 Hz to eliminate spinning sideband effects. Magnetic field homogenization and experiment adjustment were minimized, with samples kept at 4 °C to prevent metabolic changes. Spectra with standard solvent suppression (32,000 points, 256 acquisitions, 20-min total acquisition) used a NOESY pulse sequence with radiofrequency irradiation at water's resonant frequency for 2 seconds during mixing period (tm = 150 ms), T1 at 3 µs, and spectral width of 6009.62 Hz. A Carr-Purcell-Meibom-Gill pulse sequence with T2 filter suppressed macromolecule signals, using rotor-synchronized conditions with 1/rotational speed delay (200 µs) and 100 ms total spin echo time. Parameters included 128 repeats, 6009 Hz spectral width, and 32,000 data points. Spectra were processed using TOPSPIN software (v3.5), with FIDs multiplied by exponential weight function (0.3 Hz line widening), phase- and baseline-corrected, and referenced to sodium singlet at δ 0 ppm.

Several ^{1}H, ^{1}H-2D experiments were performed for component assignments. The COSY90 was acquired with water pre-turation during relaxation, spectral width of 6009 Hz in both dimensions, 2K data points in f2 and 384 increments in f1. A sinusoidal window function was applied in both dimensions with f1 zero fill. The ^{1}H, ^{1}H TOCSY experiment was recorded with water presaturation during 1.5 seconds relaxation, 6009 Hz spectral width, 70 ms mixing time, 2K data points in f2, and 384 f1 increments. Zero padding in f1 and square sinusoidal window function were applied before Fourier transform. HSQC experiments were recorded with 70 µs ^{13}C GARP decoupling, spectral widths of 6009 Hz and 22 kHz in ^{1}H and ^{13}C dimensions, 2k f2 data points and 256 f1 increments, with zero padding and square sinusoidal window function applied before Fourier transform.

XVII. Drugs

Drugs and reagents were obtained from Sigma-Aldrich (Madrid, Spain), except URO-K10 that was provided by Sundia MediTech Company (Sanghai, China) based on reaction scheme suggested (Seefeld et al., 2018); PRE084 from Cayman (Michigan, USA), and BD1047 from Tocris Bioscience (Bristol, UK); and dimemorfan and SU5416 from MedChemExpress Europe (Sollentuna, Sweden). Drugs were dissolved in DMSO or water depending on the solubility of each compound, but the final volume of DMSO

never exceeded 0.01% in organ baths and did not affect smooth muscle tone in control experiments.

XVIII. Data presentation and statistical analysis

Data are expressed as mean ± standard error of the mean (SEM) of *n* measurements where *n* identifies the number of animals or patients, unless otherwise stated. The differences between means were analysed using a paired or unpaired Student's t-test, two-way ANOVA, one-way ANOVA with a Bonferroni as post-hoc analysis, analyses of area under the curve (AUC), as appropriate. The level of significance was set at $P < 0.05$. All calculations were made using a standard software package (Prism 8.0.2, GraphPad, CA, USA)

RESULTS

CHAPTER 1: Pulmonary vascular effects of a novel K_V7 channel activator URO-K10 in the context of PAH.

1.1) URO-K10 exhibits significantly greater pulmonary vasodilation compared to classical K_V7 activators and increase the K_V current in PASMCs

First, we assessed the pulmonary vasodilator effects of URO-K10 compared to established K_V7 activators, retigabine and flupirtine, using a wire myograph (Figure 10). For this purpose, PA were initially precontracted using U46619, a TXA_2 analogue to establish a stable baseline contraction. In subsequent dose-response experiments, URO-K10 induced a significant vasodilator effect, with an Emax of 58 ± 5% and a pD2 values of 7.29 ± 0.08, unlike retigabine, which showed a minimal relaxation (Figure 10A-B). Conversely, flupirtine did not produce vasodilation beyond what was seen with the vehicle (Figure 10C-D).

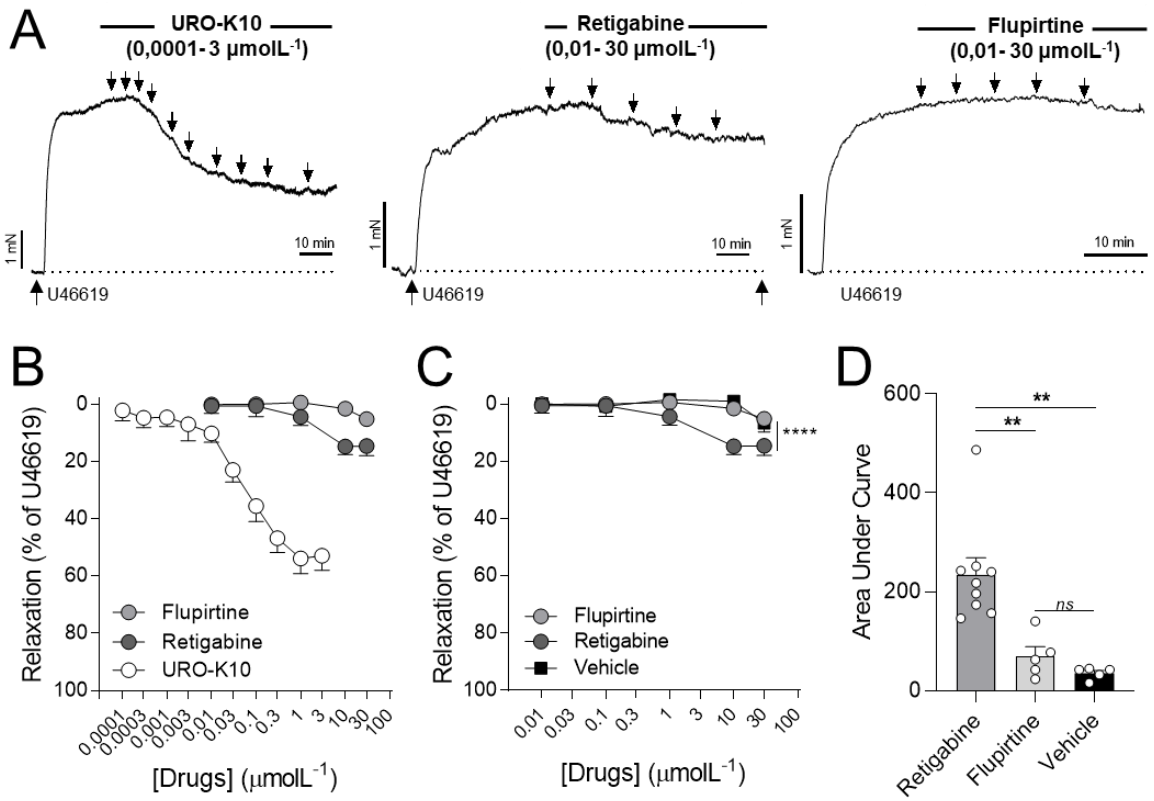

Figure 10. URO-K10 produces more potent and efficient pulmonary vasorelaxation than classical K_V7 channel activators. **(A)** Original recordings and **(B)** averaged concentration-dependent relaxant effects of URO-K10, retigabine and flupirtine in PA pre-contracted with U46619 (0.1 µmol L-1). Points represent mean ± SEM of n = 9, n = 9 and n = 5 for URO-K10, retigabine and flupirtine, respectively. **(C)** Averaged values of the

concentration dependent relaxation induced by retigabine, flupirtine and the vehicle of these drugs (DMSO) in U46619-stimulated PA. Results are expressed as a percentage of the contraction induced by U46619 (0.1 µmol L^{-1}). Significant differences from controls were analysed using two-way ANOVA. **** p< 0.0001. **(D)** Analysis of area under the curve (AUC) from panel C. ** p< 0.01, one-way ANOVA, followed by a Bonferroni post-test.

Additionally, URO-K10-induced relaxation was inhibited by the K_V7 channel blocker XE991 in a concentration-dependent manner, demonstrating the role of K_V7 channels in mediating this effect (Figure 11A). URO-K10-induced relaxation in the presence of XE991 was minimal and did not differ from that observed with the vehicle (Figure 11B). Of note, the vasodilator response of URO-K10 remained unaffected in the presence of the BK_{Ca} blocker iberiotoxin (0.1 µmol L^{-1}) (Figure 11C).

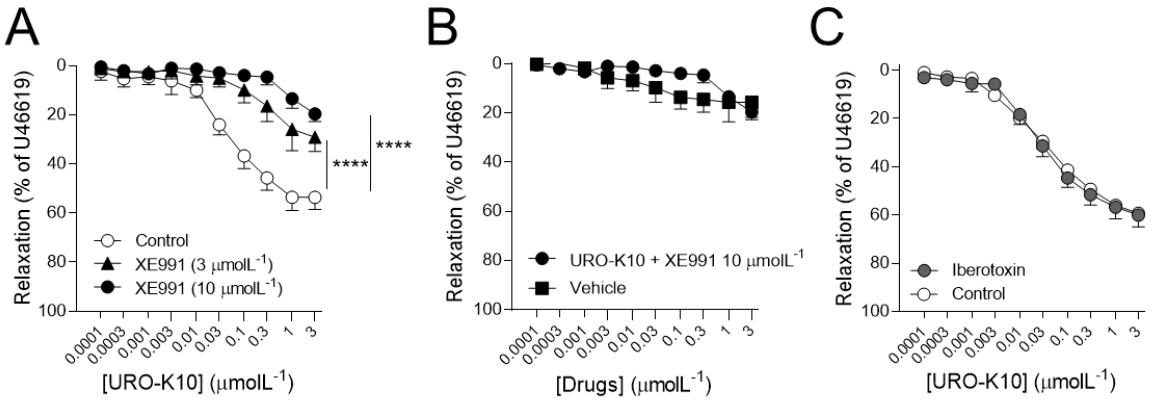

Figure 11. URO-K10 produces a pulmonary vasorelaxation via K_V7 activation and is independent of BK_{Ca} channel activation. **(A)** Averaged concentration-dependent relaxant effects of URO-K10 in the absence and in the presence of the K_V7 channel inhibitor XE991 (3 or 10 µmol L^{-1}). Points represent mean ± SEM of n = 9, n = 5 and n = 5 for URO-K10, + XE991 3 µmol L^{-1}, and + XE991 10 µmol L^{-1}, respectively. Results are expressed as a percentage of the contraction induced by U46619 (0.1 µmol L^{-1}). Significant differences from controls were analysed using two-way ANOVA. ****p< 0.0001 *vs* control. **(B)** Averaged values of the concentration-dependent relaxation induced by URO-K10 + XE991 10 µmol L^{-1} and the vehicle (DMSO) in U46619-stimulated PA. **(C)** Averaged concentration-dependent relaxation effects of URO-K10 (0.0001 - 3 µmol L^{-1}) in the absence and in the presence of iberotoxin (0.1 µmol L^{-1}) in U46619-stimulated PA. Points represent mean ± SEM of n = 7 for control and n = 6 animals for Iberiotoxin (p<0.05, unpaired t-test *vs* control).

URO-K10 also induced a more pronounced vasodilation in MA having Emax = 107 ± 3% and pD2 = 8.50 ± 0.3 (Figure 12) compared to PA. The difference was statistically significant for Emax (p<0.0001), but not for pD2 (p>0.05), as determined by unpaired t-test (n = 9 and n = 5 for PA and MA, respectively). As in PA, URO-K10-induced vasodilation in MA was inhibited by XE991, confirming the involvement of K_V7 channels (Figure 12).

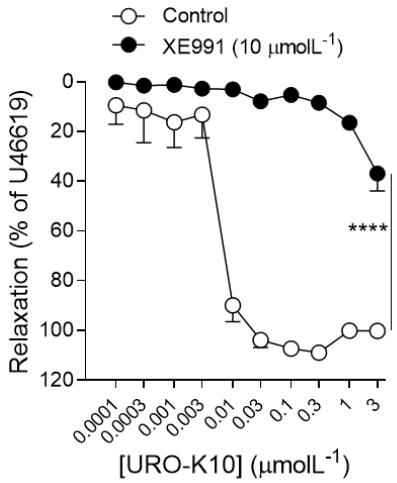

Figure 12. URO-K10 produced greater vasodilation in mesenteric arteries via K_V7 channel activation. Averaged concentration-dependent relaxation effects of URO-K10 in MA contracted with U46619 (0.3 μmol L^{-1}) in the absence and in the presence of XE991 (10 μmol L^{-1}) (****p<0.0001, n = 5, two-way ANOVA).

Supporting these findings, patch-clamp recordings from isolated PASMCs showed that URO-K10 augmented outward K_V currents (Figure 13A-B) and this effect was completely abolished when XE991 was present (Figure 13C). URO-K10-sensitive K_V current (i.e. K_V7 current) was calculated by subtracting the current recorded in the presence of the drug from that recorded in the absence of the drug, which became evident at membrane potentials above -40 mV and was abolished in the presence of XE991 (Figure 13D). The resting membrane potential of PASMCs, which was around -45 mV, remained unchanged after treatment with either URO-K10 or XE991+URO-K10 (Figure 13E-F). Moreover, application of URO-K10 vehicle (DMSO) did not elicit any outward current (Figure 13G).

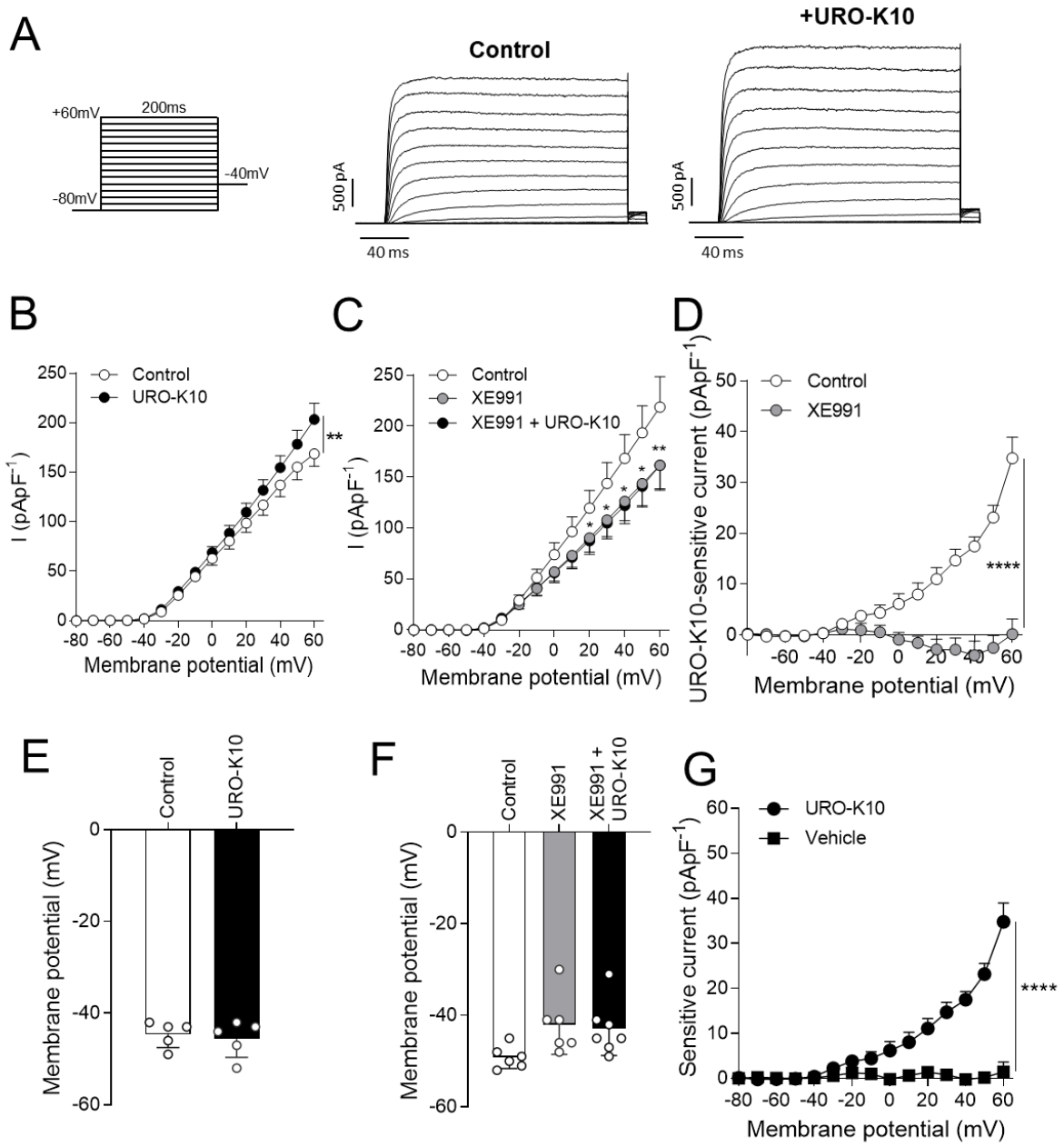

Figure 13. URO-K10 increases the K_V current by activating K_V7 channels in freshly isolated PASMCs from control rats*. (A)** Representative K^+ current traces and **(B)** K^+ current-voltage relationships measured at the end of the depolarizing pulses in the absence and in the presence of URO-K10 (0.3 µmol L^{-1}). **(C)** K^+ current-voltage relationships measured at the end of the depolarizing pulses in the absence and presence of XE911 (10 µmol L^{-1}) and XE911 + URO-K10 (n = 6, *, ** p<0.05 and 0.001 control *vs* control, two-way ANOVA followed by a Bonferroni post-test). **(D)** URO-K10-sensitive current in control and in the presence of XE991 (n=6, ****p<0.0001. Data were analysed by two-way ANOVA). **(E)** Mean values of the resting membrane potential in the absence and in the presence of URO-K10 (n=5, p>0.05, paired *t*-test) and **(F)** in the absence and in the presence of XE911 (10 µmol L^{-1}) and XE911 + URO-K10 (n = 6, p>0.05, one-way ANOVA). **(G)** URO-K10 (0,3 µmol L^{-1}) or vehicle (DMSO) -sensitive current (*p<0.0001, n=6, data were analysed by two-way ANOVA).

1.2) URO-K10 causes vasorelaxation, increases K_V currents and exerts antiproliferative effects in human PA

In the next set of experiments, we turned our focus to human tissue samples to investigate the effects of URO-K10. Remarkably, URO-K10 demonstrated significantly more potent and more effective vasodilator properties in human PA when compared to retigabine. The potency difference was evident with URO-K10 achieving a pIC_{30} of 7.0 ± 0.2 *vs* 4.4 ± 0.3 for retigabine (p<0.0001, unpaired t-test) (Figure 14A-B). Consistent with previous findings in rat PASMCs, URO-K10-induced relaxation was essentially blunted in the presence of XE991 (Figure 14C). Control experiments using the vehicle alone (DMSO), produced a negligible vasodilator effect which was statistically lower that the response triggered by retigabine (Figure 14D).

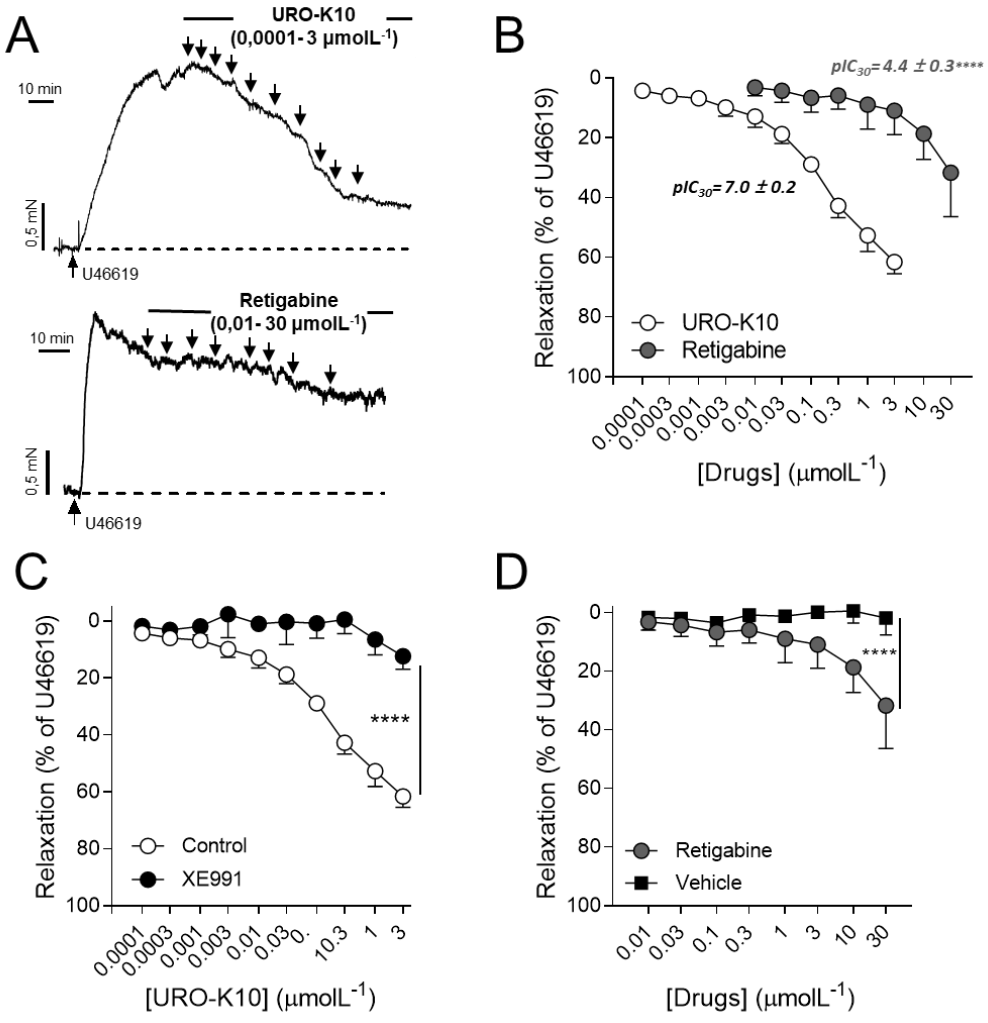

***Figure 14. URO-K10 causes vasodilatation via K_V7 activation in human PA*. (A)** Isometric tension recordings showing the effects of increasing concentrations of URO-K10 (0.0001 - 3

μmol L^{-1}) and retigabine (0.01 -30 μmol L^{-1}) on human PA contracted with U46619 (0.1 μmol L^{-1}). **(B)** Averaged concentration-dependent relaxant effects to URO-K10 and retigabine on human PA. Points represent mean ± SEM (n = 6 and 4 for URO-K10 and retigabine, respectively). **(C)** Averaged concentration-dependent relaxation effects to URO-K10 in the absence and in the presence of the K_V7 channel inhibitor XE991 (10 μmol L^{-1}) in human PA. **(D)** Averaged concentration-dependent relaxant effects of retigabine (0.01 – 30 μmol L^{-1}) or vehicle alone in human PA. Points represent mean ± SEM of n = 6 and n = 5 for panel C and D, respectively, ****p<0.0001, two-way ANOVA).

Additionally, we examined URO-K10 effects on ion channel activity in freshly isolated human PASMCs. The drug, increased K_V current density (Figure 15A-B), without altering resting membrane potential (Figure 15C). Moreover, to explore the potential antiproliferative properties of URO-K10, we treated human PASMCs with increasing concentrations of the compound. The results revealed that URO-K10 inhibited cell proliferation (Figure 15D) and showed a tendency to be inhibited by XE991 (Figure 15E n = 3, preliminary data due to limited availability of human tissue). Note that XE991 by itself reduce BrdU signal. Overall, our results support that this novel K_V7 channel modulator exhibits potent vasodilator and antiproliferative effects in both rat and human PA.

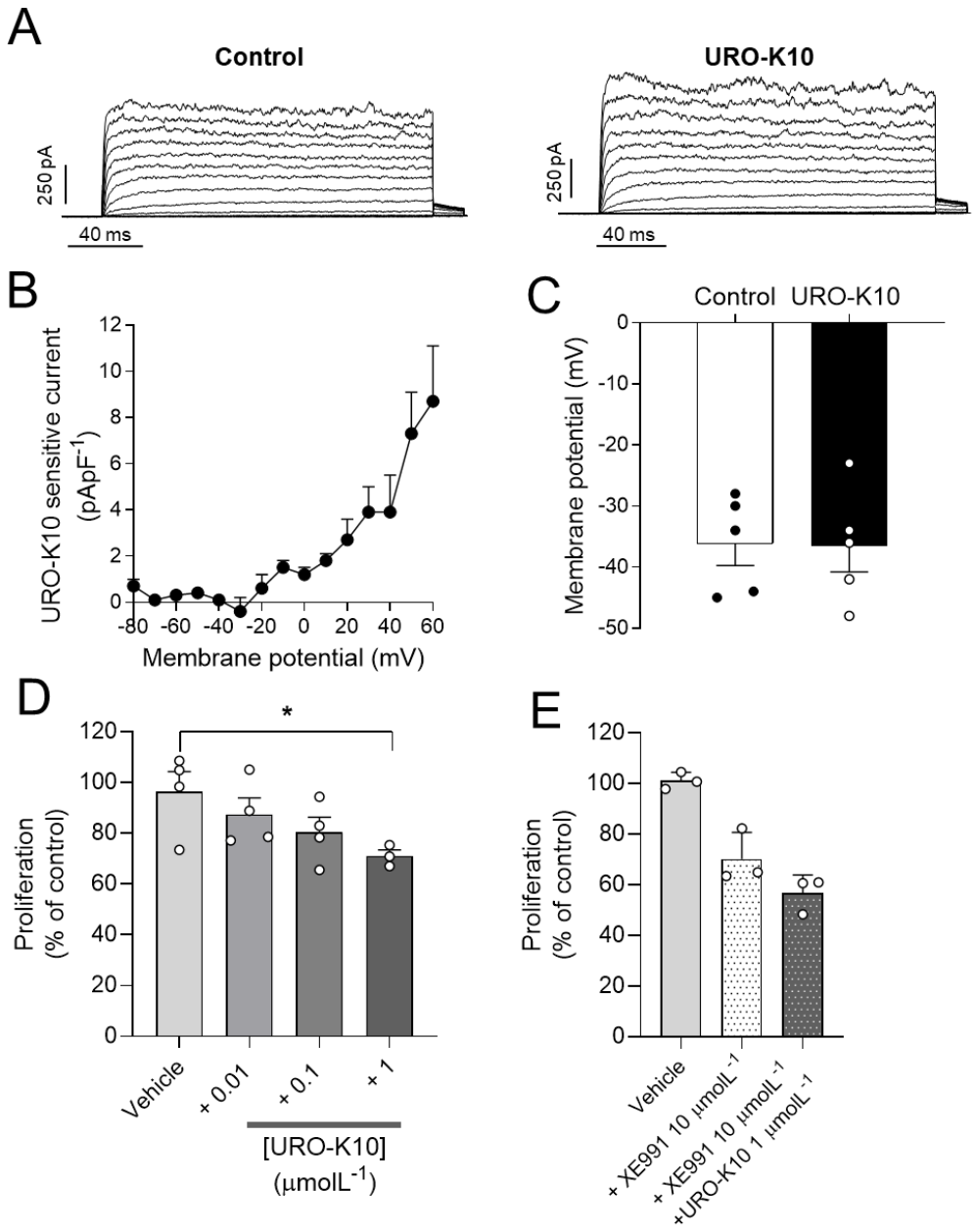

***Figure 15. URO-K10 increases K_V currents and exert an antiproliferative effect in PA and PASMCs freshly isolated from human samples*.** **(A)** Representative K^+ current traces recorded in human PASMCs in the absence and in the presence of URO-K10. **(B)** URO-K10-sensitive current measured at the end of the depolarizing pulses obtained by subtracting the K^+ current in the presence of URO-K10 from the current in the absence of the drug. **(C)** Mean values of the human PASMCs resting membrane potential in the absence and in the presence of URO-K10 (n = 5, p>0.05, paired t-test). **(D)** Concentration-dependent inhibition of BrdU incorporation induced by URO-K10 and **(E)** induced by XE991 (10 µmol L^{-1}) and by combination of XE991 + URO-K10 (1 µmol L^{-1}) in human PASMCs. Data are expressed as percentage of proliferation induced by FBS 5% (n = 4 and 3; for panel D and E, respectively, *p<0.05 *vs* vehicle, one-way ANOVA followed by a Bonferroni test.

1.3) URO-K10-induced relaxation in PA is independent of the KCNE4 ancillary subunit

Next, we explored mechanistic differences between URO-K10 and classical K_V7 activators that could explain their distinct functional behaviour, focusing on the regulatory subunit KCNE4. This ancillary subunit is known to increase K_V7.4 membrane abundance in smooth muscle cells and to be essential for the relaxation induced by S-1, a K_V7.2-7.5 activator, in MA (Abbott & Jepps, 2016; T. A. Jepps et al., 2015; Strutz-Seebohm et al., 2006). In contrast, URO-K10-induced K_V7.4 currents in heterologous systems is not enhanced by KCNE4 overexpression (Lee et al., 2020). To investigate the role of KCNE4 in URO-K10-induced pulmonary vascular effects, PA were treated with KCNE4-targeting morpholinos and using this technique a ~ 50% reduction in expression was confirmed by Western blot (Figure 16A-B). This knockdown also slightly but significantly decreased K_V7.4 expression (Figure 16C-D), without affecting K_V7.5 (Figure 16E-F).

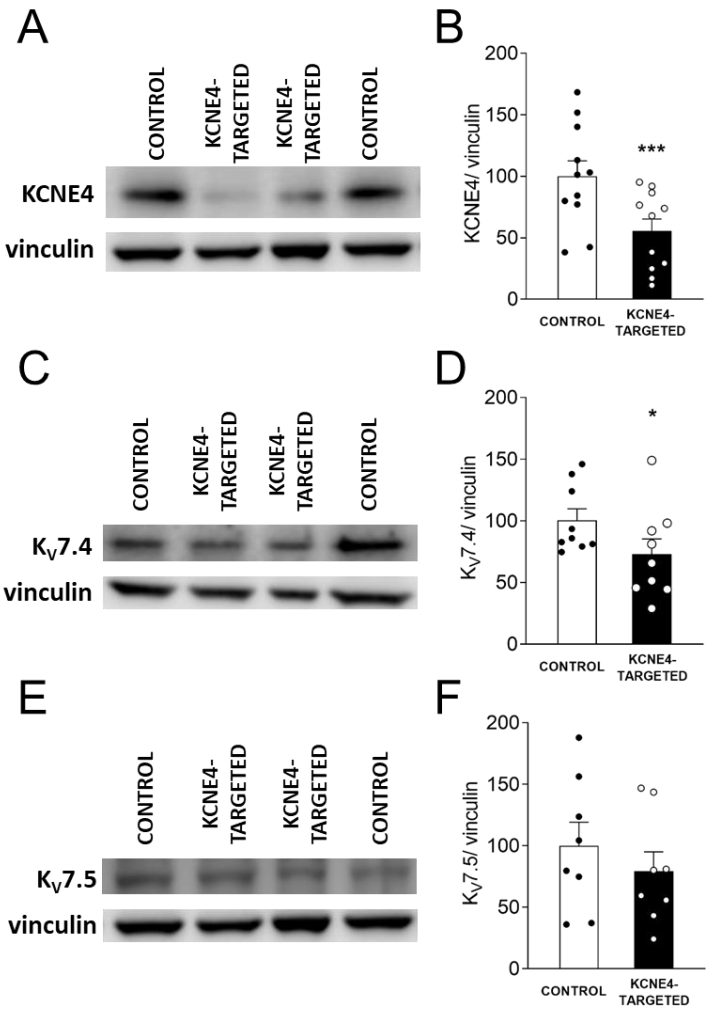

Figure 16. KCNE4-targeted morpholino effectively reduces KCNE4 and partially decreases K_V7.4 channel protein expression in PA. Representative Western blot and mean data of KCNE4 **(A-B)**, K_V7.4 channel **(C-D)** and K_V7.5 channel **(E-F)** expression in PA transfected with either a KCNE4-targeted or the respective control morpholino. Protein expression was normalized by vinculin expression. Data are shown as means ± SEM of PA from n = 8, 9 and 11 animals for K_V7.5 channel, K_V7.4 channel and KCNE4 subunit, respectively. Significant differences were analysed by using paired *t*-test. *, *** p<0.05 and 0.001 *vs* control morpholino.

Therefore, we assessed the vasodilatory responses of URO-K10 and retigabine in PA transfected with either KCNE4-targeted or control morpholinos. As shown in Figure 17, UROK-10-induced relaxation was unaffected, whereas vasodilation induced by retigabine was reduced by KCNE4 knockdown (Figure 17A-B, D-E). Moreover, the vehicle (DMSO) produced a negligible vasodilator effect, which was significantly lower than that of retigabine (Figure 17E). Similarly, flupirtine-induced relaxation in 5-HT-stimulated PA was also significantly reduced by KCNE4 knockdown (Figure 18A-B). Moreover, XE991 blocked the vasodilation induced by all drugs in control transfected PA, but its inhibitory effect on retigabine and flupirtine was absent in KCNE4-silenced PA (Figure 17C and F, Figure 18C-D). Taken together, these findings indicate that, unlike retigabine and flupirtine, URO-K10 promotes pulmonary vasodilation via K_V7 channel activation independently of KCNE4.

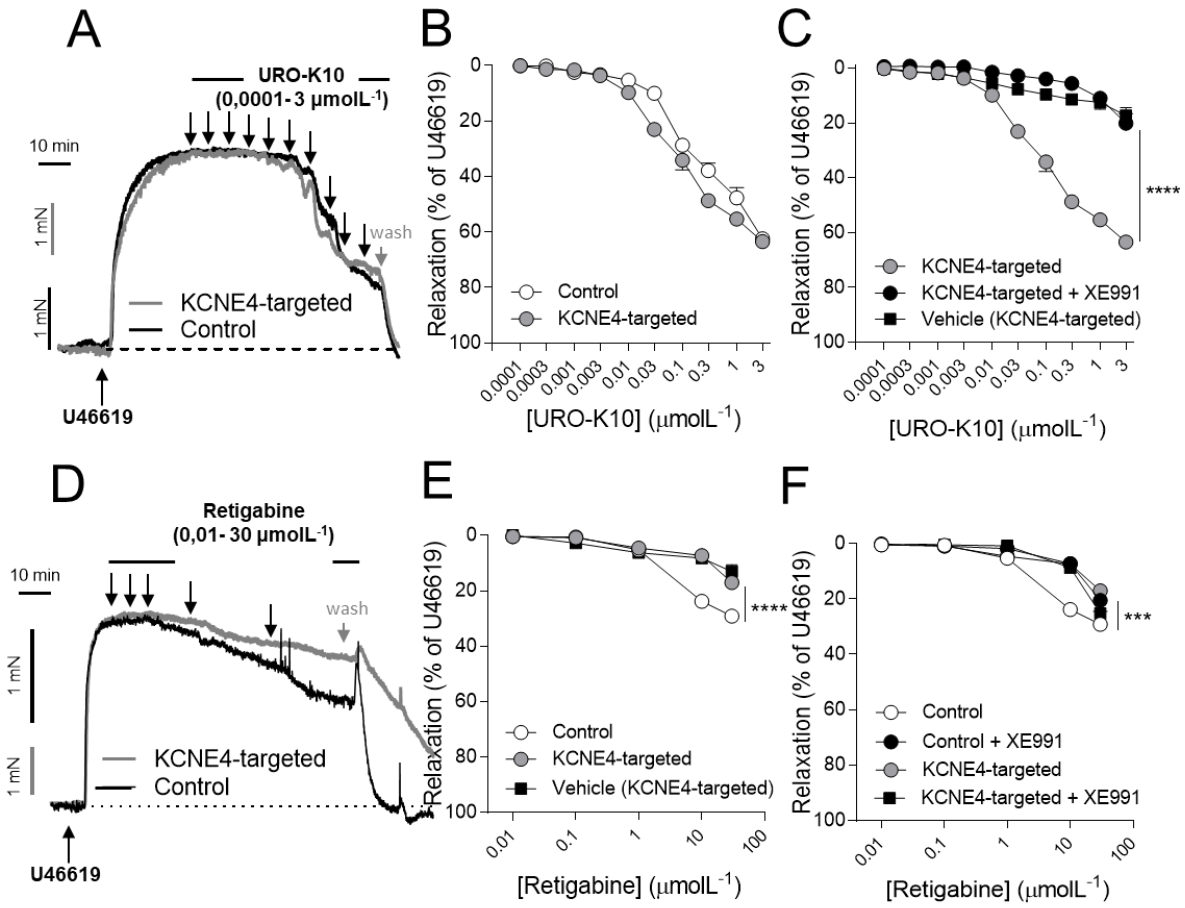

***Figure 17. KCNE4 knockdown attenuates retigabine- but not URO-K10-induced pulmonary vasodilatation*. (A and D)** Original recordings and **(B-F)** averaged values of the concentration-dependent relaxation induced by URO-K10 (0.0001 – 3 µmol L^{-1}) and retigabine

(0.01 – 30 µmol L^{-1}) and vehicle, respectively, in rat PA transfected with either a KCNE4-targeted or the respective control morpholino in the presence and in the absence of XE991 (10 µmol L^{-1}). Points represent mean ± SEM of n = 5 - 8. Significant differences were analysed by using two-way ANOVA. ***, **** p<0.001 and 0.0001 *vs* control morpholino and ***P<0.001 *vs* KCNE4 targeted.

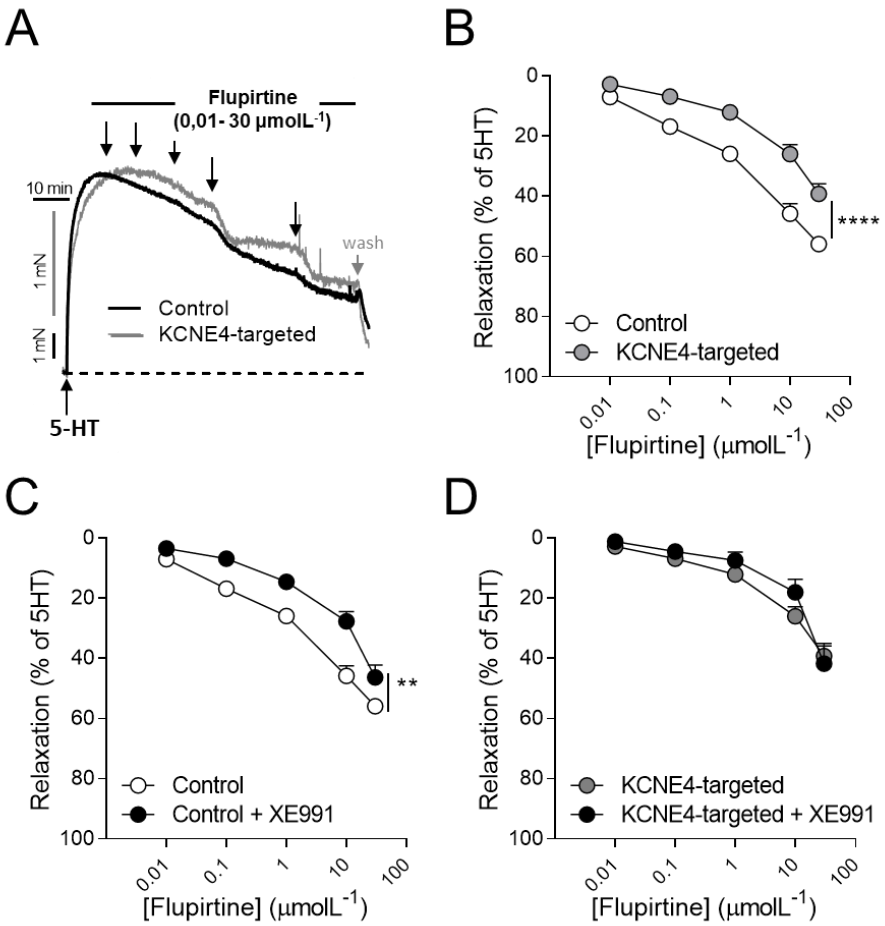

Figure 18. Flupirtine-induced pulmonary vasodilatation via activation of K_V7 channels depends on the presence of KCNE4. **(A)** Original recordings showing the concentration-dependent relaxation induced by flupirtine (0.01 – 30 µmol L^{-1}) in PA pre-contracted with serotonin (1 µmol L^{-1}) and transfected with either a KCNE4-targeted or the respective control morpholino. **(B-D)** Averaged values of flupirtine-induced relaxation in the absence and in the presence of XE991 in control or KCNE4-targeted serotonin-precontracted PA. Points represent mean ± SEM of n = 5. Significant differences were analysed by using two-way ANOVA. ** p<0.05 and **** p<0.0001.

1.4) Enhanced responses to URO-K10 in the presence of TASK-1 and K_V1.5 inhibitors

As previously mentioned, downregulation of K^+ channels, such as TASK-1 and K_V1.5, is a well-established hallmark of PAH. Therefore, to investigate the effect of URO-K10 under conditions mimicking this pathological ionic channel remodelling characteristic of the disease, we evaluated its pulmonary vascular effects in the presence of the K_V1.5 and TASK-1 channel inhibitors DPO-1 (1 µmol L^{-1}) and ML365 (1 µmol L^{-1}), respectively. Under these conditions, URO-K10 produced significantly greater relaxation compared to arteries not exposed to these potassium inhibitors (Figure 19A-B). This enhanced vasodilator was observed in PA but not in MA (Figure 20). Consistent with the expected action of DPO-1 and ML365, total K^+ current amplitude was significantly reduced in PASMCs treated with both inhibitors (Figure 19C-D). Remarkably, as shown in Figure 19C-D subsequent addition of URO-K10 resulted in a significant increase in K^+ currents. However, the URO-K10-sensitive current in PASMCs treated with ML365 + DPO-1 was comparable to those observed under control conditions (p>0.05, two-way ANOVA, n = 5 and n = 6, Figure 19E). In addition, to confirm the involvement of K_V7 channels, we examined the effects of XE991 on URO-K10-induced current in the presence of DPO-1 + ML365. Since XE991 blocked the current, these findings indicate that URO-K10 acts through K_V7 channel activation under these conditions too. Of note, exposure of ML365 + DPO-1 caused a marked membrane depolarization in PASMCs, which was repolarized by URO-K10 (Figure 19F and G).

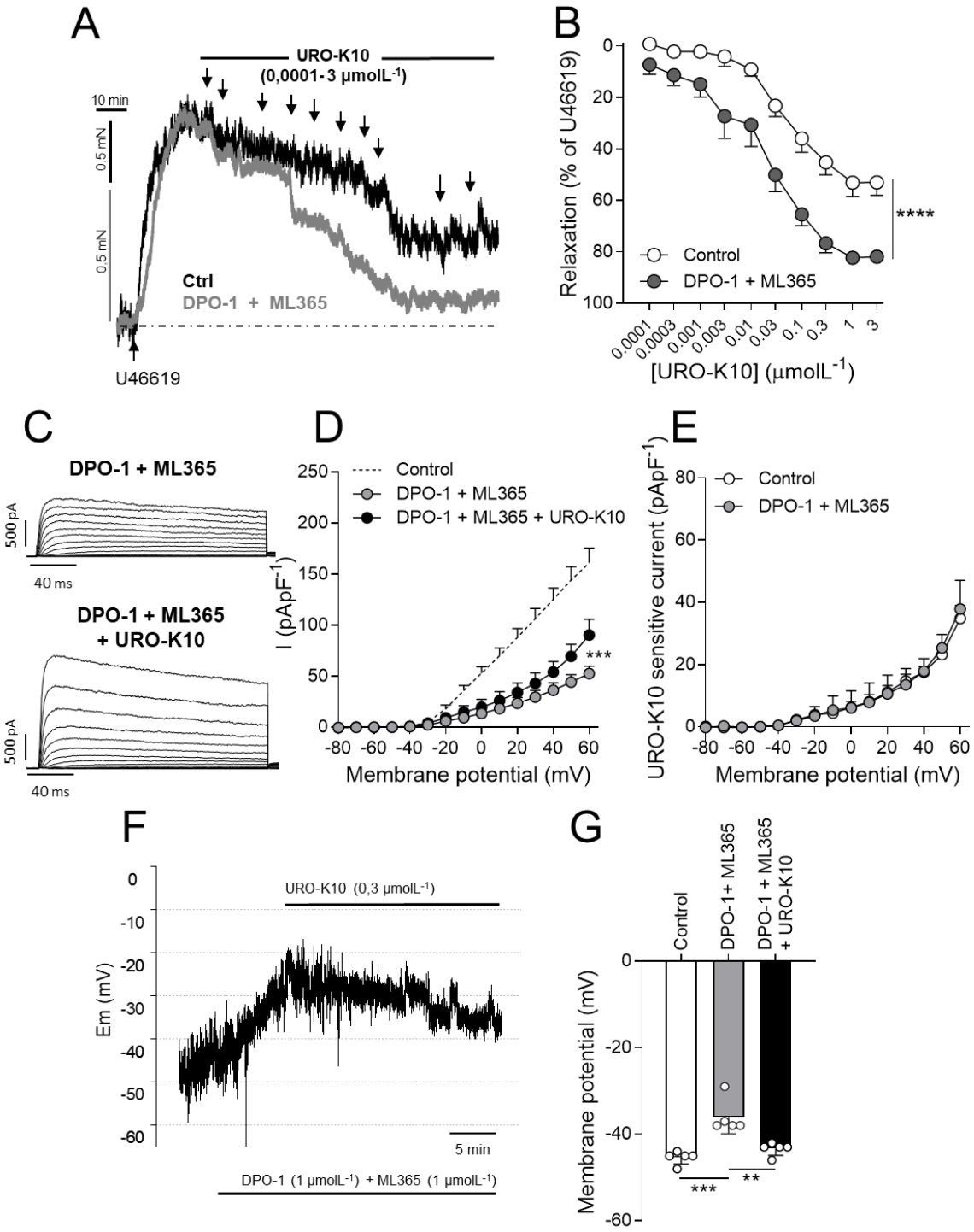

Figure 19. Enhanced pulmonary vascular effects of URO-K10 upon blockade of K_V1.5 and TASK-1 channels. URO-K10 effects were tested in rat PA incubated during 15 min with the inhibitors of K_v1.5 and TASK-1 channels, DPO-1 and ML365 respectively, to mimic the ionic remodeling that occurs in PAH. **(A)** Original recordings and **(B)** averaged data of the concentration-dependent relaxation induced by URO-K10 (0.0001 – 3 µmol L^{-1}) in PA contracted with U46619 (0.1 µmol L^{-1}) in the absence (Control) and in the presence of ML365+DPO-1 (both at 1 µmol L^{-1}) (**** p <0.0001 *vs* control, n= 5, two-way ANOVA). **(C)**

Representative K^+ current traces and **(D)** K^+ current-voltage relationships showing the effect of URO-K10 (0.3 µmol L^{-1}) in the presence of ML365+DPO-1 (n = 5, *** p <0.001 vs Control, two-way ANOVA). The dashed line represents the current-voltage relationship under control conditions. **(E)** URO-K10-sensitive current under control conditions taken from figure 2F and in presence ML365+DPO-1 calculated from data on panel D (n = 5 and n = 6, p >0.05, two-way ANOVA). **(F-G)** Representative recordings **(F)** and mean values **(G)** of the repolarizing effect of URO-K10 in the presence of ML365+DPO-1 on freshly isolated PASMCs. Points represent mean ± SEM of n = 5. Significant differences from controls were analysed by paired *t*-test, **, *** p <0.01 and ** 0.001, respectively *vs* control.

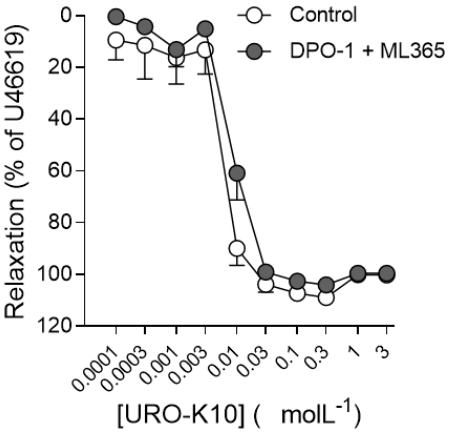

Figure 20. URO-K10 produced greater vasodilation in mesenteric arteries. Averaged concentration-dependent relaxation effects of URO-K10 (0.0001 - 3 µmol L^{-1}) in MA contracted with U46619 (0.3 µmol L^{-1}) in the absence and in the presence of ML365+DPO-1 (both at 1 µmol L^{-1}). (p > 0.05, n = 5, two-way ANOVA).

1.5) Augmented responses to URO-K10 in PA from PH animals

Finally, we examined the effects of URO-K10 on vascular reactivity in PA from MCT-PH animals. In line with our data on an *in vitro* PH model (previous section), the vasodilator efficacy of URO-K10 was significantly stronger in PA from MCT-PH rats compared to those from control animals (Emax= 60 ± 7% *vs* 102 ± 10%, p< 0.05, unpaired nested *t*-test; and pD_2: 6.31 ± 0.06 *vs* 6.48 ± 0.10, p> from n = 3 animals for the MCT group) (Figure 21A and B).In addition, we studied the electrophysiological effects of URO-K10 in PASMCs isolated from PH rats. We recorded K_V7 currents using depolarizing pulses ramps ranging from -100 to +40 mV under three situations: control situation perfused with external solution (a), after adding URO-K10 (1 µmol L^{-1}) (b), and with URO-K10 (1 µmol L^{-1}) + XE991 (30 µmol L^{-1}) (c). Figure 21(C-D) illustrate the K_V7 current and the URO-K10-induced K_V7 component, calculated by subtracting the currents at points (a)-(c) and at (b)-(c), respectively, in PASMCs from control (Figure 21C) or MCT-PH (Figure 21D) rats, revealing a marked increase in Kv7 current in both groups after treatment with this novel agonist. Very interestingly, the K_V7 current

induced by URO-K10 was significantly greater in PASMCs from PH animals compared to controls (Figure 21E).

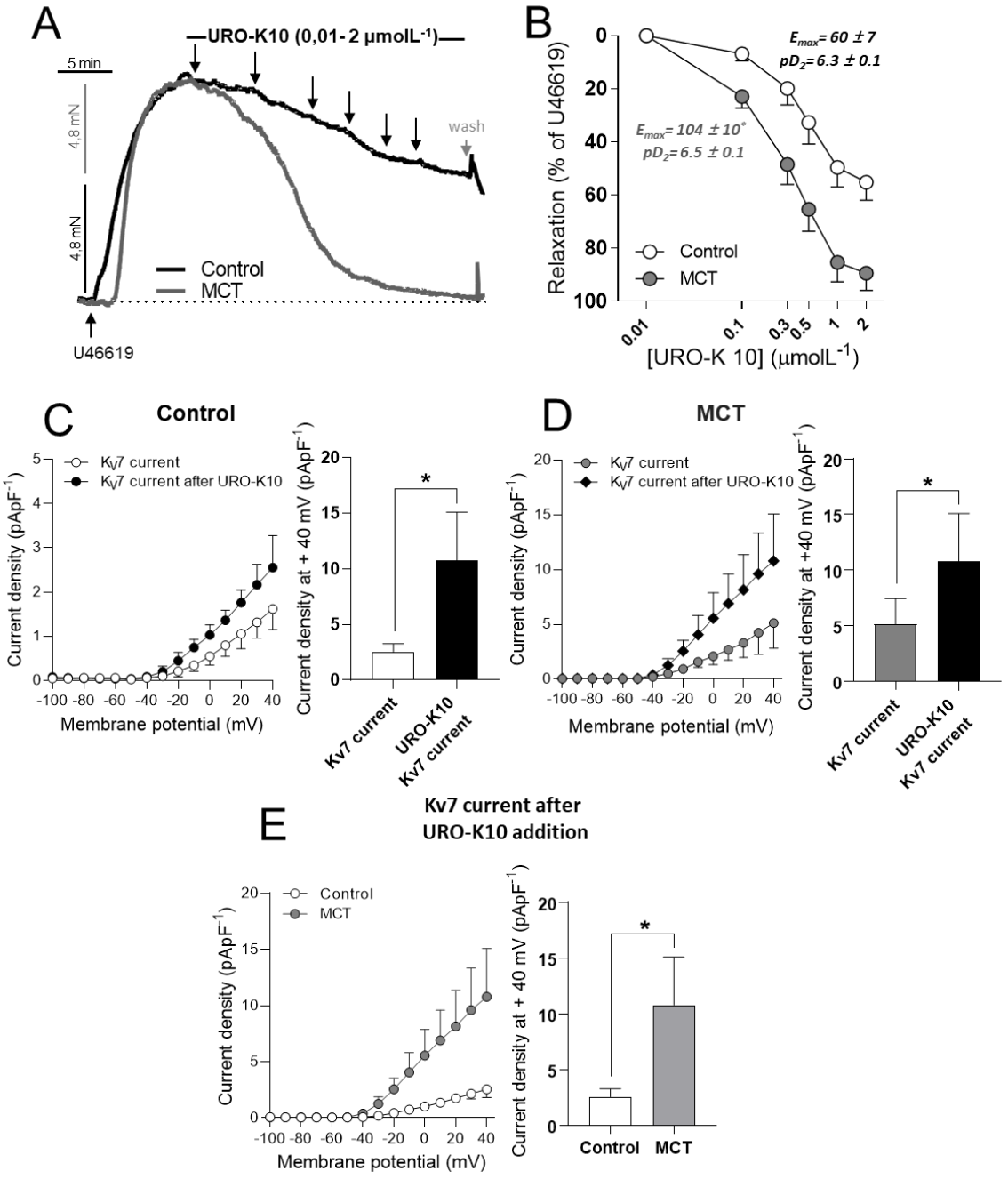

***Figure 21. Enhanced response to URO-K10 in PA from MCT-induced PH rats*. (A)** Representative recordings and **(B)** averaged data of the concentration-response curves to URO-K10 (0.0001 – 3 µmol L^{-1}) in PA from control and MCT-PH rats. Points represent mean ± SEM (n = 12 and 10 arteries from n = 3 animal per group). p <0.05, unpaired nested *t*-test *vs* Control. **(C-D)** Current-voltage relationships (left panel) and inset of current density at + 40 mV (right panel) obtained after applying depolarizing ramp pulses from -100 mV to + 40 mV

for 3 s. These data show the effects of URO-K10 (1 µmol L^{-1}) on K_V7 currents in freshly isolated PASMCs from control **(C)** or MCT-PH **(D)** rats. The K_V7 current and the K_V7 current after URO-K10 represent the XE991 (30 µmol L^{-1})-sensitive current in the absence and in the presence of URO-K10, respectively. **(E)** Current-voltage relationships (left panel) and inset of current density at + 40 mV (right panel) of K_V7 current after URO-K10 in PASMCs from control or MCT-PH rats. Data were analysed using a nested analysis at +40 mV current, * p <0.05 *vs* K_V7 current or *vs* Control. Points represent mean ± SEM of 6 cells from n = 3 (control group) and 8 cells from n = 3 (MCT-group).

CHAPTER 2: Effects of the S1R agonist PRE084 on $K_V1.5$ activity and cardiopulmonary function in an experimental model of PAH.

2.1) In vivo administration of the S1R agonist PRE084 enhances attenuated K_V1.5 channel activity in PA from Hpx/Su rats

K_V1.5 channel activity (measured as DPO-1-sensitive current) was determined in isolated PASMCs from either normoxic, Hpx/Su and Hpx/Su+PRE084-exposed animals. Representative K^+ current traces in the absence and presence of DPO-1 (1 μmol L^{-1}) are shown in Figure 22A. As expected, total K^+ and DPO-1-sensitive currents (Figure 22B and C, respectively) which correspond to the K_V1.5 component were markedly decreased in PASMCs from Hpx/Su rats. Similarly, reduced DPO-1-insensitive currents (Figure 22D) in these animals indicates that other K^+ channels are also impaired in PAH. Notably, PRE084 treatment in Hpx/Su rats improved the total K^+ current and the K_V1.5 channel activity but not the DPO-1-insensitive component. Furthermore, PASMCs from PRE084-treated rats had a more hyperpolarized membrane potential than Hpx/Su rats, reaching similar levels to those of normoxic rats (Figure 22E). In line with the higher K_V1.5 channel activity, depolarization induced by DPO-1 was more pronounced in PASMCs from PRE084-treated than that from vehicle-treated Hpx/Su rats (Figure 22F). Interestingly, PASMCs obtained from Hpx/Su rats showed an abnormally increased membrane capacitance, which is indicative of larger cell size, and this was attenuated by PRE084 (Figure 22G).

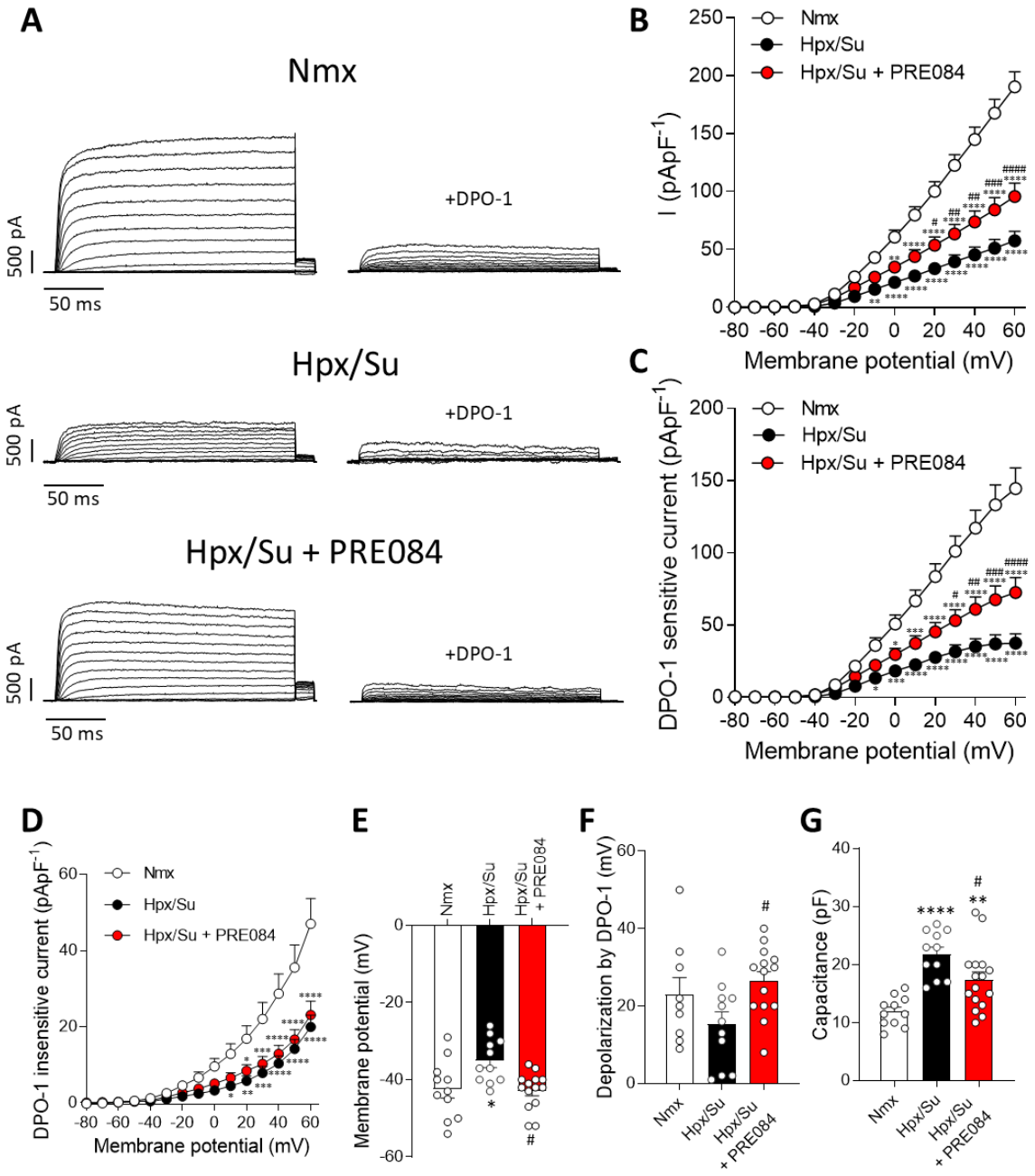

***Figure 22. In vivo administration of PRE084 increases K_V1.5 currents in PASMCs from Hpx/Su rats*.** **(A)** Representative K^+ currents traces in PASMC from the three experimental groups: Normoxia (Nmx), Hypoxia + SU5416 (Hpx/Su) and Hypoxia + SU5416 + PREO084 (Hpx/Su +PRE084). Currents were recorded in the absence (*left*) and in the presence of DPO-1 (1 µmol L^{-1}) (*right*). **(B)** K^+ current-voltage relationships measured at the end of the depolarizing pulses and normalized by the cell capacitance of PASMCs from Nmx (white), Hpx/Su (black) and Hpx/Su + PRE084 (red). **(C)** The DPO-1 sensitive current obtained by subtracting the K^+ current in the presence of DPO-1 from the current in the absence of the drug; and the DPO-1 insensitive current **(D)** of the three groups. Points represent mean ± SEM (n=11, 11 and 14 cells, from N= 5, 7 and 5 rats from Nmx, Hpx/Su and Hpx/Su + PRE084, respectively). ****$p <$ 0.0001 *vs* Nmx and #### $p <$ 0.0001 *vs* Hpx/Su (Two-way repeated

measures ANOVA followed by Bonferroni's *post hoc* test). **(E)** Mean values of the resting membrane potential and **(F)** mean values of membrane depolarization induced by DPO-1 in PASMCs. **(G)** Average PASMCs membrane capacitance. For panels E, F and G *, ** and ****$p <$ 0.05, 0.01 and 0.0001 *vs* Nmx and #$p <$ 0.05 *vs* Hpx/Su (One-way ANOVA followed by Bonferroni's *post hoc* test).

2.2) The in vivo effects of PRE084 are not associated with changes on K_V1.5 channels expression in isolated pulmonary arteries

Impairment of K_V1.5 channel activity present in Hpx/Su animals was associated with changes in K_V1.5 protein expression in isolated PA (Figure 23A-B). Thus, Western blots revealed that PA from these animals had lower levels of the fully glycosylated mature channel (upper band) and augmented levels of the core-glycosylated immature form (lower band). These changes were unaffected by PRE084 treatment. In addition, PA from Hpx/Su rats showed a significant upregulation of S1R (Figure 23A-B), which did not seem to be affected by the administration of PRE084. To provide further insight into the potential mechanism underlying the augmentation of K_V1.5 channel activity by PRE084, we performed *in vitro* studies to analyse the presence of the channel in the plasma membrane of PASMCs using immunocytochemistry. We observed that 24 h incubation with PRE084 treatment (20 µmol L^{-1}) caused a considerable increase of K_V1.5 channel expression in the cell membrane (Figure 24). These data suggest that PRE084, rather than affecting total K_V1.5 channel expression or maturation, increases the localisation of the channel in the membrane.

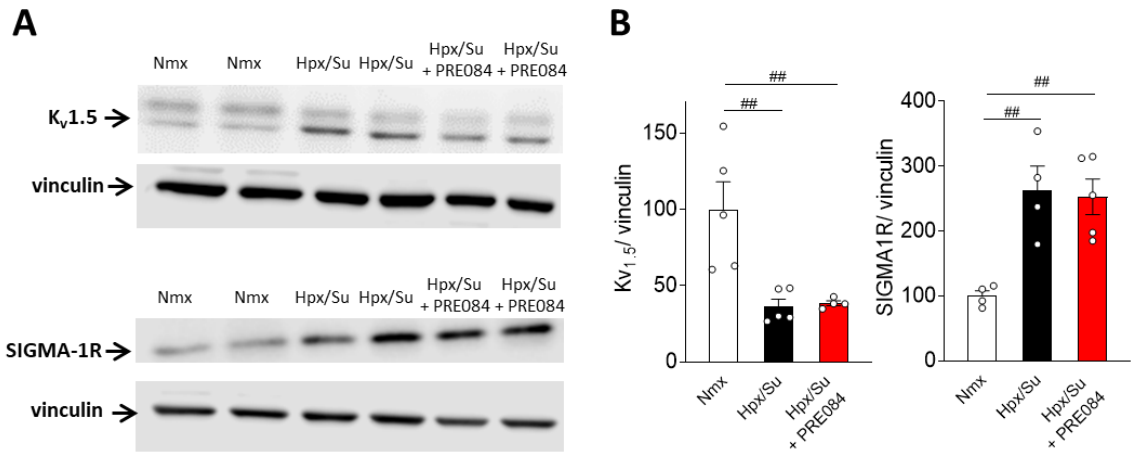

Figure 23. PRE084 administration in the Hpx/Su- induced PAH in vivo model does restore the reduced K_V1.5 channel expression in PA. **(A)** Representative Western blot and **(B)** total

K_V1.5 and S1R protein expression were quantified in PA from the three experimental groups. The two bands of the K_V1.5 channel are observed, where the upper band is the mature, fully glycosylated channel, and the lower band is the immature core-glycosylated channel. Protein expression was normalized by vinculin expression. Data are shown as mean ± SEM of PA from n= 4-5 animals per group. $^{**}p < 0.01$ *vs* Nmx (One-way ANOVA followed by Bonferroni's *post hoc* test).

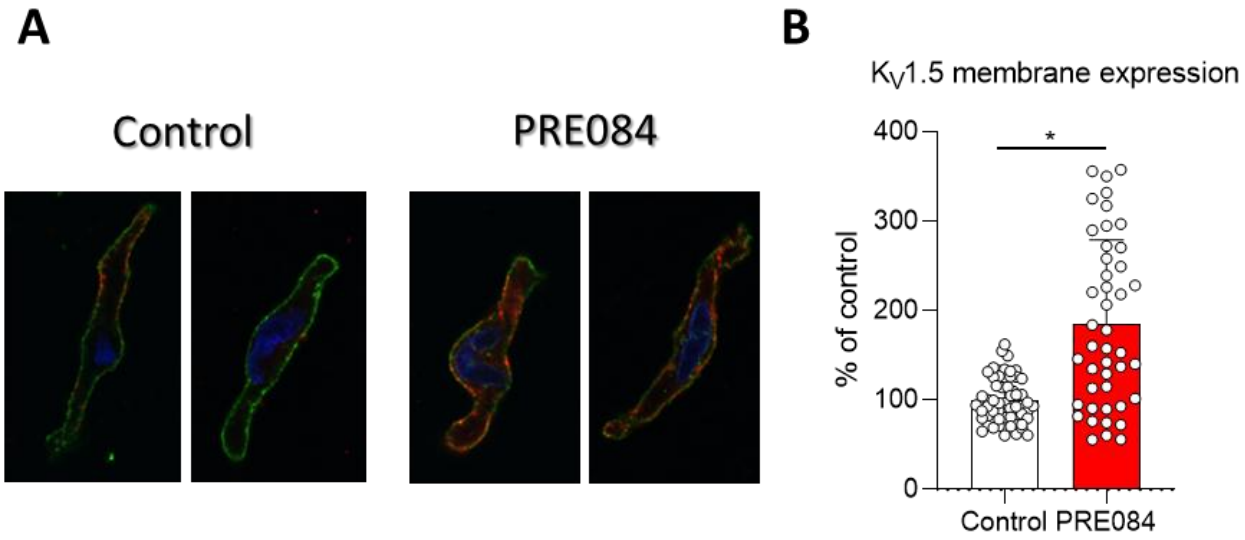

Figure 24. 24 h incubation with PRE084 increased the K_V1.5 membrane expression in rat PASMCs. **(A)** Four representative images of immunocytochemistry staining of rat PASMCs which was done using a membrane marker wheat germ agglutinin (WGA) (green), a primary rabbit anti-K_V1.5 antibody (red) and DAPI (blue). **(B)** K_V1.5 membrane expression represented as % of control. Each bar shows the mean ± SEM (*n* = 54-57 cells from n = 5 animals in each group). $^{*}p < 0.05$ *vs* control (Nested t-test).

2.3) PRE084 improves pulmonary vascular function in Hpx/Su rats

Isolated PA from the three different groups were firstly contracted with KCl (80 mmol L^{-1}), which led to similar vasoconstrictor responses in the three groups (1.01 ± 0.14, 1.01 ± 0.23 and 1.41 ± 0.3 mN/mm^2). We also studied the effect of 5-HT as pulmonary vasoconstrictor in PA from the three experimental groups. Consistent with the expected higher vasoreactivity, PA from Hpx/Su model exhibited a clear hyperreactivity to 5-HT compared to those from Nmx group (Figure 25A -B). Treatment with PRE084 partially reversed the hypercontractility to 5-HT, which was particularly evident at lower concentrations of this agonist (Figure 25A-B). To further explore the role of K_V1.5 channels in the modulation of pulmonary vascular tone in the three

experimental groups, we examined the effect of the K_V1.5 channel inhibitor DPO-1 on Phe-induced vasoconstriction. Cumulative concentrations of Phe were tested on each PA, first in the absence (control) and subsequently in the presence of DPO-1. As expected, the K_V1.5 inhibitor potentiated Phe-induced contraction in PA from Nmx rats (Figure 25C), whereas no significant potentiation was observed in PA from Hpx/Su rats (Figure 25D). Interestingly, PA from Hpx/Su + PRE084 rats demonstrated a clear potentiation of Phe-induced contraction in the presence of DPO-1 (Figure 25E), suggesting that *in vivo* treatment with PRE084 produces a heightened sensitivity to the K_V1.5 channel inhibitor on pulmonary vascular reactivity.

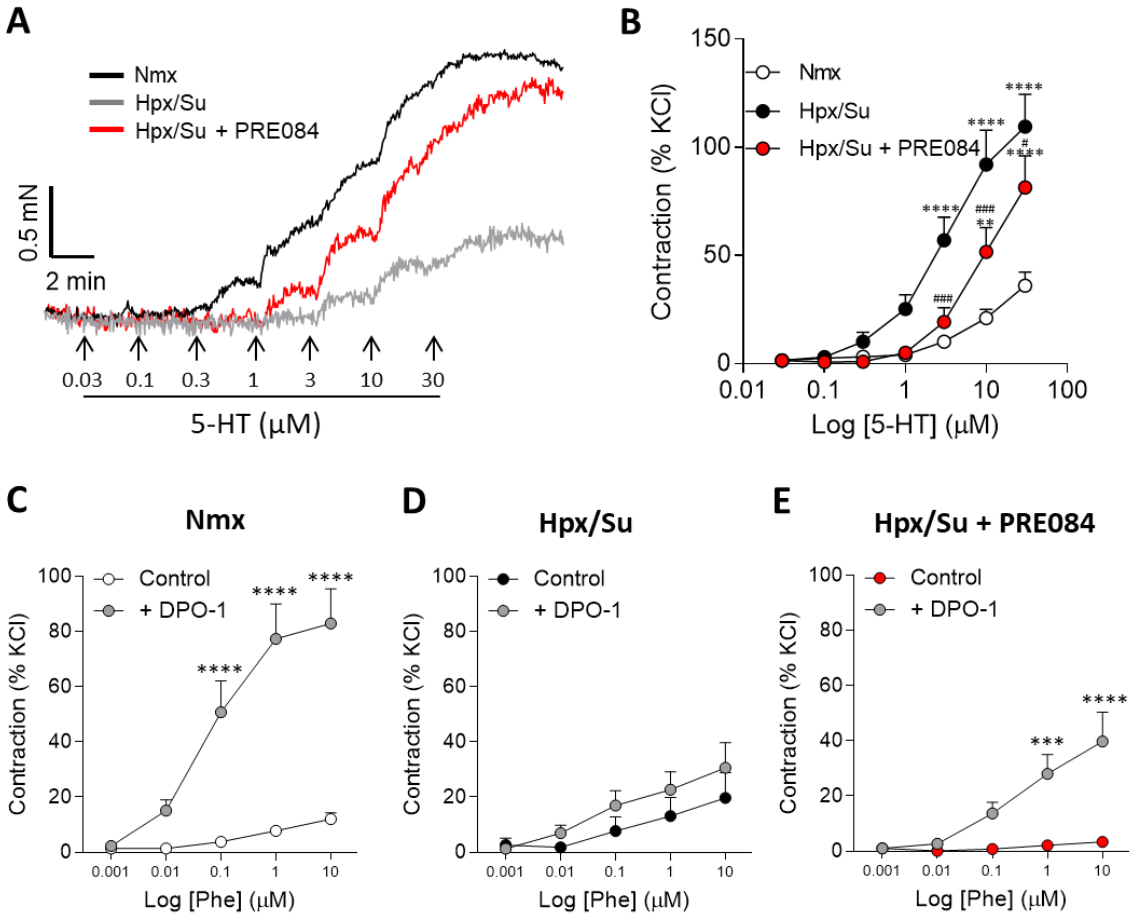

Figure 25. In vivo administration of PRE084 decreases vasoconstriction in PA of Hpx/Su rats. **(A)** Representative recordings and **(B)** averaged data of the concentration-response curves to serotonin (5-HT, 30 nmol L^{-1}- 30 µmol L^{-1}) on PA from Nmx (white-grey), Hpx/Su (black) and Hpx/Su + PRE084 (red) rats. Points represent mean ± SEM (n= 8, 8 and 9 for Nmx, Hpx/Su and Hpx/Su + PRE084). ****$p <$ 0.0001 *vs* Nmx and # and ### $p <$ 0.05 and 0.001 *vs* Hpx/Su (Two-way repeated measures ANOVA followed by Bonferroni's *post hoc* test). **(C-E)** Mean concentration-response curves to phenylephrine (Phe) (1 nmol L^{-1}-10

µmol L^{-1}) in the absence (control) and in the presence of DPO-1 (1 µmol L^{-1}) on PA from the three groups. Points represent mean ± SEM (n= 10, 7 and 9 for Nmx, Hpx/Su and Hpx/Su + PRE084). *** and ****p < 0.001 and 0.0001 *vs* control (Two-way repeated measures ANOVA followed by Bonferroni's *post hoc* test).

We also evaluated the potential protective effects of PRE084 on the PA endothelial dysfunction characteristic of PAH. Original recordings of acetylcholine-induced endothelium-dependent vasodilation in the three groups are shown in Figure 26A. PA from Hpx/Su rats showed a clear impairment of endothelium-dependent relaxation which was partially restored by PRE084 (Figure 26A-B). In contrast, the reduced relaxant response to the guanylyl cyclase stimulator riociguat in PA of Hpx/Su rats was not improved by PRE084 (Figure 26C).

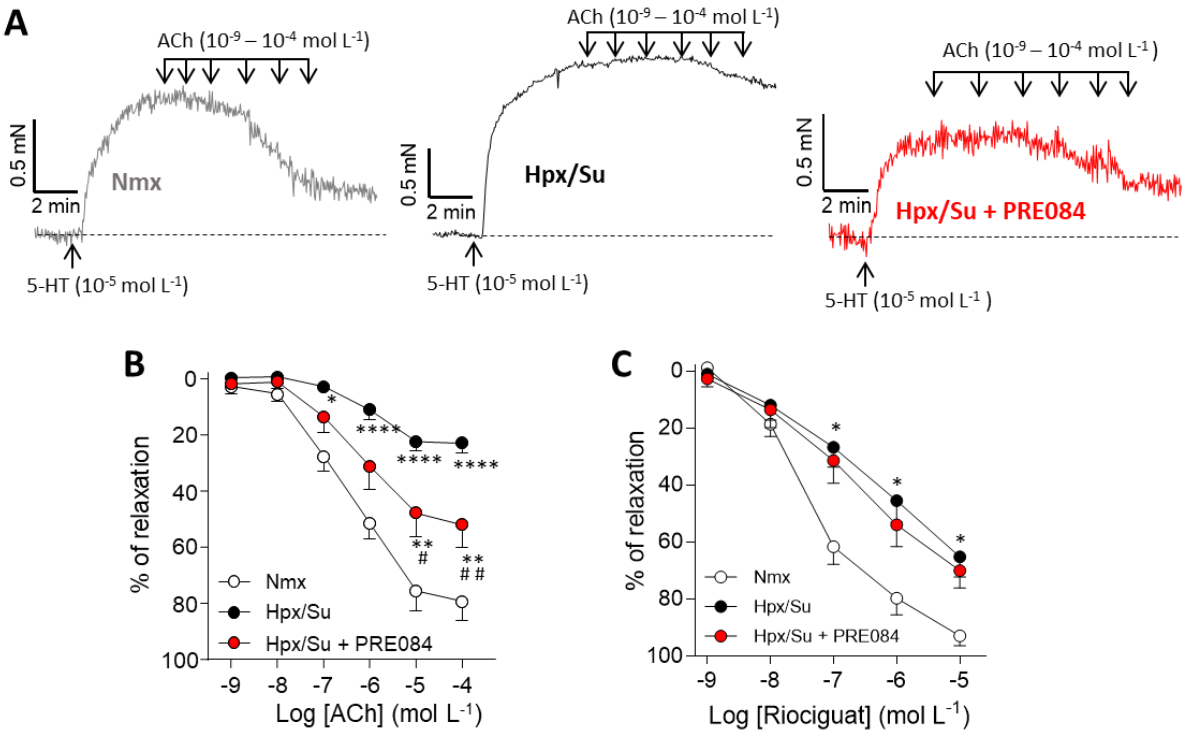

***Figure 26. PRE084 partially attenuates the impaired endothelial-dependent relaxation but not the diminished response to riociguat in PA from Hpx/Su in vivo model of PAH*. (A)** Originals recordings and **(B)** average concentration-dependent relaxant effects to acetylcholine (1 nmol L^{-1}- 100 µmol L^{-1}) on PA precontracted with 5-HT (10 µmol L^{-1}) of the Nmx (grey-white), Hpx/Su (black) and Hpx/Su + PRE084 (red). Points represent mean ± SEM (n = 11, 8 and 10 for Nmx, Hpx/Su and Hpx/Su + PRE084). **(C**) Average concentration-dependent

relaxant effects to riociguat (1 nmol L^{-1}- 10 µmol L^{-1}) on PA precontracted with 5-HT (10 µmol L^{-1}) of the three experimental groups. Points represent mean ± SEM (n = 10, 7 and 8 for Nmx, Hpx/Su and Hpx/Su + PRE084). *, ** and**** $p < 0.05$, 0.01 and 0.0001 *vs* Nmx and # and ## $p < 0.05$ and 0.01 *vs* Hpx/Su (Two-way ANOVA followed by Bonferroni's *post hoc* test).

2.4) PRE084 partially attenuated pulmonary vascular remodelling in Hpx/Su rats

As previously mentioned, pulmonary vascular remodelling is a hallmark of PAH. This was observed in Hpx/Su rats, which showed an increase of the number of detected vessels (Figure 27B) and a higher proportion of fully muscularised PA and a lower proportion of non-muscularised PA (Figure 27A and C). Additionally, muscularised PA from these animals exhibited medial hypertrophy (Figure 27D) and increased vascular occlusion (Figure 27E). PRE084-treated rats showed a reduction in the proportion of fully muscularised PA and an increased proportion of non-muscularised PA, along with a reduced vessel count compared to Hpx/Su-untreated animals (Figure 27B and C). However, no differences were observed in media wall thickness (Figure 27D) or vascular occlusion (Figure 27E) between treated and untreated animals.

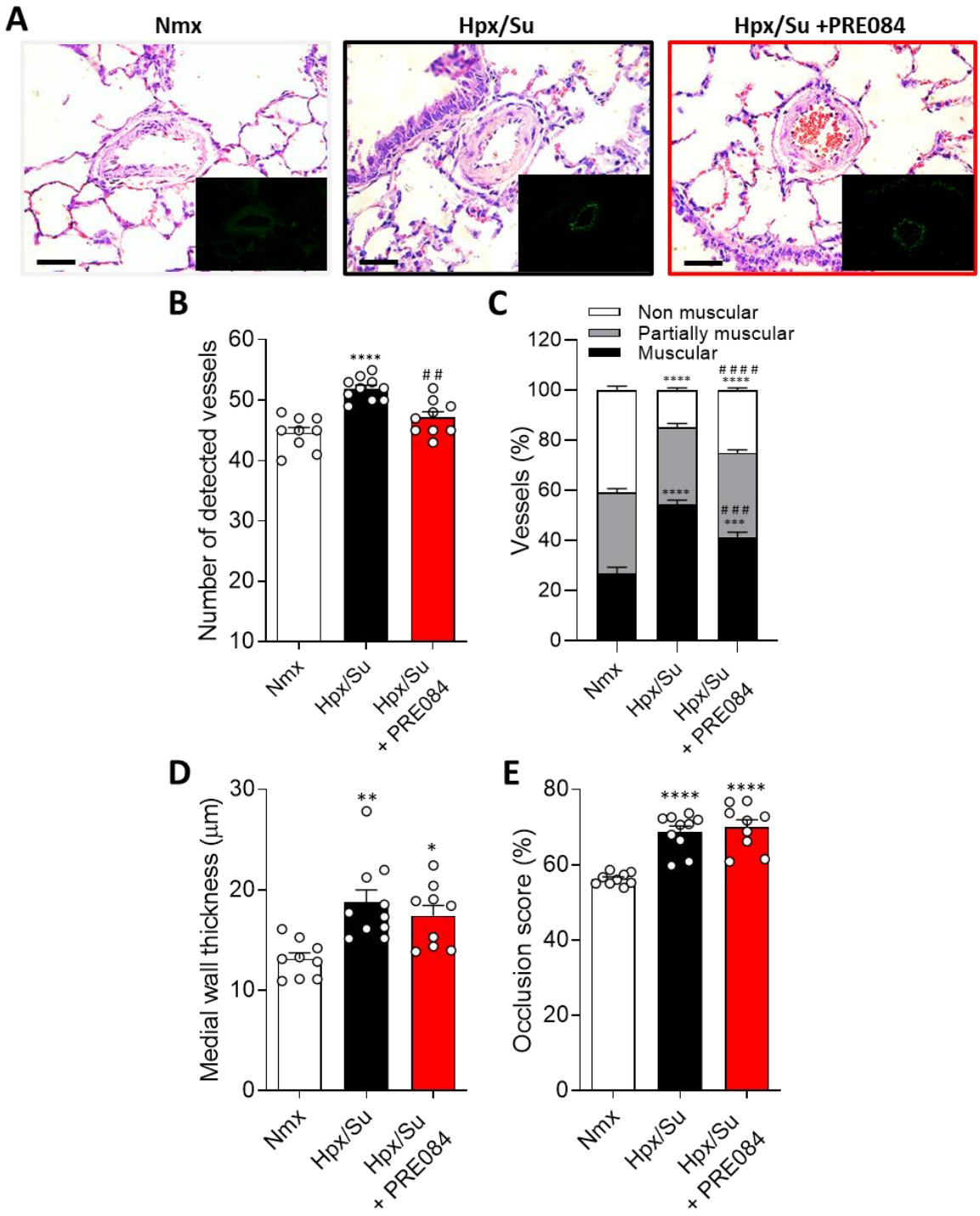

Figure 27. PRE084 attenuates pulmonary vascular remodelling in Hpx/Su-induced PAH rats. **(A)** Representative cross-sectional views of lung histology of Nmx, Hpx/Su and Hpx/Su + PRE084 (scale bar, 50 µm). **(B)** Number of vessels analysed per animal from the three groups. **(C)** Percentage of muscular, partially muscular and non-muscular arteries in the different treatment groups. **(D)** Percent wall thickness of PA and **(E)** luminal occlusion score. Each bar shows the mean ± SEM (n = 9-11 animals in each group). *** and ****p < 0.001 and 0.0001 *vs* Nmx and #### p < 0.0001 *vs* Hpx/Su (one-way ANOVA followed by Boferroni's *post hoc* test).

2.5) PRE084 ameliorates RV dysfunction in Hpx/Su rats

To follow the progression of cardiac and pulmonary disease, all animals of the three groups underwent echocardiographic evaluation before (basal) and at the end of the three-week treatment. As expected, Hpx/Su rats exhibited reduced pulmonary artery acceleration time normalized to ejection time ratio (PAAT/PAET) (Figure 28A) and pulmonary artery velocity-time integral (PAVTI) indicating impaired pulmonary blood flow (Annexes table1). Moreover, these animals also showed signs of RV dysfunction as evidenced by lower TAPSE values. No significant changes were observed in PAAT/PAET and PAVTI between PRE084- and vehicle-treated Hpx/Su rats at the end of the treatment period. However, PRE084-treated rats displayed an improvement in ventricular function, as evidenced by an increase in TAPSE values (Figure 28B).

After echocardiographic evaluation, hemodynamic studies were performed by right heart catheterization to measure right ventricular systolic (RVSP) and diastolic (RVDP) pressures, as well as right ventricle contractility (dP/dTMax) and relaxation (dP/dTMin) to estimate RV function. Figure 28C shows original recordings of RV pressure in the three groups. In line with expectations, rats exposed to Hpx/Su developed an increase in RVSP (Figure 28D) and RVDP (Figure 28E), augmented RV contractility (Figure 28F) and reduced RV relaxation (Figure 28G). Of note, PRE084 treatment significantly attenuated the increased RVSP (Figure 28D) and RV contractility (Figure 28F) and the decreased RV relaxation (Figure 28G) observed in Hpx/Su rats.

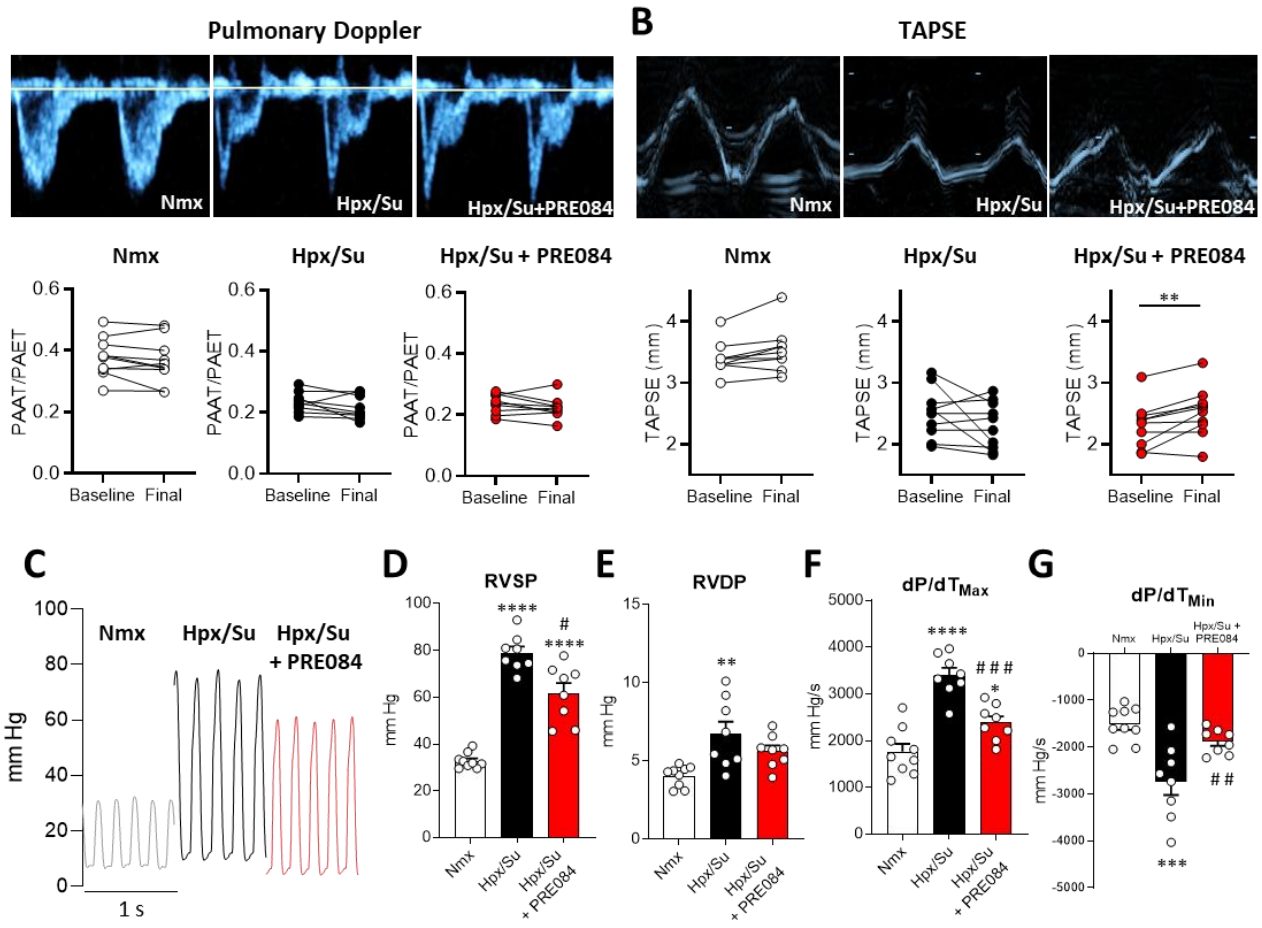

Figure 28. PRE084 attenuated the progression of right ventricle dysfunction in Hpx/Su rats. **(A)** Representative pulse-wave Doppler tracings of Nmx, Hpx/Su and Hpx/Su + PRE084 rats. Pulmonary artery acceleration per ejection time (PAAT/PAET) ratio was assessed before (*basal*) and at the end of the three-week treatment (*final*). **(B)** Tricuspid annular plane systolic excursion (TAPSE) tracings and TAPSE data quantification of the three experimental groups in *basal* and *final* time. n= 8 rats per group. $^{**}p < 0.01$ *basal vs final* (Paired t-test). **(C)** Original recordings of RV pressure in each treatment group. (D) Right ventricular systolic pressure (RVSP) and diastolic pressure (RVDP). **(F)** Rate in pressure change over time during systole (dP/dT_{Max}) and **(G)** diastole (dP/dT_{Min}). Each bar shows the mean ± SEM (*n* = 8-9 animals in each group). For panels D-G *, **, *** and ****$p < 0.05$, 0.01, 0.001 and 0.0001 *vs* Nmx and #, ## and ###$p < 0.05$, 0.01 and 0.001 *vs* Hpx/Su (One-way ANOVA followed by Bonferroni's *post hoc* test).

After recording RV hemodynamics of the RV, the catheter was introduced in the pulmonary artery to measure pulmonary arterial pressure. Hpx/Su animals showed increases in systolic (Figure 29B), diastolic (Figure 29C), and mean (Figure 29D)

pulmonary arterial pressures. Of note, administration of treatment with PRE084 was associated with reduced systolic pulmonary arterial pressure (sPAP) (Figure 29B).

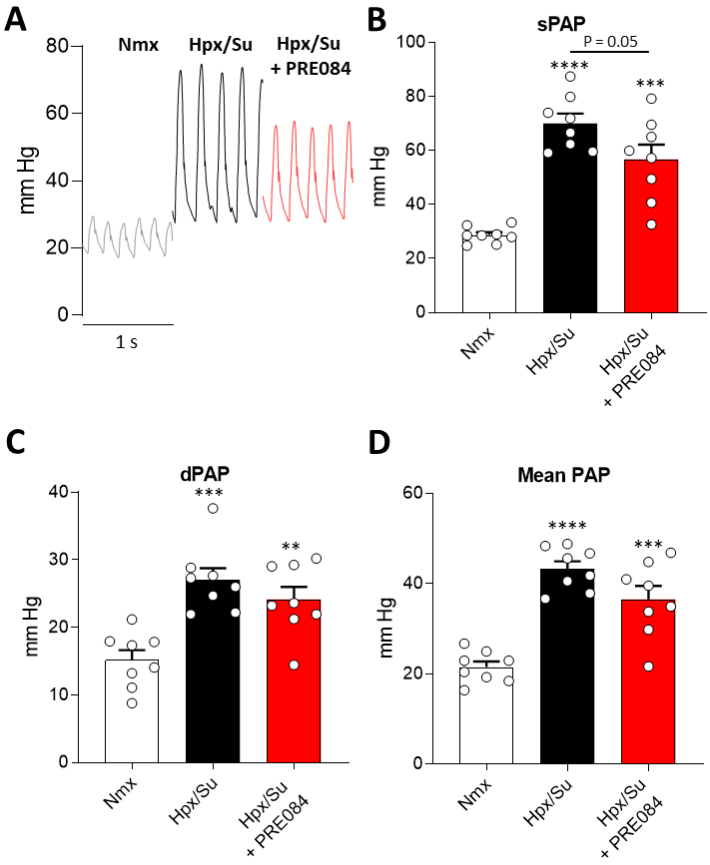

Figure 29. PRE084 tends to attenuate pulmonary hemodynamic alterations in the Hpx/Su PAH model. **(A)** Original recordings of pulmonary pressure in each treatment group. (**B-D)** Systolic, diastolic and mean pulmonary arterial pressure (sPAP, mPAP, and dPAP, respectively) in Nmx, Hpx/Su and Hpx/Su + PRE084. Each bar shows the mean ± SEM (*n* = 8 animals in each group). ****$p < 0.0001$ *vs* Nmx and (One-way ANOVA followed by Bonferroni's *post hoc* test).

2.6) PRE084 attenuates cardiac remodelling in Hpx/Su rats

Consistent with the haemodynamic findings, Hpx/Su rats developed RV hypertrophy, as confirmed by an elevated Fulton index and cardiomyocyte cross-sectional area (CSA), both of chich were significantly reduced by PRE084 treatment (Figure 30B-D). Echocardiographic analysis at weeks 3 and 5 further confirmed the progression of RV hypertrophy in Hpx/Su animals, which was attenuated by PRE084 administration (Figure 30A). Regarding myocardial fibrosis, measured by Sirius Red staining, revealed a significant increase in the Hpx/Su group, which was reversed by PRE084 treatment (Figures 30E–F).

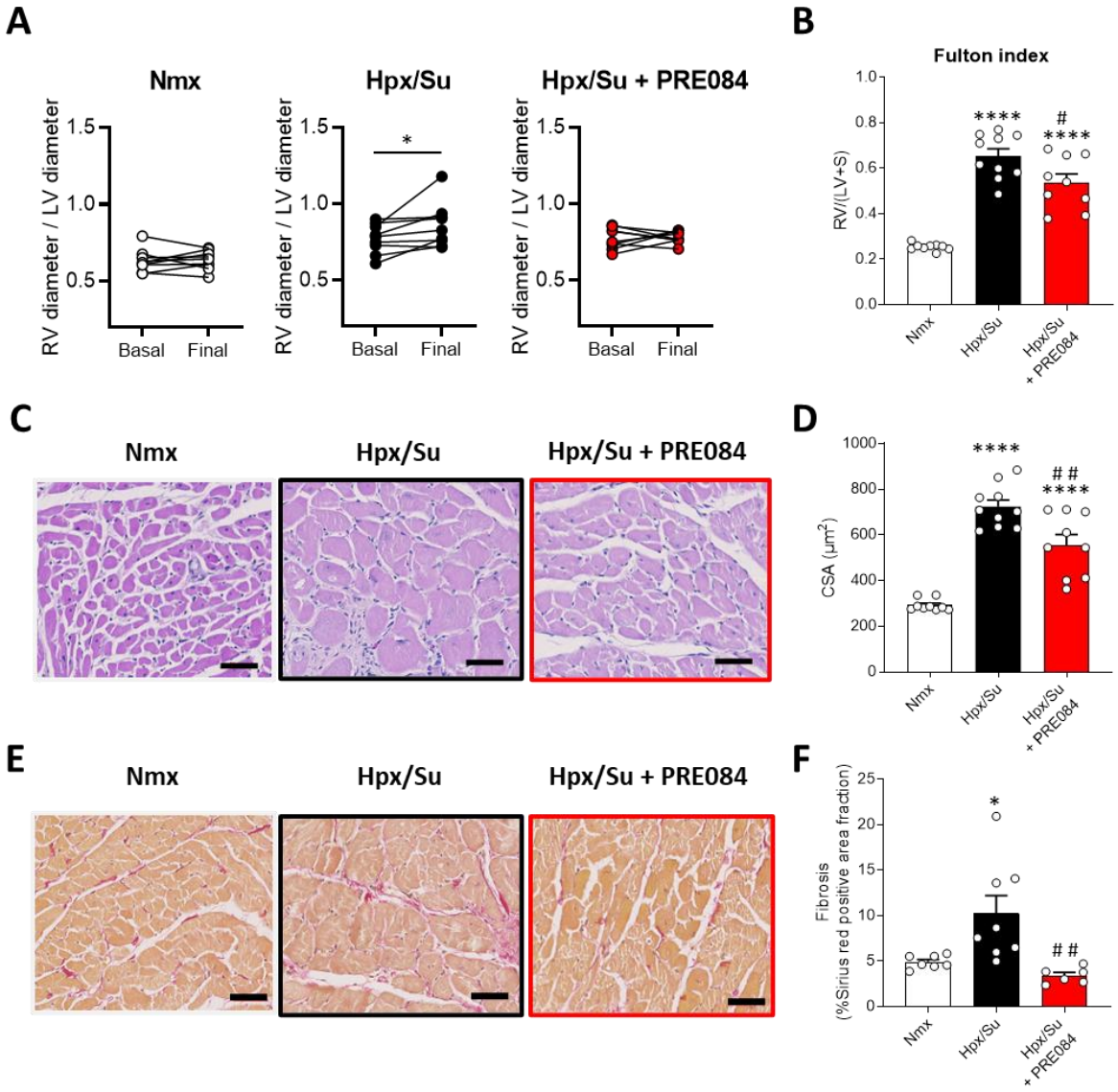

Figure 30. PRE084 attenuates right ventricle remodelling in Hpx/Su rats. **(A)** Ratio of the diameter of the right ventricle (RV) diameter and the left ventricle (LV) was measured before (*basal*) and at the end of the three-weeks treatment (*final*). *$p < 0.05$ *baseline vs* final (Paired t-test). **(B)** Fulton index (RV/LV+S) in the groups. **(C)** Representative cross-sectional views of RV histology stained with hematin/eosin (scale bar, 50 µm) y **(E)** sirius red (scale bar, 50 µm). **(D)** Quantitative analysis of cardiac myocyte cross-sectional area (CSA) and **(F)** the percent of fibrosis. Each bar shows the mean ± SEM (n = 6-10 animals in each group). For panels B, D and F * and ****$p < 0.05$ and 0.0001 *vs* Nmx and # and ## $p < 0.05$ and 0.01 *vs* Hpx/Su (One-way ANOVA followed by Bonferroni's *post hoc* test).

Finally, a metabolic analysis of RV samples detected 4 metabolites which were significantly altered in RV of Hpx/Su rats compared to controls (Figure 31, Supplemental Table 2). Thus, lactate (Figure 31A) was upregulated while glutamine +

carnitine (Figure 31C), creatine (Figure 31B) and inositol (Figure 31D) were downregulated. Of note, RV inositol levels were restored in PRE084-treated (Figure 31D). Furthermore, protein quantification analysis in RV showed that the pAkt/AKT ratio was increased in Hpx/Su and that treatment with PRE084 was able to completely restore it (Figure 31 E-F), while peNOS/eNOS levels were not affected in any of the three groups (Figure 31 G-H).

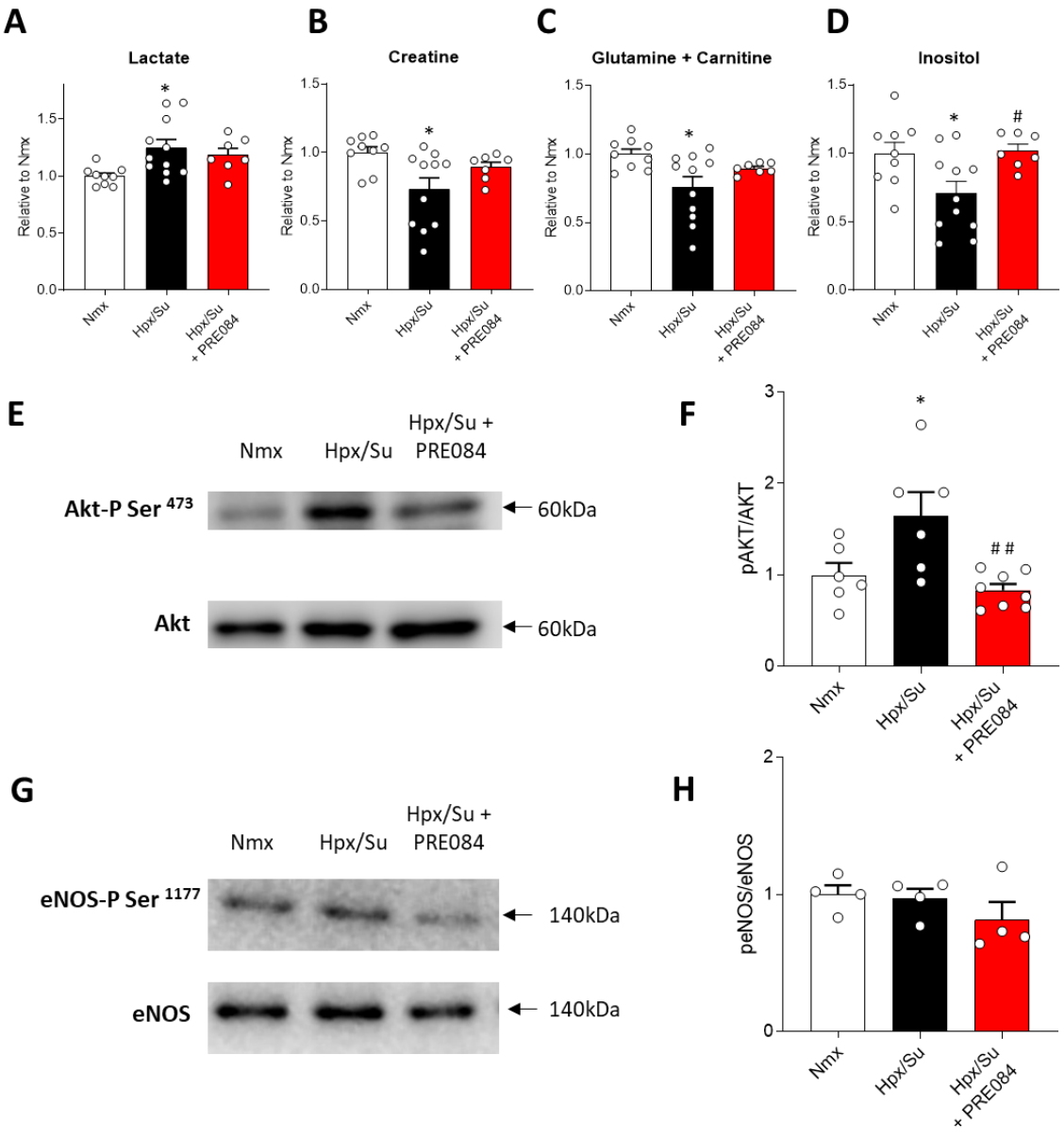

Figure 31. PRE084 attenuates right ventricle inositol levels and ratio pAKT/AKTt in Hpx/Su rats. **(A)** Lactate, **(B)** creatine, **(C)** glutamine and carnitine and **(D)** inositol levels in RV of the three groups. Each bar shows the mean ± SEM (*n* = 7-10 animals in each group). **(E and G)** Representative Western Blot and (F and H) total ratio of pAKT/AKT and peNOS/eNOS protein expression were quantified in RV from the three experimental groups. Each bar shows the

mean ± SEM (*n* = 4-7 animals in each group). * $p < 0.05$ *vs* Nmx and # and ## $p < 0.05$ and 0.01 *vs* Hpx/Su (One-way ANOVA followed by Bonferroni's *post hoc* test).

CHAPTER 3: Modulation of $K_V1.5$ channels by the approved drugs fluoxetine and dimemorfan which exhibit S1R agonist activity

3.1) Dimemorfan and fluoxetine increase K_V1.5 currents in rat PASMCs

Given the role of the S1R in modulating the activity of K_V1.5 channels, in this chapter we assessed the possible modulation of these channels by approved drugs known to exhibit S1R agonist activity. For this purpose, we incubated rat PA for 24 h in the absence or presence of dimemorfan (5 µmol L^{-1}) or fluoxetine (0.3 µmol L^{-1}) and their respective vehicles. Following the isolation of rat PASMCs and whole-cell patch-clamp recordings, incubation with fluoxetine and dimemorfan was found to augment the total K_V current (Figure 32A-B and Figure 33A-B). We then determined whether the K_V1.5 current, which represents the main component of the total K_V current in pulmonary vasculature (Remillard et al., 2007), was enhanced by fluoxetine and dimemorfan. To that end, cells were perfused using 1 µmol L^{-1} of DPO-1, a selective K_V1.5 channel inhibitor, which produced a marked reduction of the K_V currents (Figure 32A and Figure 33A). Therefore, the DPO-1sensitive current that reflects the K_V1.5 channel component was significantly higher in rat PASMCs incubated with fluoxetine and dimemorfan (Figure 32C and Figure 33C). By contrast, these drugs did not affect DPO-1-insensitive currents, which indicates that the augmentation of the K^+ current by both marketed drugs is mainly due to K_V1.5 channels (Figure 32D and Figure 33D). Neither resting membrane potential (Figures 32E and 33E) nor DPO-1-induced membrane depolarization (Figures 32F and 33F) showed significant differences between cells untreated or treated with dimemorfan or fluoxetine.

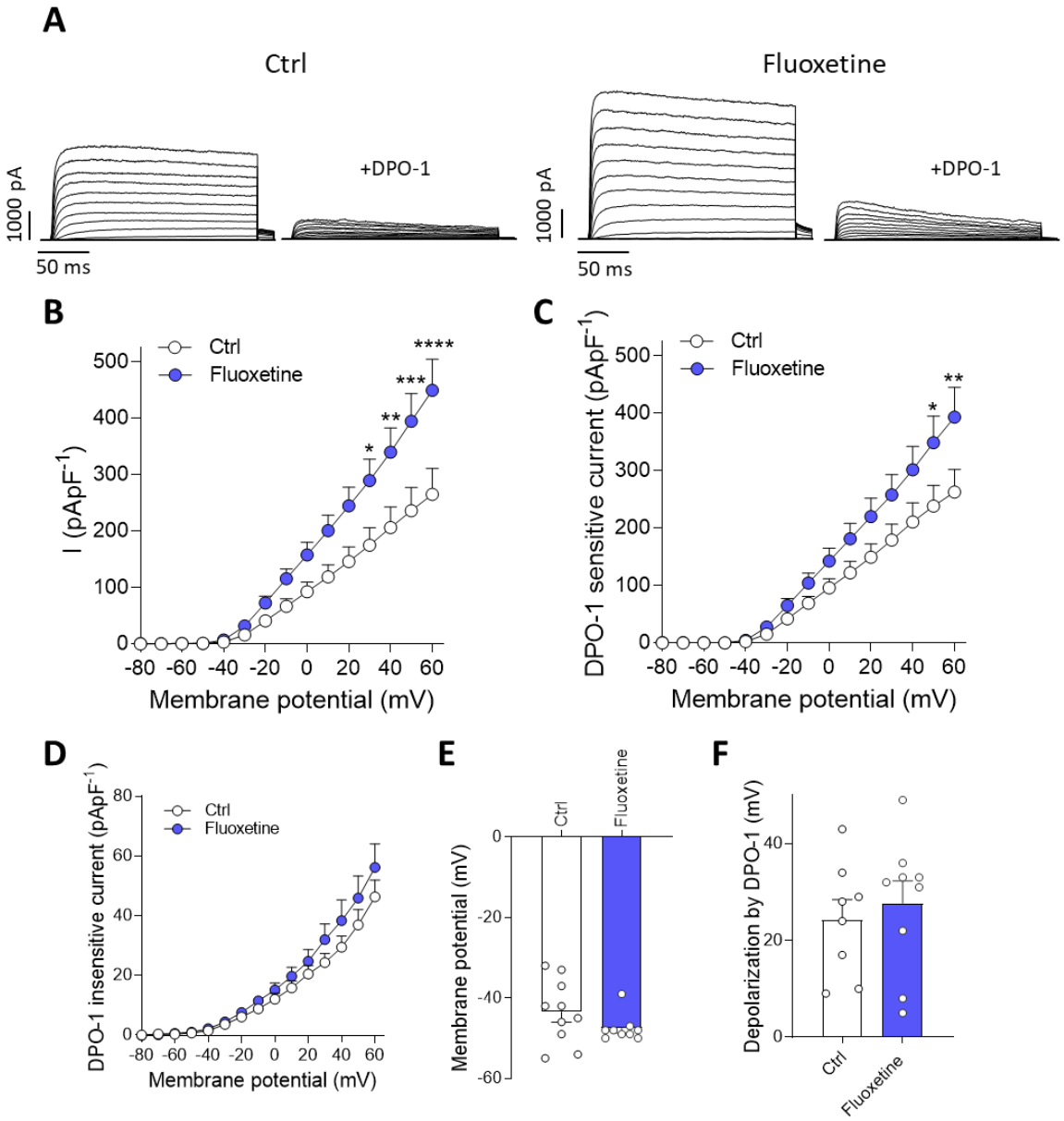

Figure 32. Effects of fluoxetine on K_V currents in freshly isolated rat PASMCs. **(A)** Representative K^+ current traces from rat PASMC after 24 h incubation with vehicle (Ctrl) (*left*) or fluoxetine (0,3 µmol L^{-1}) (*right*). Currents were recorded in the absence and in the presence of DPO-1 (1 µmol L^{-1}). **(B)** K^+ current-voltage relationships measured at the end of the depolarizing pulses and normalized by the cell capacitance after treatment with vehicle (*white*) or fluoxetine (*blue*). **(C)** K^+ current-voltage relationships of the DPO-1 sensitive and **(D)** the DPO-1 insensitive currents. **(E)** Mean values of the resting membrane potential and **(F)** membrane depolarization induced by DPO-1 in control and fluoxetine-incubated rat PASMCs. Points represent mean ± SEM (n= 8-10 cels from n = 5 and 6 rats from Ctrl and with fluoxetine, respectively). *, **, *** and ****p < 0.05, 0.01, 0.001 and 0.0001 *vs* Ctrl. Data were analysed by two-way ANOVA followed by Bonferroni's *post hoc* test in panel B-C-D, and by a two-tailed unpaired student t-test in panels E and F.

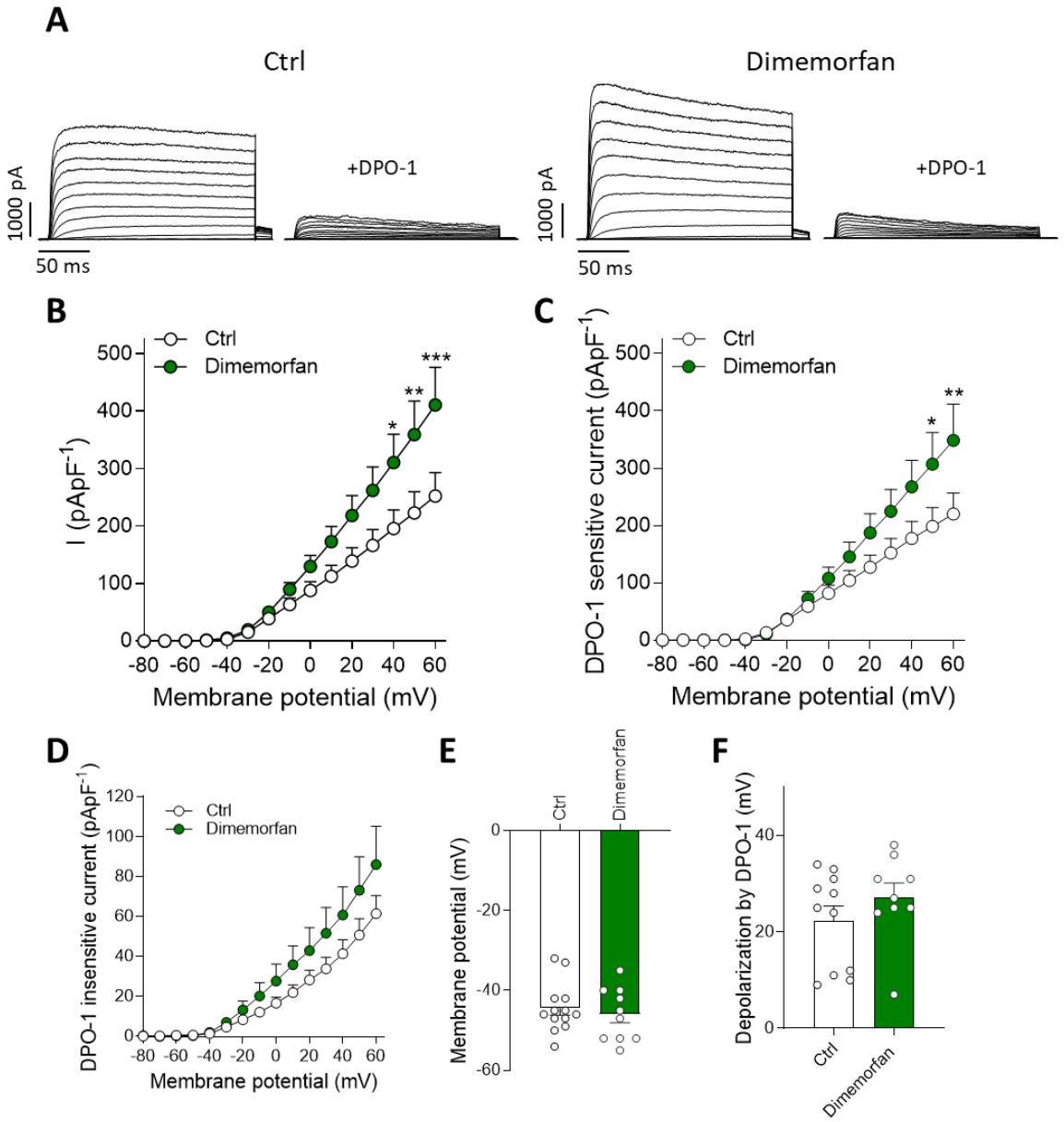

***Figure 33. Effects of dimemorfan on K_V currents in freshly isolated rat PASMCs*. (A)** Representative K^+ current traces from rat PASMC after 24 h incubation with vehicle (Ctrl) (*left*) or dimemorfan (5 µmol L^{-1}) (*right*). Currents were recorded in the absence and in the presence of DPO-1 (1 µmol L^{-1}). **(B)** K^+ current-voltage relationships measured at the end of the depolarizing pulses and normalized by the cell capacitance after treatment with vehicle (*white*) or dimemorfan (*green*). **(C)** K^+ current-voltage relationships of the DPO-1 sensitive and **(D)** the DPO-1 insensitive currents. **(E)** Mean values of the resting membrane potential and **(F)** membrane depolarization induced by DPO-1 in control and dimemorfan-incubated rat PASMCs. Points represent mean ± SEM (n= 9-13 cels from n = 5 and 6 rats from Ctrl and with dimemorfan, respectively). *, ** and *** $p < 0.05$, 0.01 and 0.001 *vs* Ctrl. Data were analysed by two-way ANOVA followed by Bonferroni's *post hoc* test in panel B-C-D, and by a two tailed unpaired student t-test in panels E and F.

3.2) Dimemorfan and fluoxetine increase K_V1.5 mediated S1R activation in rat PASMCs

After this initial characterization of the effects of both drugs, we wanted to determine whether the observed increase in K_V currents was indeed the result of an activation of S1R. For that, rat PA were incubated during 24 h with 10 µmol L^{-1} BD1047, a selective S1R inhibitor, in the absence and in the presence of dimemorfan (5 µmol L^{-1}) or fluoxetine (0.3 µmol L^{-1}). Our patch-clamp data showed that the enhancing effects of fluoxetine and dimemorfan on K_V currents were fully prevented by BD1047, confirming the role of S1R (Figure 34).

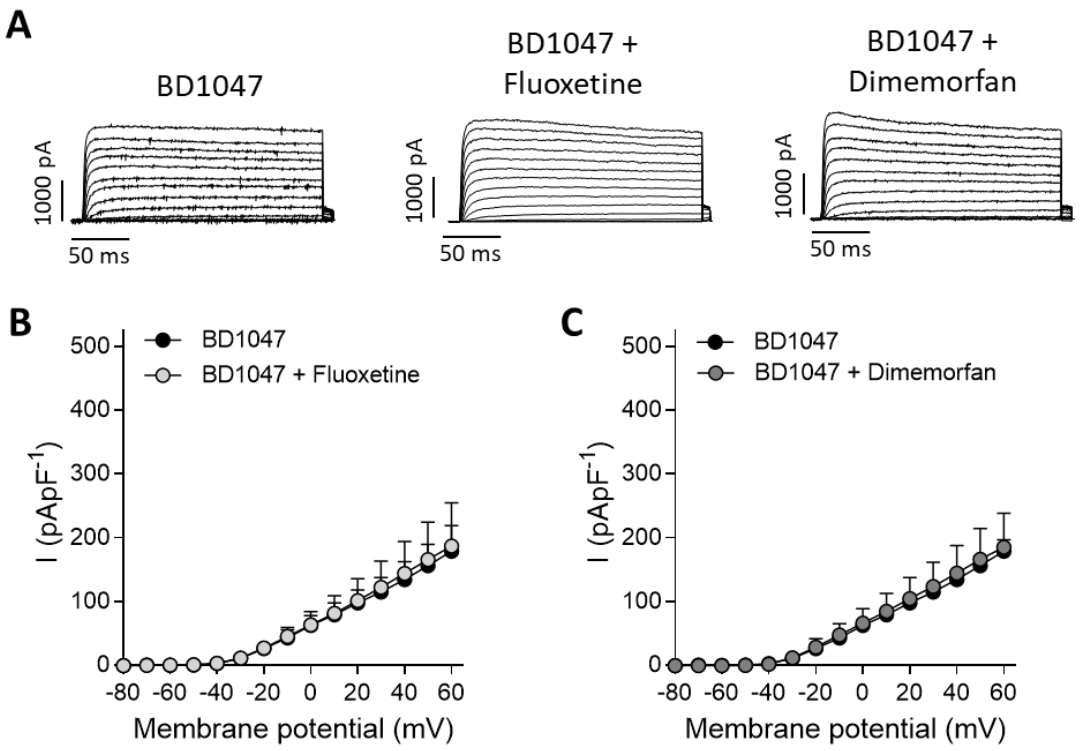

***Figure 34. S1R activation underlies the increase on K^+ currents induced by fluoxetine and dimemorfan*. (A)** Representative K^+ currents traces from rat PASMC following 24 h incubation with BD1047 (10 µmol L^{-1}) (*left*), BD1047 (10 µmol L^{-1}) + fluoxetine (0,3 µmol L^{-1}) (*middle*) and BD1047 (10 µmol L^{-1}) + dimemorfan (5 µmol L^{-1}) (*right*). **(B-C)** K^+ current-voltage relationships measured at the end of the depolarizing pulses and normalized by the cellular capacitance of PASMCs incubated with BD1047, BD1047 + fluoxetine **(B)** or BD1047 + dimemorfan **(C).** Points represent mean ± SEM (n= 12, 12 and 14, respectively, from n = 5 rats per each group). Data were analysed by two-way ANOVA followed by Bonferroni's *post hoc* test.

3.3) Dimemorfan increases K_V1.5 in human PASMCs

Next, we aimed to confirm these findings in human tissue. Therefore, we incubated freshly isolated human PA for 24 h with the vehicle (control) or dimemorfan (5 µmol L^{-1}). Remarkably, dimemorfan caused a pronounced increase in the K_V current present in human PASMCs (Figure 35).

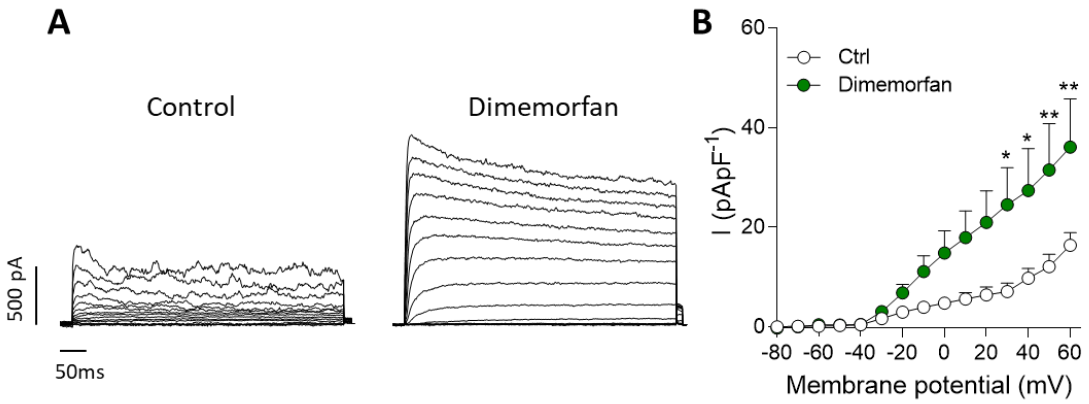

Figure 35. Effects of dimemorfan on K_V currents in freshly isolated human PASMCs. **(A)** Representative K^+ currents traces from human PASMC following 24 h incubation with the vehicle (control) or dimemorfan (5 µmol L^{-1}). **(B)** K^+ current-voltage relationships measured at the end of the depolarizing pulses and normalized by the cellular capacitance of human PASMCs incubated dimemorfan**.** Points represent mean ± SEM (n = 7 cells per group, from n = 3 human sample). Data were analysed by two-way ANOVA followed by Bonferroni's *post hoc* test.

3.4) Dimemorfan does not affect nor modulate the expression of K_V1.5 channels in rat PA

Next, we focused on whether these effects on the increase in K_V1.5 current correlates with an augmentation in channel expression. For this purpose, we incubated rat PA for 24 h in the absence or presence of dimemorfan (5 µmol L^{-1}) with and without BD1047 (10 µmol L^{-1}) and quantified proteins by Western Blot. As it can be seen in Figure 36, no significant changes in K_V1.5 channel expression were observed after incubation with dimemorfan.

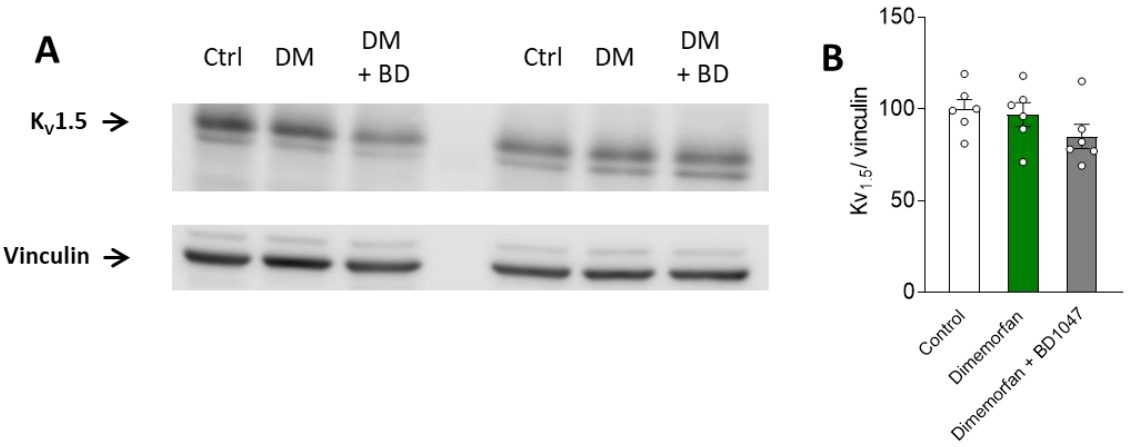

Figure 36. The effects of dimemorfan on K^+ currents are not related to changes in K_V1.5 channel expression in PA. **(A)** Representative Western blot and **(B)** total K_V1.5 protein expression were quantified in rat PA incubated with the vehicle (Ctrl), dimemorfan (5 µmol L^{-1}) or dimemorfan (5 µmol L^{-1}) + BD1047 (10 µmol L^{-1}). Protein expression was normalized by vinculin expression. Data are shown as mean ± SEM of PA from n = 6 animals per group. Data were analysed by two-way ANOVA followed by Bonferroni's *post hoc* test.

3.5) Treatment with dimemorfan and fluoxetine decreases contraction in rat pulmonary arteries through to K_V1.5 enhancement

As mentioned in the introduction, K_V1.5 channel activity and expression are closely associated with the regulation of pulmonary vascular tone. Therefore, we tested whether 24 h incubation with dimemorfan or fluoxetine affects pulmonary vascular reactivity using wire myographs. Of note, both drugs reduced the pulmonary vasoconstriction induced by Phe (Figure 37A-B and Figure 38A-B) and these effects disappeared in the presence of DPO-1 (1 µmol L^{-1}) (Figure 37A and C and Figure 38A and C). This latter strongly suggests that the decrease in contraction observed with fluoxetine and dimemorfan is mainly due to an increase in K_V1.5 channel activity.

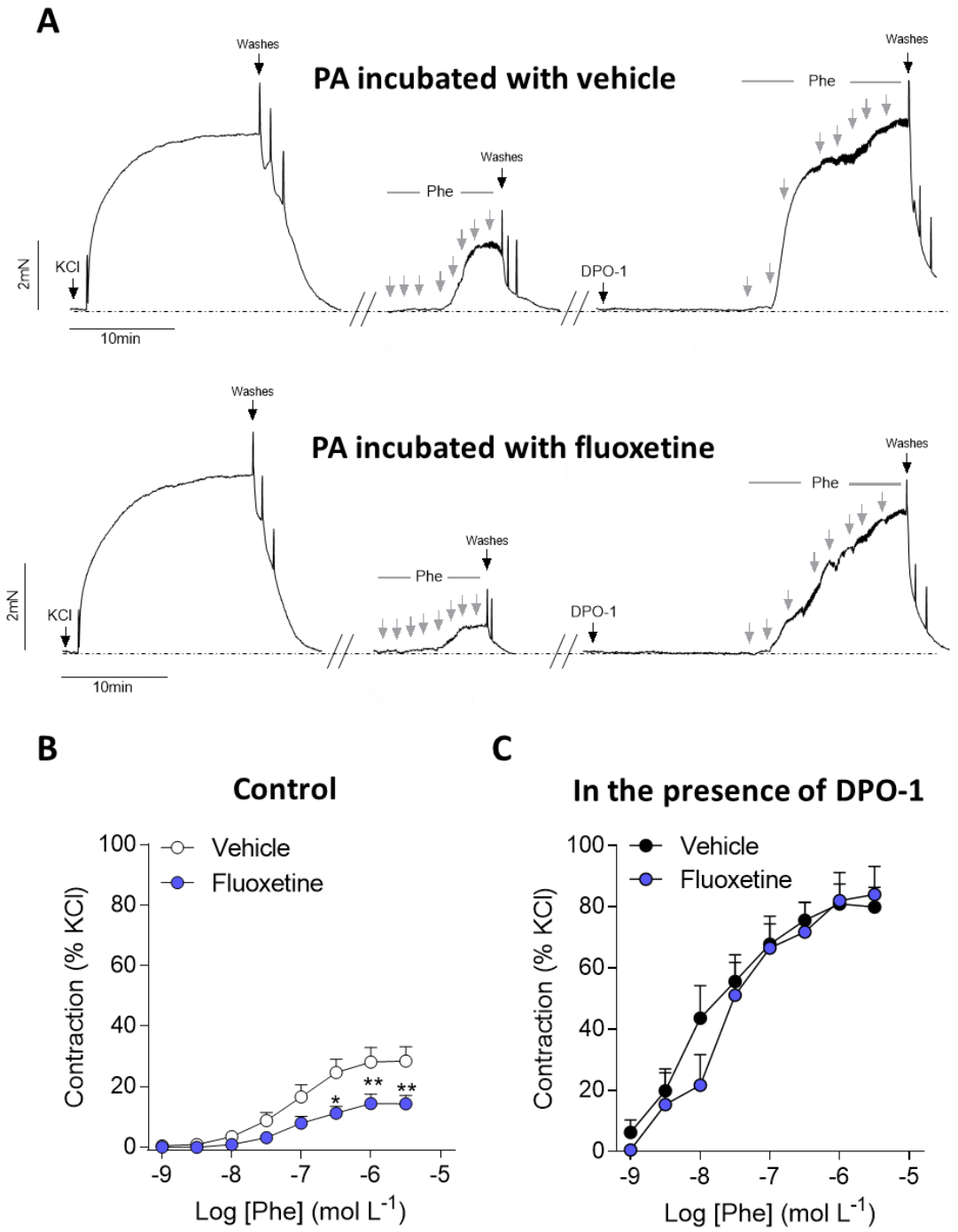

***Figure 37. Treatment with fluoxetine decreases pulmonary vasoconstriction due to $K_V1.5$ channel enhancement*. (A)** Representative recordings of the contraction to KCl (80 mmol L^{-1}) and the concentration-response curves to phenylephrine (Phe) (1 nmol L^{-1}- 3 µmol L^{-1}) in the absence and in the presence of DPO-1 (1 µmol L^{-1}) in PA previously incubated with vehicle (Ctrl) or fluoxetine (0,3 µmol L^{-1}). **(B-C)** Average data of the concentration-response curves to Phe in the absence (B) and in the presence of DPO-1 (C) in PA treated with the vehicle (white) or fluoxetine (blue). Points represent mean ± SEM (n=10 and 8 arteries from n = 6 and 5 animals for vehicle and fluoxetine, respectively). * and ** $p < 0.05$ and 0.01 *vs* vehicle (Two-way ANOVA followed by Bonferroni's *post hoc* test).

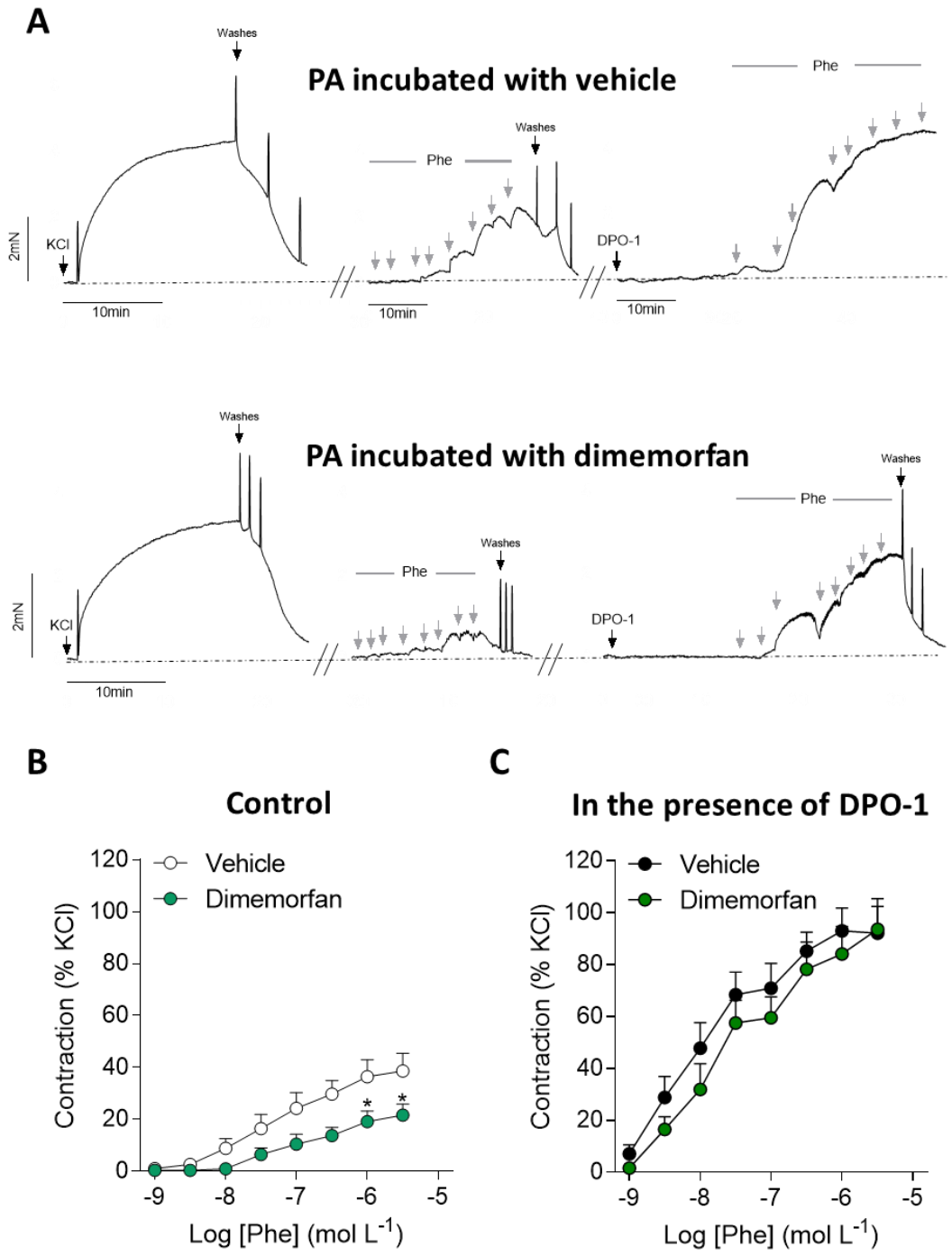

***Figure 38. Treatment with dimemorfan decreases pulmonary vasoconstriction due to K_V1.5 channel enhancement*. (A)** Representative recordings of the contraction to KCl (80 mmol L^{-1}) and the concentration-response curves to phenylephrine (Phe) (1 nmol L^{-1}- 3 µmol L^{-1}) in the absence and in the presence of DPO-1 (1 µM) in PA previously incubated with vehicle (Ctrl) or dimemorfan (5 µmol L^{-1}). **(B-C)** Average data of the concentration-response curves to Phe in the absence (B) and in the presence of DPO-1 (C) in PA treated with vehicle (white) or dimemorfan (green). Points represent mean ± SEM (n =12 and 10 arteries from n = 5 and 7 animals for the vehicle and dimemorfan, respectively). *$p < 0.05$ *vs* vehicle (Two-way ANOVA followed by Bonferroni's *post hoc* test).

3.6) Fluoxetine and dimemorfan enhance KV1.5 activity in PASMCs from hypoxia + SU5416-induced PAH rats

Finally, we studied the possible beneficial effects of dimemorfan and fluoxetine on K_V1.5 channel activity in PASMCs isolated from Hpx/Su PH rats. As expected, K_V currents present in PASMCs from Hpx/Su rats were much lower than those from control rats. Importantly, treatment of PA with fluoxetine or dimemorfan for 24 h was able to markedly increase K_V currents, resulting in a remarkable recovery of attenuated K_V currents characteristic of these PH animals (Figure 39A-B and Figure 40A-B). As can be seen in Figures 39D and 40D, the increase in current induced by fluoxetine or dimemorfan was prevented by BD1047, confirming an involvement of S1R activation. In addition, DPO-1 sensitive currents (Figure 39C and Figure 40C) and DPO-1-induced membrane depolarization (Figure 39F and Figure 40F) were significantly higher in rat PASMCs incubated with fluoxetine or dimemorfan, suggesting an increased contribution of K_V1.5 channel activity in these treated cells. Moreover, fluoxetine and dimemorfan significantly hyperpolarised the resting membrane potential of these cells toward more physiological values, similar to those found in healthy rats. (Figure 39E and Figure 40E).

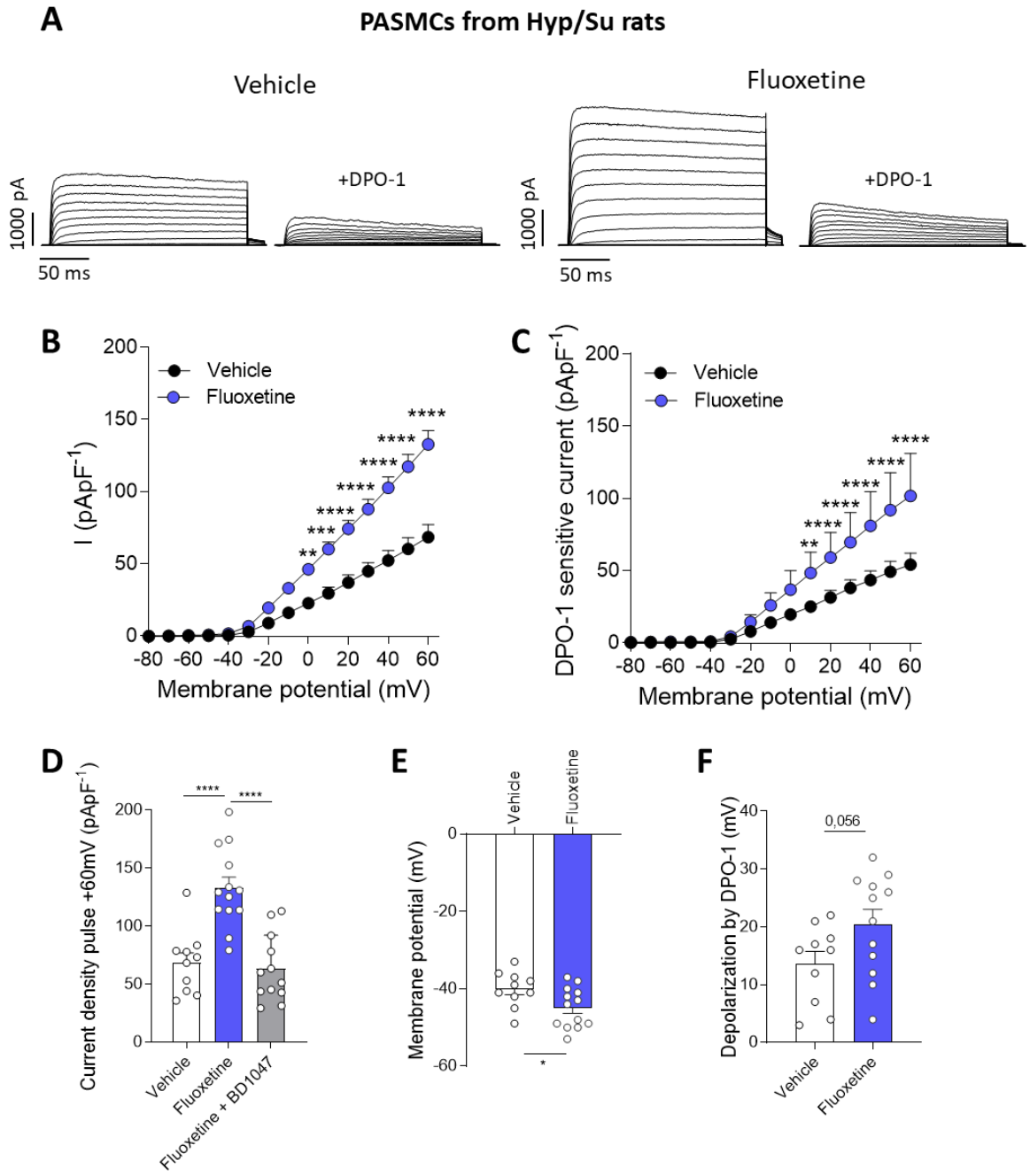

Figure 39. Effects of fluoxetine on K⁺ currents in PASMCs isolated from Hpx/Su rats. **(A)** Representative K^+ currents of PASCM derived from Hpx/Su PH rats after 24 h incubation with the vehicle (*left*) or fluoxetine (0,3 µmol L^{-1}) (*right*). Currents were recorded in the absence and in the presence of DPO-1 (1 µmol L^{-1}). **(B)** Total K_V and **(C)** DPO-1 sensitive current-voltage relationships measured at the end of the depolarizing pulses and normalized by cell capacitance of PASMCs after 24 h incubation with vehicle (*black*) or fluoxetine (*blue*). **(D)** Values of current density at +60 mV in PASMCs after treatment with vehicle, fluoxetine or fluoxetine + BD1047 (10 µmol L^{-1}). **(E)** Mean values of the resting membrane potential and **(F)** membrane depolarization induced by DPO-1. Points represent mean ± SEM (n= 10-13 cells from N= 5 rats). For panel B and C **, *** and ****$p < 0.01$, 0.001 and 0.0001 *vs* Vehicle (Two-way ANOVA followed by Bonferroni's *post hoc* test). For panel D **** $p < 0.0001$ (One-way ANOVA followed by Bonferroni test). For panel E and F * $p < 0.05$ (Unpaired t-test).

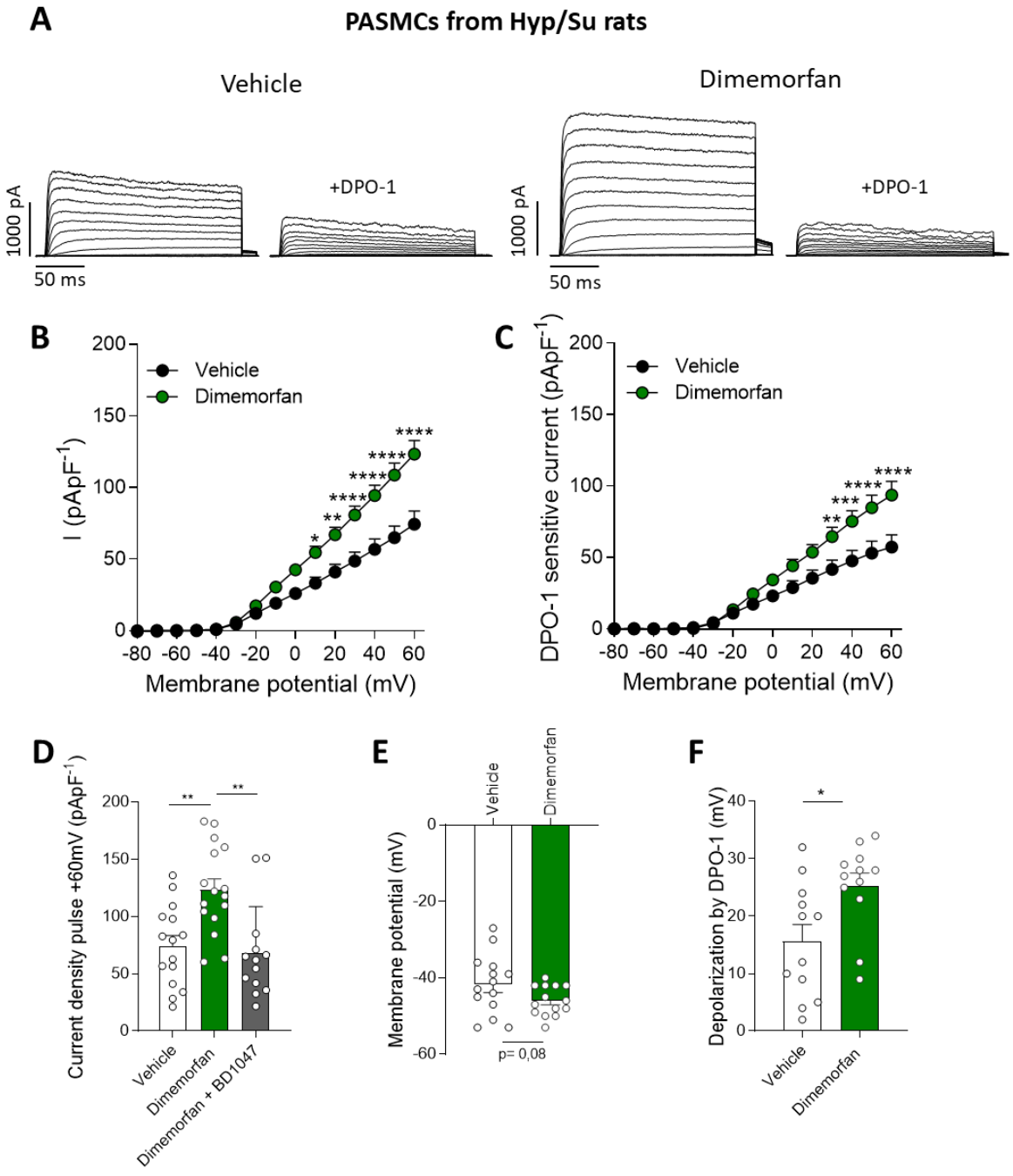

***Figure 40. Effects of dimemorfan on K⁺ currents in PASMCs isolated from Hpx/Su rats*. (A)** Representative K^+ currents of PASCM from PA derived from Hpx/Su PH rats after 24 h incubation with vehicle (*left*) or dimemorfan (5 µmol L^{-1}) (*right*). Currents were recorded in the absence and in the presence of DPO-1 (1 µmol L^{-1}). **(B)** Total K_V and **(C)** DPO-1 sensitive current-voltage relationships measured at the end of the depolarizing pulses and normalized by cell capacitance of PASMCs after 24 h incubation with vehicle (*black*) or dimemorfan (*green*). **(D)** Values of current density at +60 mV in PASMCs after treatment with the vehicle, dimemorfan or dimemorfan + BD1047 (10 µmol L^{-1}). **(E)** Mean values of the resting membrane potential and **(F)** membrane depolarization induced by DPO-1. Points represent mean ± SEM (n = 12-16 cells from n = 5 and 6 rats). For panel B-C *, **, *** and ****$p < 0.05$, 0.01, 0.001

and 0.0001*vs* Ctrl (Two-way ANOVA followed by Bonferroni's *post hoc* test). For panel D ** $p <$ 0.01 (One-way ANOVA followed by Bonferroni test). For panel E and F * $p < 0.05$ (Unpaired t-test).

DISCUSSION

The main objective of this Doctoral Thesis was to identify new pharmacological strategies to improve K_V channel activity in the context of pulmonary hypertension. Our efforts have focused on evaluating novel modulators of K_V7 and $K_V1.5$ channels and determining their potential to improve the attenuated K_V channel activity characteristic of pulmonary vascular diseases such as pulmonary arterial hypertension. Data from this Thesis show URO-K10 as a novel K_V7 channel activator that exhibits an enhanced pharmacological response in the pulmonary vasculature compared to other available activators. Furthermore, S1R is identified as an interesting target to enhance $K_V1.5$ channel activity and improve cardiopulmonary function and remodeling in the context of PH. Finally, the potential of already approved drugs (fluoxetine and dimemorfan) to increase $K_V1.5$ channel activity through their ability to activate S1R is addressed. Taken together, the findings derived from this Doctoral Thesis provide relevant information about several pharmacological strategies to target K_V channels with potential applications for pulmonary vascular diseases such as PH.

In the first chapter of the Thesis, we demonstrate that URO-K10, through the activation of K_V7 channel, increases K_V currents in PASMCs and induces a very potent and effective vasodilation in rat PA, displaying greater efficacy than other K_V7 channel activators. These vascular effects were also confirmed in human PA and notably, URO-K10 exhibits antiproliferative properties in human PASMCs. Unlike retigabine and flupirtine, the action of URO-K10 is not dependent on the auxiliary subunit KCNE4. Furthermore, its vasodilatory effects are enhanced under conditions that mimic the ionic remodelling associated with PAH. Finally, URO-K10 improves vascular responses and K_V currents in PA and PASMCs from the MCT-PH rats. Hence, our findings indicate that URO-K10 is a KCNE4-independent K_V7 channel activator with potent pulmonary vascular activity.

K_V7 channels are key in the regulation of vascular smooth muscle tone, making their activation an attractive pharmacological strategy for the treatment of smooth muscle disorders (Barrese et al., 2018; Borgini et al., 2021; Haick & Byron, 2016; T. Jepps et

al., 2013; Mondejar-Parreño et al., 2020; Stott et al., 2014). Flupirtine and retigabine, K_V7.2-K_V7.5 channel activators previously marketed as analgesic and anticonvulsant drugs respectively, were withdrawn from the market due to adverse effects (Brickel et al., 2012; Michel et al., 2012; Puls et al., 2011). In this context, we evaluated the pulmonary vascular effects of URO-K10, a novel K_V7 channel activator that enhances K^+ currents in K_V7.4- and K_V7.5 channel-expressing HEK293 cells and induces relaxation in mesenteric arteries at low concentration (Lee et al., 2020). We show that URO-K10 was a highly effective relaxant in human and rat PA. Its effect was abolished by XE991, a K_V7 channel inhibitor, but not by the BK_{Ca} channel inhibitor iberotoxin. This supports the idea that the main mechanisms of URO-K10 is the activation of K_V7 channels. Although XE991 did not completely abolish the URO-K10-induced vasodilation, this is line with the fact that, at this concentration, XE991 inhibited but did not fully block K_V7.4 and K_V7.5 currents in HEK293 cells (Lee et al., 2020). The abolition of the URO-K10 sensitive current and the relaxation comparable to the vehicle in the presence of XE991 demonstrate that activation of K_V7 channels represents the main mechanism action of the drug. Patch-clamp experiments in isolated PASMCs showed that URO-K10 significantly increases the amplitude of K_V7 currents at test potentials positive to -30 mV. In line with this, the drug did not alter the resting membrane potential ranging from -51 to -44 mV, indicating a negligible effect under basal conditions. Conversely, in depolarized PASMCs, such as those following vasoconstrictor stimulation, URO-K10 exerted a marked repolarizing effect.

URO-K10 exhibited a much more potent and efficient pulmonary vasodilation than retigabine, flupirtine (present study), and other previously reported K_V7 activators (Mondéjar-Parreño et al., 2020; Morales-Cano et al., 2021). In line with these data, Lee et al., described greater efficacy of URO-K10 in increasing K_V7.4 currents compared to ML213, a K_V7.2-7.5 enhancer (Lee et al., 2020). Importantly, the K^+ channel activation and the stronger pulmonary vasodilatory effects of URO-K10 compared to retigabine were reproduced in human tissues. Although XE991 also blocked these effects in human PA, we were unable to confirm the nature of the URO-K10-induced current in human PASMCs due to limitation of human tissue. Nevertheless, we found clear antiproliferative effects of URO-K10 in human PASMCs,

which contrasts with data reported for retigabine (Mondéjar-Parreño et al., 2020). This antiproliferative effect was attenuated in the presence of XE991, although this should be interpreted with caution due to limited samples size and the possibility that K_V7 blockade may also affect cell viability (Cidad et al., 2012). Taken together, these data indicate that URO-K10 is a novel K_V7 channel opener with pronounced vasodilator and antiproliferative effects on pulmonary vessels.

The pronounced pulmonary vascular effects of URO-K10 suggest a distinctive pharmacological profile compared to most currently available K_V7 enhancers. Retigabine and other structurally diverse K_V7 activators are considered pore-targeted openers, interacting with a conserved tryptophan residue in the channel's pore domain through a carbonyl oxygen present in their molecular structures (R. Y. Kim et al., 2015; Lange et al., 2009; Schenzer et al., 2005; Wuttke et al., 2005). URO-K10 also contains a carbonyl oxygen and point mutations experiments suggest that this compound (Compound 25 in the study of Seefeld MA et al.) likewise binds to the conserved tryptophan residue found in $K_V7.2$- $K_V7.5$ channels (Seefeld et al., 2018). We investigated whether the auxiliary subunit KCNE4 contributes to the higher efficacy of URO-K10 compared to retigabine and flupirtine. In fact, this subunit has been shown to enhance $K_V7.4$ channel function (T. A. Jepps et al., 2015) and to contribute to vasodilation elicited by retigabine and S-1 (Abbott & Jepps, 2016). In agreement with these reports, we found that deletion of KCNE4 attenuated the vasodilatory responses to retigabine and flupirtine. Interestingly, URO-K10-induced vasorelaxation remained unaffected following KCNE4 deletion. These findings are consistent with those by Lee et al., who found that, KCNE4 was not required for URO-K10 to shift the voltage-sensitivity of $K_V7.4$ -7.5 and, in fact, inhibited the effect of URO-K10 on channel conductance (Lee et al., 2020). Our data indicates that KCNE4 is critical for the pulmonary vascular effects induced by retigabine and flupirtine, but not for those mediated by URO-K10.

KCNE4 plays a dual role in modulating both the function and expression of K_V7 channels. For instance, overexpression of KCNE4 has been shown to reduce $K_V7.4$ expression in heterologous systems (Strutz-Seebohm et al., 2006), while paradoxically increasing its presence at the membrane abundance (T. A. Jepps et al.,

2015). Conversely, the knockdown of KCNE4 with morpholino treatment led to decrease in K_V7.4 membrane expression in arterial smooth muscle cells (T. A. Jepps et al., 2015). Additionally, mesenteric arteries from male KCNE4 KO mice exhibit significantly reduced levels of K_V7.4 protein (Abbott & Jepps, 2016). Consistent with these data, we observed that KCNE4 deletion resulted in diminished total K_V7.4 protein expression. Interestingly, this downregulation of K_V7.4 did not affect URO-K10 induced vasorelaxation. This was unexpected, considering that URO-K10 directly activates K_V7.4 channels (Lee et al., 2020), which are considered main contributors of the K_V7 channel family in the vascular tissues. However, it's important to consider that KCNE4 deletion does not affect K_V7.5 protein expression, and that URO-K10 can also activate K_V7.3 and K_V7.5 channels, albeit less efficiently (Seefeld et al., 2018). Therefore, it is possible that activation of other K_V7 subtypes channels may compensate for the moderate (by a 25%) reduction in K_V7.4, thereby preserving URO-K10-induced relaxation in arteries treated with KCNE4-targeting morpholinos. Supporting this idea, previous studies have shown that downregulation of K_V7.4 channels does not affect relaxation of some K_V7 channel agonists. For example, mesenteric artery dilation in response to ML-213 was not affected in female *KCNE4* KO mice despite clear K_V7.4 downregulation (Abbott & Jepps, 2016).

PAH is commonly associated with the downregulation of various K^+ channels, particularly K_V1.5 and TASK-1 channels (Antigny et al., 2016; Gurney et al., 2003; Lambert, Boet, et al., 2018; Mondejar-Parreño et al., 2019; Morales-Cano et al., 2014; Olschewski et al., 2017; Wang et al., 1997; J. X.-J. Yuan et al., 1998; X.-J. Yuan et al., 1998). Based on this, we decided to evaluate the effects of URO-K10 under conditions that mimic the ionic remodelling characteristic of PAH by pharmacologically inhibiting K_V1.5 and TASK-1 channels. In a previous study using this approach, we observed that retigabine-induced K^+ currents, membrane hyperpolarization and vasodilation were significantly enhanced (Mondéjar-Parreño et al., 2020). In that context, we also detected an increased presence of KCNE4 at the cell membrane and suggested that this subunit might be involved in the enhanced effects observed with retigabine. Herein we found that pulmonary artery relaxation induced by URO-K10 was also enhanced in the presence of K_V1.5 and TASK-1 blockers. However, the

URO-K10-sensitive K^+ current did not differ from that observed under control conditions. This leads us to speculate that while KCNE4 may play a role in the electrophysiological and vascular effects of retigabine ad similar compounds, it may not be involved in the effects mediated by URO-K10. Although the precise mechanism behind the increased hyperpolarization and relaxation induced by URO-K10 remains unclear, it is likely that the drug exerts stronger effects when the membrane is more depolarized, close to the voltage threshold of K_V7 channel activation, as occurs in the case when $K_V1.5$ and TASK-1 channels are inhibited.

The impairment of the NO/cGMP and the PGI_2 signalling pathway is a hallmark in PAH (Galiè et al., 2019; Klinger & Kadowitz, 2017; Schermuly et al., 2011). Current therapeutic strategies for PAH, including sildenafil, riociguat and selexipag, primarily target these pathways by enhancing NO/cGMP signalling or activating the prostacyclin receptor. Notably, K_V7 channel activation has been shown to contribute significantly to the vasodilatory effects of both riociguat and sildenafil (Al-Chawishly et al., 2022; Mondéjar-Parreño et al., 2019), and more recently, have been also implicated in the selexipag-induced vasodilation (Baldwin et al., 2022). Interestingly, although the vasodilatory response mediated by NO/cGMP pathway is often diminished in various models of PH (Christou et al., 2018; Mam et al., 2010; Milara et al., 2016; Sikarwar et al., 2018), the effects of $K_V7$channels activators tend to be preserved or even improved (Mondéjar-Parreño et al., 2020). In line with this, we observed similar behaviour for URO-K10, but noteworthy, this novel K_V7 agonist can achieve a full vasodilation in PA from PH models. Additionally, URO-K10-induced K^+ currents were significantly greater in PASMCs from PH animals compared to those from healthy animals.

In the second chapter of the Doctoral Thesis, we investigated the therapeutic potential of the S1R agonist PRE084 in the Hpx/Su PAH model. We found that *in vivo* administration of PRE084 in pulmonary hypertensive rats significantly attenuated pulmonary vasoconstriction, improved endothelial and RV function, and reduced RV pressure and hypertrophy. These protective effects were associated with enhanced

K_V1.5 channel activity in PASMCs, as well as inhibition of the PI3K/Akt signalling pathway and restoration of inositol levels in the RV. Taken together, these results support the concept that targeting S1R may represent a promising multi-faceted therapeutic strategy in PAH.

S1R is a multimodal chaperone protein engaged in numerous pathophysiological processes. It exhibits pleiotropic signalling and acts as a multifunctional inter-organelle signalling protein, regulating a variety of cellular functions such as protein folding, oxidative stress, inflammation, apoptosis, angiogenesis, and cell proliferation among others. S1R is also involved in ion channel regulation, endoplasmic reticulum-mitochondrial communication, lipid metabolism, and mitochondrial homeostasis. Therefore, due to its versatility, S1R has been suggested as a potential target for several cardiovascular diseases (Lewis et al., 2020; Munguia-Galaviz et al., 2023).

As mentioned in the Introduction section, a hallmark of PAH pathophysiology is the downregulation of K^+ channels, particularly K_V1.5 and TASK-1, in pulmonary vasculature. This ionic remodelling contributes to membrane depolarization of PASMCs, pulmonary vasoconstriction, hyperproliferation and impaired apoptosis (Boucherat et al., 2015; Mondejar-Parreño et al., 2019; Mondéjar-Parreño et al., 2021; Vera-Zambrano, Lago-Docampo, et al., 2023; X. J. Yuan et al., 1998). We have previously reported that S1R finely regulates K_V1.5 channel activity and that PRE084, S1R agonist, enhances K_V1.5 current in PASMCs *in vitro*, thereby limiting pulmonary vasoconstriction and proliferation (Vera-Zambrano, Baena-Nuevo, et al., 2023).

In the present Thesis we provide evidence that such phenomena also occur after *in vivo* administration of PRE084. Importantly, this drug partially restored the downregulated K^+ currents observed in PASMCs from PH animals, specially increasing DPO-1-sensitive currents while leaving DPO-1-insensitive currents unchanged. This suggests a selective enhancement of K_V1.5 channel activity by the S1R agonist. Nevertheless, we cannot exclude that other K^+ channels such as K_V1.2, which is also regulated by S1R (Kourrich et al., 2013) and may be downregulated in PH, may also improve with PRE084 treatment. The enhancement of K_V1.5 channel

activity due to PRE084 treatment was reflected in an increased effects of DPO-1 on membrane potential and on pulmonary vascular reactivity. Notably, PRE084 shifted the resting membrane potential of PASMCs toward more negative values than those observed in cells from Hpx/Su animals, effectively restoring the levels found in PASMCs from Nmx animals. In line with this, treatment with PRE084 dampened the enhanced pulmonary vasoconstriction found in PH animals. Intriguingly, these functional changes were not associated with an increase in total $K_V1.5$ protein expression in pulmonary arteries. However, membrane localization of $K_V1.5$ in isolated PASMCs was significantly increased, suggesting enhanced channel trafficking to the cell surface. Similarly, S1R activation does not affect total $K_V1.2$ expression but induces its trafficking to the plasma membrane in the nucleus (Kourrich et al., 2013). Interestingly, S1R expression was upregulated in Hpx/Su PA, which may potentiate the effects of S1R agonist, like PRE084, under these pathological conditions. In this regard, *in vivo* treatment with PRE084 increased $K_V1.5$ currents to a higher extent than observed *in vitro* in control animals (Vera-Zambrano, Baena-Nuevo, et al., 2023). Finally, PRE084 treatment also partially ameliorated the pulmonary endothelial dysfunction found in Hpx/Su model, which could be attributed to its anti-inflammatory actions. Thus, PRE084 has been shown to protect against endothelial cell inflammation and permeability in acute lung injury (Mahamed et al., 2023).

In addition to the improvements in pulmonary vascular function, PRE084 treatment also exerted beneficial effects on pulmonary vascular remodelling. It reversed the increased membrane capacitance observed in PASMCs from Hpx/Su rats, suggesting antihypertrophic effects at cellular level. Moreover, the lungs of Hpx/Su animals displayed an increased number of detected vessels, a higher percentage of muscularized vessels and a reduced percentage of non-muscularized arteries, as previously reported (Serdjebi et al., 2024), which were substantially restored by PRE084 treatment. However, no significant differences were observed in medial layer thickening or vessel occlusion between PH and PRE084-treated animals, which could explain the more pronounced effect of PRE084 on RV pressure compared to pulmonary arterial pressure. In line with our findings, fluvoxamine, an antidepressant

with S1R agonistic properties, was shown to improve RV function in the monocrotaline model of PH with negligible effects on pulmonary arterial pressure (Sun et al., 2022).

RV dysfunction is considered a critical determinant of PH outcome (Hsu et al., 2016; Vonk-Noordegraaf et al., 2013). As expected, both RV contractile and diastolic dysfunction were found in Hpx/Su rats, which were clearly ameliorated by PRE084 treatment. Consistent with our data, marketed drugs displaying S1R agonistic properties such as fluvoxamine, fluoxetine or dehydroepiandrosterone have been shown to improved RV function in other rat models of PH (Sun et al., 2022; Zhai et al., 2009; Y.-T. Zhang et al., 2019). Likewise, S1R activation has been reported to improve cardiac function in a rat model of post-infarction heart failure (Zhao et al., 2022).

Cardiac hypertrophy and fibrosis contribute to the development of RV remodelling and heart failure in PAH (Vonk-Noordegraaf et al., 2013). PRE084 treatment significantly reduced cardiomyocyte hypertrophy and ventricle wall thickness. Consistent with other studies, we found increased collagen deposition in the RV of Hpx/Su rats, assessed by Sirius red staining (Milano et al., 2025; Mirani et al., 2025). This effect was substantially reduced by PRE084, suggesting alleviation of RV fibrosis development. Taken together, our data indicate that PRE084 slows the progression of RV dysfunction and remodelling in PH.

The cardioprotective effects of S1R agonists have been attributed to their ability to modulate cell proliferation, growth, apoptosis, fibrosis and angiogenesis through multiple signalling cascades (Almaamari et al., 2025; Lewis et al., 2020; Munguia-Galaviz et al., 2023). In our study, RV from PH animals showed no changes in eNOS or p-eNOS expression, but elevated levels of the anti-apoptotic protein Bcl-2, which were unaffected by PRE084 treatment. Notably, the p-Akt/Akt ratio was increased in RV from Hpx/Su rats, indicating the activation of PI3K/Akt pathway, which plays a role in cell growth and survival and has been associated with RV hypertrophy due to pressure overload (Yang et al., 2014). Similarly, up-regulation of p-Akt has been reported in rodent lungs with hypoxia-induced PH (Tang et al., 2015), PASMCs from PAH patients (Tang et al., 2015), and in hypertrophied human right atria (Yang et al., 2014). Moreover, deletion of Akt attenuates hypoxia-induced PH and RV

hypertrophy (Tang et al., 2015). Notably, PRE084 treatment reversed the p-Akt up-regulation, suggesting that modulation of the PI3K/AKT pathway may contribute to its protective effects on RV hypertrophy.

Our metabolic analysis revealed increased levels of lactate and decreased levels of glutamine + carnitine, creatine and inositol in RV from Hpx/Su. These results were also shown in a recent study by Banerjee S et al (Banerjee et al., 2022) in PH rats induced by Hpx/Su or monocrotaline. Importantly, PRE084 treatment restored inositol levels in the RV. Inositol 1,4,5-trisphosphate (IP3) plays a critical role as an intracellular second messenger involved in cardiac homeostasis, participating in excitation–contraction coupling and electrical signalling. Reduced levels of myo-inositol can disrupt these processes and have been associated with cardiac dysfunction after myocardial infarction (McKirnan et al., 2019). Moreover, supplementation with inositols ameliorates cardiac dysfunction and hypertrophy induced by high-fat diet (L'Abbate et al., 2020) and lithium (L'Abbate et al., 2024). Thus, normalization of inositol levels due to PRE084 treatment may contribute to the observed improvements in RV function and structure.

These findings demonstrate that PRE084 markedly improves both functional and morphological alterations associated with PH but could not restore them completely. Importantly, our experimental design focused on evaluating the therapeutic efficacy of PRE084 in an established model of PAH, thereby it more closely resembles the real clinical situation. However, this approach is more challenging than preventive strategies when it comes to demonstrating drug efficacy. In fact, numerous drugs have shown beneficial effects in a preventive but not in a therapeutic approach (Antigny et al., 2016; Chaudhary et al., 2021; Huh et al., 2011; Sztuka et al., 2018).

PAH is a complex and multifactorial disease which involve a great number of cellular processes and mechanisms (Bousseau et al., 2023; Humbert et al., 2019; Rabinovitch et al., 2014); consequently, targeting a single mechanism is often insufficient. In fact, combination therapies targeting different pathways are the current standard of care in PAH (Chin et al., 2024). In this regard, the multifunctional nature of the Sigma-1 receptor, through the modulation of a variety of intracellular

signalling pathways, makes it a potential pharmacological target of great interest in PAH.

To further evaluate other more viable strategies targeting S1R, in the final chapter of the Doctoral Thesis, we assessed the potential of approved drugs (i.e. fluoxetine and dimemorfan) with S1R agonistic properties to enhance K_V1.5 channel activity in PA. Drug repurposing aims to find new therapeutic applications for existing drugs, but the process still presents significant challenges in disease treatment. It offers potential benefits like reduced development time and costs, but it faces hurdles such as financial and regulatory barriers, and the need for robust clinical evidence (Recino et al., 2025). As outlined in the Introduction, PAH is a rare disease associated with poor prognosis and with few effective therapies available. In particular, little attention has been given to the ionic remodelling characteristic of the disease as a therapeutic target. Thus, we took advantage of the identification of S1R as a potential target for enhancing K_V1.5 channel activity in order to evaluate the ability of approved drugs with S1R agonist activity to enhance channel activity. In this regard, several approved drugs exhibit S1R agonist activity, though this may not be their primary mechanism of action. These include, among other, certain antidepressants like fluoxetine and fluvoxamine (Hashimoto, 2015; Ishima et al., 2014) and the cough suppressants dimemorfan and dextromethorphan (Nguyen et al., 2014; Y. Shen et al., 2008). In the present Thesis we have evaluated the effects of fluoxetine and dimemorfan and found that both drugs were indeed highly effective to increase K_V1.5 current through S1R activation.

Previous studies have shown that fluoxetine exerts protective effects in monocrotaline-induced HAP (Guignabert et al., 2005; Zhai et al., 2009) and in mice with SM22α-targeted overexpression of the serotonin transporter (5-HTT) (Guignabert et al., 2009). This led to the assumption that inhibition of the 5-HTT was responsible for the observed beneficial effects of fluoxetine (Guignabert et al., 2005, 2009). Although previous studies have suggested that the protective effects of fluoxetine may be associated with an increase in K_V1.5 channel expression (Dai et al., 2012; Zhai et al., 2009), our study is the first to demonstrate a clear augmentation of K_V1.5 channel activity by the drug, independent of changes in protein expression.

Fluoxetine and other antidepressants from the same pharmacological group (5-HTT inhibitors) are considered highly selective for blocking serotonin reuptake, rather than that of norepinephrine or dopamine. However, they are not entirely specific and can still act on additional targets, including S1R and acid sphingomyelinase, having some off-target effects, that may contribute to a range of potential beneficial or side effects (Di Rosso et al., 2016; Gulbins et al., 2013; Xiao et al., 2025). In our study, we found that the electrophysiological effects of fluoxetine on PASMCs were prevented by a S1R antagonist. Moreover, this profile (enhancement of K_V1.5 currents without changes in protein expression) was similar to that observed with the selective S1R activator PRE084. Moreover, this profile was shared with the chemically unrelated drug dimemorfan, which also has S1R agonist activity. Taken together, these data demonstrate that fluoxetine and dimemorfan are effective enhancers of the K_V1.5 channel through S1R activation. Remarkably, the effects of dimemorfan on K_V1.5 channel activity were also confirmed in freshly isolated human PASMCs.

As we had observed with the selective S1R agonist PRE084, the increase in K_V1.5 channel activity induced by fluoxetine or dimemorfan was associated with a significant reduction in pulmonary vasoconstriction, which was prevented in the presence of the K_V1.5 channel blocker DPO-1. These data indicate that the increase in K_V1.5 channel activity induced by these drugs limits cell depolarisation in response to vasoconstrictor stimuli, leading to a reduction in pulmonary vascular tone. It is significant that fluoxetine and dimemorfan were also able to markedly improve K_V1.5 channel activity and restore resting membrane potential values in PASMCs from animals with PH. Altogether, these data strongly suggest that these drugs may represent a viable strategy for rescuing the attenuated activity of these channels in the context of this disease.

This Doctoral Thesis provides relevant insights into new avenues aimed at improving the activity of K_V channels in pulmonary circulation. In particular, both the new K_V7 channel activator with an improved profile, URO-K10, and drugs modulating K_V1.5 channels via S1R may represent promising pharmacological strategies for enhancing K_V channel function in various clinical applications, such as PAH.

GRAPHICAL ABSTRACT 1

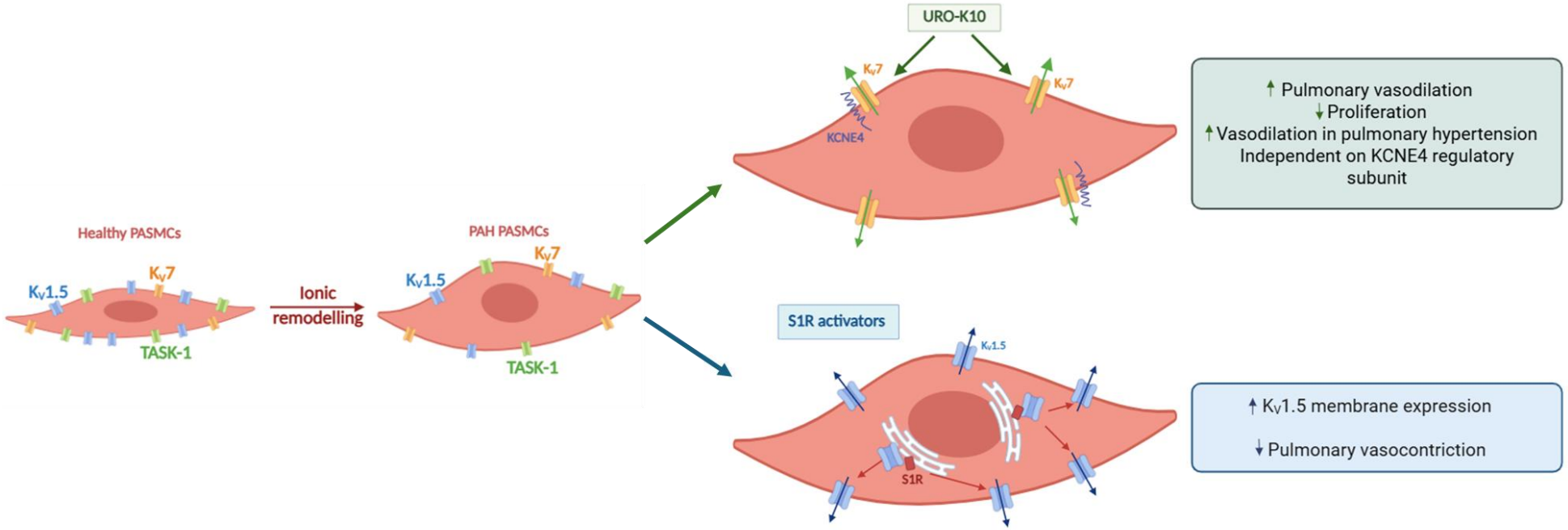

Figure 41: Graphical abstract. The thesis aims to counteract the ionic remodelling characteristic of pulmonary arterial hypertension through two complementary approaches: (1) enhancing K_V7 currents via the modulator URO-K10, and (2) increasing $K_V1.5$ currents through activation of the sigma-1 receptor.

GRAPHICAL ABSTRACT 2

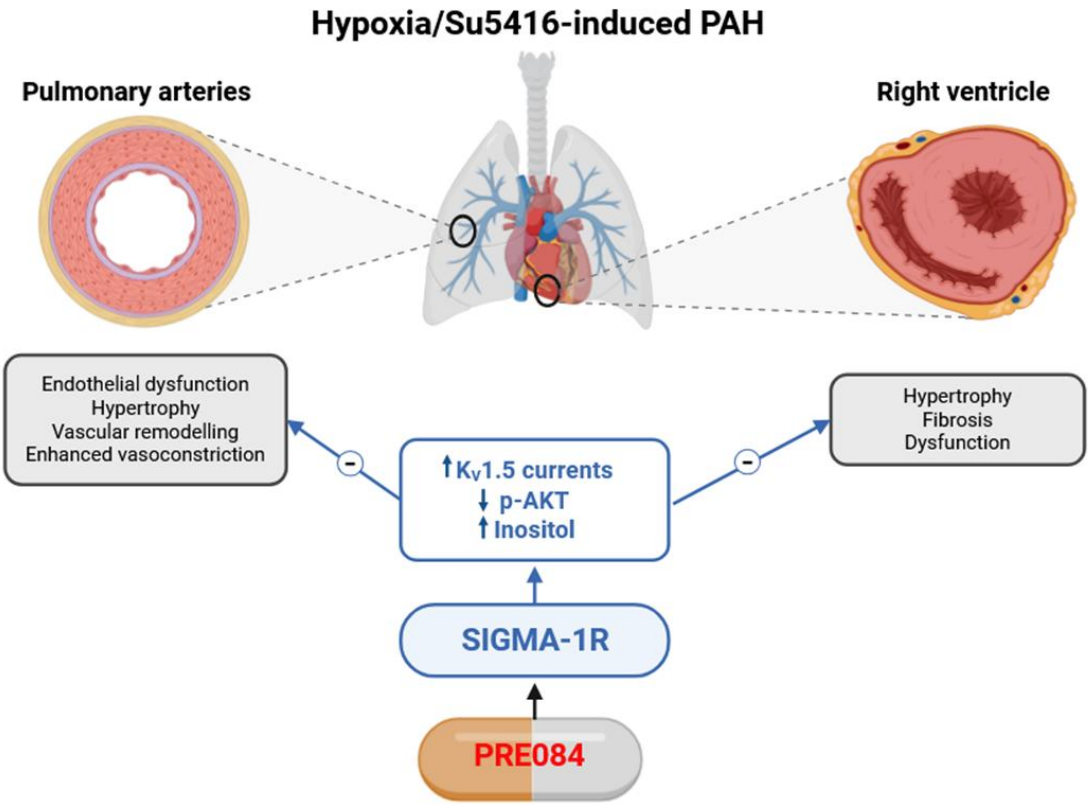

Figure 42: Graphical abstract specific of the chapter 2. The sigma-1 receptor agonist PRE-084 exerts beneficial effects in an experimental model of pulmonary arterial hypertension induced by chronic hypoxia and SU5416.

CONCLUSIONS

Considering all the work described in the previous chapters, and considering the objectives stated in the present Doctoral Thesis, the following conclusions can be drawn:

1. URO-K10 is an effective K_V7 channel activator that increased K_V currents in PASMC and induced more potent and effective vasodilation than the classical agonists retigabine and flupirtine in rat and human pulmonary arteries. In addition, it exhibits antiproliferative effects in human PASMC.
2. Unlike traditional K_V7 agonists, the vasodilatory effects of URO-K10 occurred independently of the auxiliary subunit KCNE4, suggesting a distinctive mechanism of action.
3. URO-K10 induced more effective vasodilation under PAH conditions, both in arteries that mimic ionic remodelling and in those of monocrotaline-induced PAH. This supports the idea that novel K_V7 channel activators with enhanced properties may be useful in PAH therapy.
4. The *in vivo* administration of the S1R agonist PRE084 significantly improved pulmonary vascular function in the Hpx/Su model of PAH, enhanced $K_V1.5$ channel activity in PASMCs, attenuated hypercontraction, and partially restored endothelium-dependent vasodilation. These effects were not associated with changes in total $K_V1.5$ protein levels but with increased trafficking into the plasma membrane.
5. *In vivo* administration of PRE084 in the Hpx/Su model of PAH improved pulmonary vascular remodelling by reversing vascular muscularization. These findings support a role for the S1R in modulating both the functional and structural components of pulmonary vascular pathology.
6. PRE084 exerted significant cardioprotective effects by attenuating RV dysfunction, reducing hypertrophy and fibrosis, lowering RV systolic pressure, and showing a tendency to reduce pulmonary artery pressure. These benefits appear to be, at least in part, by modulating the pAKT pathway and restoring inositol levels. Hence, these findings highlight the pleiotropic benefits of S1R activation in right ventricular remodelling.

7. The approved drugs, dimemorfan and fluoxetine increased K_V1.5 currents in PASMC via S1R activation and attenuated vasoconstriction in rat PA. In addition, these drugs enhanced K_V1.5 activity in PASMC from hypoxia+Su5416-induced PAH rats. These findings are highly relevant as they identify S1R as a potential novel pharmacological target in cardiovascular diseases associated with an impaired K_V1.5 channel function. Moreover, they underscore the therapeutic relevance of drug repurposing, demonstrating that already marketed drugs may be effectively repositioned for the treatment of diseases such a as PAH.

ANNEXES

	Nmx		Hpx/Su		Hpx/Su + PRE084	
	Basal	**Final**	**Basal**	**Final**	**Basal**	**Final**
Pulmonary arterial flow and structure						
PA diameter (cm)	3.17 ± 0.05	3.26 ± 0.03	3.01 ± 0.07	3.29 ± 0.08	3.18 ± 0.08	3.36 ± 0.08
PAPSV (m/s)	0.97 ± 0.03	0.97 ± 0.03	0.87 ± 0.03	0.86 ± 0.04	0.91 ± 0.04	0.92 ± 0.04
PAVTI (cm)	5.61 ± 0.24	5.73 ± 0.22	3.97 ± 0.27	3.73 ± 0.38 ***	4.24 ± 0.24	4.50 ± 0.31 *
PAAT (ms)	29.22 ± 1.86	27.33 ± 1.99	16.53 ± 0.86	15.47 ± 0.98 ***	17.87 ± 0.75	16.90 ± 0.82 ***
PAET (ms)	74.56 ± 2.20	72.89 ± 2.39	71.02 ± 2.04	72.25 ± 3.84	76.15 ± 1.45	76.42 ± 1.63
HR (bpm)	351.67 ± 8.09	352.33 ± 7.67	352.60 ± 6.72	335.20 ± 11.68	351.75 ± 11.31	339.35 ± 11.02
PAAT/PAET	0.39 ± 0.02	0.38 ± 0.02	0.23 ± 0.01	0.22 ± 0.01 ***	0.23 ± 0.01	0.22 ± 0.01 ***
Aortic flow and structure						
AoVTI (cm)	5.03 ± 0.18	5.32 ± 0.47	3.40 ± 0.35	3.73 ± 0.33 **	3.30 ± 0.23	3.82 ± 0.37 *
HR (bpm)	355.89 ± 7.66	357.78 ± 8.14	351.33 ± 5.42	353.10 ± 21.31	356.20 ± 12.44	334.30 ± 8.70
Aorta diameter (mm)	2.84 ± 0.08	2.90 ± 0.09	2.42 ± 0.09	2.78 ± 0.10	2.62 ± 0.08	2.70 ± 0.06
RV function and structure						
TAPSE (cm)	3.41 ± 0.09	3.54 ± 0.12	2.51 ± 0.13	2.31 ± 0.12 ***	2.31 ± 0.12	2.53 ± 0.13 ***
s' (m/s)	0.06 ± 0.00	0.06 ± 0.00	0.04 ± 0.00	0.04 ± 0.00 ***	0.04 ± 0.01	0.04 ± 0.01 ***
RVA diastole (cm^2)	0.39 ± 0.01	0.39 ± 0.01	0.47 ± 0.04	0.52 ± 0.04 *	0.44 ± 0.02	0.48 ± 0.03
RVA systole (cm^2)	0.27 ± 0.01	0.27 ± 0.01	0.35 ± 0.03	0.39 ± 0.03 *	0.33 ± 0.01	0.37 ± 0.03 *
RAA max (cm^2)	0.27 ± 0.02	0.27 ± 0.02	0.32 ± 0.03	0.35 ± 0.04 *	0.31 ± 0.01	0.33 ± 0.02
RAA min (cm^2)	0.18 ± 0.01	0.19 ± 0.01	0.23 ± 0.02	0.24 ± 0.03	0.19 ± 0.01	0.23 ± 0.02
RV diameter (mm)	5.21 ± 0.16	5.27 ± 0.07	5.74 ± 0.26	6.09 ± 0.21 **	5.72 ± 0.15	5.96 ± 0.21 *
RV/LV diameter	0.63 ± 0.02	0.64 ± 0.02	0.77 ± 0.03	0.84 ± 0.05 ***	0.78 ± 0.02	0.78 ± 0.01 **
RVFAC (%)	30.98 ± 2.50	29.88 ± 2.25	25.69 ± 1.70	25.70 ± 2.56	25.29 ± 1.42	23.60 ± 1.45
LV function and structure						
LVAWT systole (cm)	3.22 ± 0.12	3.19 ± 0.11	3.63 ± 0.25	3.98 ± 0.20 *	3.56 ± 0.21	3.38 ± 0.16
LVID systole (cm)	4.42 ± 0.14	4.49 ± 0.14	2.96 ± 0.27	2.23 ± 0.46 ***	3.23 ± 0.34	3.89 ± 0.41 #
LVPWT systole (cm)	2.86 ± 0.16	2.80 ± 0.15	3.18 ± 0.20	3.81 ± 0.27 **	3.10 ± 0.20	2.98 ± 0.19
LVAWT diastole (cm)	1.69 ± 0.09	1.68 ± 0.07	2.13 ± 0.14	2.05 ± 0.14	1.97 ± 0.10	1.91 ± 0.08
LVID diastole (cm)	8.27 ± 0.16	8.34 ± 0.15	6.49 ± 0.24	6.83 ± 0.24 ***	7.01 ± 0.23	7.44 ± 0.28 *
LVPWT diastole (cm)	1.87 ± 0.14	1.81 ± 0.11	2.41 ± 0.16	2.52 ± 0.13 **	2.16 ± 0.18	1.96 ± 0.09
EI	0.94 ± 0.02	0.95 ± 0.02	0.74 ± 0.05	0.71 ± 0.05 ***	0.82 ± 0.04	0.76 ± 0.04 **
LV mass (g)	0.91 ± 0.06	0.90 ± 0.05	0.89 ± 0.04	0.97 ± 0.05	0.87 ± 0.07	0.86 ± 0.05
LVFS (%)	46.50 ± 1.35	46.21 ± 1.30	54.28 ± 3.86	68.14 ± 5.56 **	54.02 ± 4.56	48.58 ± 4.13 #
LVCO (ml/min^{-1})	114.27 ± 7.39	124.45 ± 9.44	55.69 ± 8.65	82.84 ± 11.99 *	64.03 ± 6.11	74.02 ± 8.03 **

Supplemental Table 1. ***Echocardiography evaluation***. Results are expressed as mean ± SEM. Two-way ANOVA repeated measures with Sidak method for post hoc comparisons. *P<0.05, **P<0.01, ***P<0.001 vs Nmx; #P<0.05, vs Hpx/Su. PA: pulmonary artery, PAPSV: pulmonary artery peak systolic velocity, PAVTI: pulmonary artery velocity time integral, PAAT: pulmonary artery acceleration time, PAET: pulmonary artery ejection time, HR: heart rate, AoPSV: aortic peak systolic velocity, AoVTI: aortic velocity time integral, TAPSE: *Tricuspid Annular Plane Systolic Excursion* , s´: tricuspid annulus peak systolic velocity, RVA: right ventricular area, RAA: right atrial area, RVFAC: right ventricle fractional area change, LVAWT: left ventricular

anterior wall thickness, LVID: left ventricular internal diameter, LVPWT: left ventricular posterior wall thickness, EI: excentric index, LVFS: left ventricular fractional shortening, LVCO: left ventricular cardiac output.

Metabolite	**Nmx (n=9)**	**Hpx/Su (n=11)**	**Hpx/Su + PRE084 (n=7)**
Lactate	1 ± 0.02	1.24 ± 0.07 *	1.32 ± 0.13
Alanine	1 ± 0.02	0.98 ± 0.05	1.08 ± 0.06
Acetate	1 ± 0.03	0.89 ± 0.05	1.02 ± 0.01
Glutamine + Glutamic acid	1 ± 0.03	0.86 ± 0.06	0.98 ± 0.01
Glutamic acid + Lipids	1 ± 0.02	0.99 ± 0.04	0.91 ± 0.03
Glutamic acid	1 ± 0.03	0.91 ± 0.07	1.04 ± 0.01
Glutamine + Carnitine	1 ± 0.04	0.76 ± 0.07 *	0.89 ± 0.01
Gluthathione	1 ± 0.03	0.94 ± 0.07	1.07 ± 0.03
Hypotaurine	1 ± 0.03	0.93 ± 0.07	1.04 ± 0.03
Creatine	1 ± 0.04	0.73 ± 0.08 *	0.89 ± 0.03
Dimethylsulfone	1 ± 0.13	1.29 ± 0.19	1.33 ± 0.18
Choline	1 ± 0.05	0.84 ± 0.08	1.01 ± 0.04
Carnitine	1 ± 0.03	0.89 ± 0.09	0.98 ± 0.02
Taurine	1 ± 0.04	1.17 ± 0.11	1.28 ± 0.08
Glycine	1 ± 0.05	0.93 ± 0.10	1.12 ± 0.05
Inositol	1 ± 0.08	0.70 ± 0.08 *	1.02 ± 0.04 #
Ascorbate	1 ± 0.04	0.80 ± 0.09	1.01 ± 0.05
Carnitine + Gluthathione	1 ± 0.03	0.94 ± 0.07	1.10 ± 0.03

Supplemental Table 2. ***Levels of metabolites detected in right ventricle from Nmx, Hpx/Su or Hpx/Su + PRE084 rats.*** Concentrations of detected metabolites are shown relative to mean Nmx group levels. * <0.05 vs Nmx; # <0.05 vs Hpx/Su. Values represent the mean ± s.e.m. of n=9-10 animals.

BIBLIOGRAPHY

Abbott, G. W. (2020). KCNQs: Ligand- and Voltage-Gated Potassium Channels. *Frontiers in Physiology*, *11*. https://doi.org/10.3389/fphys.2020.00583

Abbott, G. W., & Jepps, T. A. (2016). KCNE4 Deletion Sex-Dependently Alters Vascular Reactivity. *Journal of Vascular Research*, *53*(3–4), 138–148. https://doi.org/10.1159/000449060

Abdullah, C. S., Alam, S., Aishwarya, R., Miriyala, S., Panchatcharam, M., Bhuiyan, M. A. N., Peretik, J. M., Orr, A. W., James, J., Osinska, H., Robbins, J., Lorenz, J. N., & Bhuiyan, Md. S. (2018). Cardiac Dysfunction in the Sigma 1 Receptor Knockout Mouse Associated With Impaired Mitochondrial Dynamics and Bioenergetics. *Journal of the American Heart Association*, *7*(20). https://doi.org/10.1161/JAHA.118.009775

Ackerman, M. J., & Clapham, D. E. (1997). Ion Channels — Basic Science and Clinical Disease. *New England Journal of Medicine*, *336*(22), 1575–1586. https://doi.org/10.1056/NEJM199705293362207

Adão, R., Barreira, B., Paternoster, E., Morales-Cano, D., Olivencia, M. A., Quintana-Villamandos, B., Rodríguez-Chiaradía, D. A., Cogolludo, A., & Perez-Vizcaino, F. (2025). Vitamin D as an add-on therapy to phosphodiesterase-5 inhibitor in experimental pulmonary arterial hypertension. *American Journal of Physiology-Lung Cellular and Molecular Physiology*, *328*(2), L253–L259. https://doi.org/10.1152/ajplung.00319.2024

Adão, R., Mendes-Ferreira, P., Santos-Ribeiro, D., Maia-Rocha, C., Pimentel, L. D., Monteiro-Pinto, C., Mulvaney, E. P., Reid, H. M., Kinsella, B. T., Potus, F., Breuils-Bonnet, S., Rademaker, M. T., Provencher, S., Bonnet, S., Leite-Moreira, A. F., & Brás-Silva, C. (2018). Urocortin-2 improves right ventricular function and attenuates pulmonary arterial hypertension. *Cardiovascular Research*, *114*(8), 1165–1177. https://doi.org/10.1093/cvr/cvy076

Al-Chawishly, M., Loveland, O., & Gurney, A. M. (2022). Kv7 Channels in Cyclic-Nucleotide Dependent Relaxation of Rat Intra-Pulmonary Artery. *Biomolecules*, *12*(3), 429. https://doi.org/10.3390/biom12030429

Almaamari, A., Sultan, M., Zhang, T., Qaed, E., Wu, S., Qiao, R., Duan, Y., Ding, S., Liu, G., & Su, S. (2025). Sigma-1 Receptor Specific Biological Functions, Protective Role, and Therapeutic Potential in Cardiovascular Diseases. *Cardiovascular Toxicology*, *25*(4), 614–630. https://doi.org/10.1007/s12012-025-09975-5

Antigny, F., Hautefort, A., Meloche, J., Belacel-Ouari, M., Manoury, B., Rucker-Martin, C., Péchoux, C., Potus, F., Nadeau, V., Tremblay, E., Ruffenach, G., Bourgeois, A., Dorfmüller, P., Breuils-Bonnet, S., Fadel, E., Ranchoux, B., Jourdon, P., Girerd, B., Montani, D., … Perros, F. (2016). Potassium Channel Subfamily K Member 3 (KCNK3) Contributes to the Development of Pulmonary Arterial Hypertension. *Circulation*, *133*(14), 1371–1385. https://doi.org/10.1161/CIRCULATIONAHA.115.020951

Austin, E. D., & Loyd, J. E. (2014). The Genetics of Pulmonary Arterial Hypertension. *Circulation Research*, *115*(1), 189–202. https://doi.org/10.1161/CIRCRESAHA.115.303404

Aydar, E., Palmer, C. P., Klyachko, V. A., & Jackson, M. B. (2002). The Sigma Receptor as a Ligand-Regulated Auxiliary Potassium Channel Subunit. *Neuron*, *34*(3), 399–410. https://doi.org/10.1016/S0896-6273(02)00677-3

Babicheva, A., Ayon, R. J., Zhao, T., Ek Vitorin, J. F., Pohl, N. M., Yamamura, A., Yamamura, H., Quinton, B. A., Ba, M., Wu, L., Ravellette, K. S., Rahimi, S., Balistrieri, F., Harrington, A., Vanderpool, R. R., Thistlethwaite, P. A., Makino, A., & Yuan, J. X.-J. (2020). MicroRNA-mediated downregulation of K+ channels in pulmonary arterial hypertension. *American Journal of Physiology-Lung Cellular and Molecular Physiology*, *318*(1), L10–L26. https://doi.org/10.1152/ajplung.00010.2019

Baldwin, S. N., Forrester, E. A., McEwan, L., & Greenwood, I. A. (2022). Sexual dimorphism in prostacyclin-mimetic responses within rat mesenteric arteries: A novel role for KV 7.1 in shaping IP receptor-mediated relaxation. *British Journal of Pharmacology*, *179*(7), 1338–1352. https://doi.org/10.1111/bph.15722

Banerjee, S., Hong, J., & Umar, S. (2022). Comparative analysis of right ventricular metabolic reprogramming in pre-clinical rat models of severe pulmonary hypertension-induced right ventricular failure. *Frontiers in Cardiovascular Medicine*, *9*, 935423. https://doi.org/10.3389/fcvm.2022.935423

Bankhead, P., Loughrey, M. B., Fernández, J. A., Dombrowski, Y., McArt, D. G., Dunne, P. D., McQuaid, S., Gray, R. T., Murray, L. J., Coleman, H. G., James, J. A., Salto-Tellez, M., & Hamilton, P. W. (2017). QuPath: Open source software for digital pathology image analysis. *Scientific Reports*, *7*(1), 16878. https://doi.org/10.1038/s41598-017-17204-5

Barrese, V., Stott, J. B., & Greenwood, I. A. (2018). KCNQ-Encoded Potassium Channels as Therapeutic Targets. *Annual Review of Pharmacology and Toxicology*, *58*(1), 625–648. https://doi.org/10.1146/annurev-pharmtox-010617-052912

Benson, M. D., Li, Q.-J., Kieckhafer, K., Dudek, D., Whorton, M. R., Sunahara, R. K., Iñiguez-Lluhí, J. A., & Martens, J. R. (2007). SUMO modification regulates inactivation of the voltage-gated potassium channel Kv1.5. *Proceedings of the National Academy of Sciences*, *104*(6), 1805–1810. https://doi.org/10.1073/pnas.0606702104

Bhuiyan, Md. S., & Fukunaga, K. (2009). Stimulation of Sigma-1 receptor signaling by dehydroepiandrosterone ameliorates pressure overload-induced hypertrophy and dysfunctions in ovariectomized rats. *Expert Opinion on Therapeutic Targets*, *13*(11), 1253–1265. https://doi.org/10.1517/14728220903264064

Bhuiyan, Md. S., Tagashira, H., Shioda, N., & Fukunaga, K. (2010). Targeting sigma-1 receptor with fluvoxamine ameliorates pressure-overload-induced hypertrophy and dysfunctions. *Expert Opinion on Therapeutic Targets*, *14*(10), 1009–1022. https://doi.org/10.1517/14728222.2010.509348

Borgini, M., Mondal, P., Liu, R., & Wipf, P. (2021). Chemical modulation of Kv7 potassium channels. *RSC Medicinal Chemistry*, *12*(4), 483–537. https://doi.org/10.1039/D0MD00328J

Boucherat, O., Chabot, S., Antigny, F., Perros, F., Provencher, S., & Bonnet, S. (2015). Potassium channels in pulmonary arterial hypertension. *European Respiratory Journal*, *46*(4), 1167–1177. https://doi.org/10.1183/13993003.00798-2015

Bousseau, S., Sobrano Fais, R., Gu, S., Frump, A., & Lahm, T. (2023). Pathophysiology and new advances in pulmonary hypertension. *BMJ Medicine*, *2*(1), e000137. https://doi.org/10.1136/bmjmed-2022-000137

Brevnova, E. E., Platoshyn, O., Zhang, S., & Yuan, J. X. J. (2004). Overexpression of human KCNA5 increases IK(V) and enhances apoptosis. *American Journal of Physiology - Cell Physiology*, *287*(3), C715–C722. https://doi.org/10.1152/ajpcell.00050.2004

Brickel, N., Gandhi, P., VanLandingham, K., Hammond, J., & DeRossett, S. (2012). The urinary safety profile and secondary renal effects of retigabine (ezogabine): A first-in-class antiepileptic drug that targets KCNQ (K_v 7) potassium channels. *Epilepsia*, *53*(4), 606–612. https://doi.org/10.1111/j.1528-1167.2012.03441.x

Budhiraja, R., Tuder, R. M., & Hassoun, P. M. (2004). Endothelial Dysfunction in Pulmonary Hypertension. *Circulation*, *109*(2), 159–165. https://doi.org/10.1161/01.CIR.0000102381.57477.50

Burg, E. D., Remillard, C. V, & Yuan, J. X. (2008). Potassium channels in the regulation of pulmonary artery smooth muscle cell proliferation and apoptosis: pharmacotherapeutic implications. *British Journal of Pharmacology*, *153*(S1). https://doi.org/10.1038/sj.bjp.0707635

Chandy, K. G., & Norton, R. S. (2017). Peptide blockers of Kv 1.3 channels in T cells as therapeutics for autoimmune disease. *Current Opinion in Chemical Biology*, *38*, 97–107. https://doi.org/10.1016/j.cbpa.2017.02.015

Chaudhary, K. R., Deng, Y., Yang, A., Cober, N. D., & Stewart, D. J. (2021). Penetrance of Severe Pulmonary Arterial Hypertension in Response to Vascular Endothelial Growth Factor Receptor 2 Blockade in a Genetically Prone Rat Model Is Reduced by Female Sex. *Journal of the American Heart Association*, *10*(15), e019488. https://doi.org/10.1161/JAHA.120.019488

Chen, B., Jin, Y., Pool, C. M., Liu, Y., & Nelin, L. D. (2022). Hypoxic pulmonary endothelial cells release epidermal growth factor leading to vascular smooth muscle cell arginase-2 expression and proliferation. *Physiological Reports*, *10*(11), e15342. https://doi.org/10.14814/phy2.15342

Chin, K. M., Gaine, S. P., Gerges, C., Jing, Z.-C., Mathai, S. C., Tamura, Y., McLaughlin, V. V, & Sitbon, O. (2024). Treatment algorithm for pulmonary arterial hypertension. *The European Respiratory Journal*, *64*(4). https://doi.org/10.1183/13993003.01325-2024

Choi, W. S., Khurana, A., Mathur, R., Viswanathan, V., Steele, D. F., & Fedida, D. (2005). Kv1.5 Surface Expression Is Modulated by Retrograde Trafficking of Newly Endocytosed Channels by the Dynein Motor. *Circulation Research*, *97*(4), 363–371. https://doi.org/10.1161/01.RES.0000179535.06458.f8

Christou, H., Hudalla, H., Michael, Z., Filatava, E. J., Li, J., Zhu, M., Possomato-Vieira, J. S., Dias-Junior, C., Kourembanas, S., & Khalil, R. A. (2018). Impaired Pulmonary Arterial Vasoconstriction and Nitric Oxide–Mediated Relaxation Underlie Severe Pulmonary Hypertension in the Sugen-Hypoxia Rat Model. *The Journal of Pharmacology and Experimental Therapeutics*, *364*(2), 258–274. https://doi.org/10.1124/jpet.117.244798

Cidad, P., Jiménez-Pérez, L., García-Arribas, D., Miguel-Velado, E., Tajada, S., Ruiz-McDavitt, C., López-López, J. R., & Pérez-García, M. T. (2012). Kv1.3 Channels Can Modulate Cell Proliferation During Phenotypic Switch by an Ion-Flux Independent Mechanism. *Arteriosclerosis, Thrombosis, and Vascular Biology*, *32*(5), 1299–1307. https://doi.org/10.1161/ATVBAHA.111.242727

Climent, B., Santiago, E., Sánchez, A., Muñoz-Picos, M., Pérez–Vizcaíno, F., García-Sacristán, A., Rivera, L., & Prieto, D. (2020). Metabolic syndrome inhibits store-operated Ca2+ entry and calcium-induced calcium-release mechanism in coronary artery smooth muscle. *Biochemical Pharmacology*, *182*, 114222. https://doi.org/10.1016/j.bcp.2020.114222

Coetzee, W. A., Amarillo, yimy, Chiu, J., Chow, A., Lau, D., McCORMACK, T., Morena, H., Nadal, M. S., Ozaita, A., Pountney, D., Saganich, M., De miera, eleazar vega-saenz, & Rudy, B. (1999). Molecular Diversity of K + Channels. *Annals of the New York Academy of Sciences*, *868*(1), 233–255. https://doi.org/10.1111/j.1749-6632.1999.tb11293.x

Cogolludo, A., Frazziano, G., Cobeño, L., Moreno, L., Lodi, F., Villamor, E., Tamargo, J., & Perez-Vizcaino, F. (2006). Role of Reactive Oxygen Species in Kv Channel Inhibition and Vasoconstriction Induced by TP Receptor Activation in Rat Pulmonary Arteries. *Annals of the New York Academy of Sciences*, *1091*(1), 41–51. https://doi.org/10.1196/annals.1378.053

Cogolludo, A., Moreno, L., Bosca, L., Tamargo, J., & Perez-Vizcaino, F. (2003). Thromboxane A2 -Induced Inhibition of Voltage-Gated K+ Channels and Pulmonary Vasoconstriction. *Circulation Research*, *93*(7), 656–663. https://doi.org/10.1161/01.RES.0000095245.97945.FE

Cogolludo, A., Moreno, L., Frazziano, G., Moral-Sanz, J., Menendez, C., Castaneda, J., Gonzalez, C., Villamor, E., & Perez-Vizcaino, F. (2008). Activation of neutral sphingomyelinase is involved in acute hypoxic pulmonary vasoconstriction. *Cardiovascular Research*, *82*(2), 296–302. https://doi.org/10.1093/cvr/cvn349

Cogolludo, A., Moreno, L., Lodi, F., Frazziano, G., Cobeño, L., Tamargo, J., & Perez-Vizcaino, F. (2006). Serotonin Inhibits Voltage-Gated K+ Currents in Pulmonary Artery Smooth Muscle Cells. *Circulation Research*, *98*(7), 931–938. https://doi.org/10.1161/01.RES.0000216858.04599.e1

Cogolludo, A., Moreno, L., & Villamor, E. (2007). Mechanisms Controlling Vascular Tone in Pulmonary Arterial Hypertension: Implications for Vasodilator Therapy. *Pharmacology*, *79*(2), 65–75. https://doi.org/10.1159/000097754

Cogolludo, A., Villamor, E., Perez-Vizcaino, F., & Moreno, L. (2019). Ceramide and Regulation of Vascular Tone. *International Journal of Molecular Sciences*, *20*(2), 411. https://doi.org/10.3390/ijms20020411

Cole, W. C., & Welsh, D. G. (2011). Role of myosin light chain kinase and myosin light chain phosphatase in the resistance arterial myogenic response to intravascular pressure. *Archives of Biochemistry and Biophysics*, *510*(2), 160–173. https://doi.org/10.1016/j.abb.2011.02.024

Dai, F., Mao, Z., Xia, J., Zhu, S., & Wu, Z. (2012). Fluoxetine protects against big endothelin-1 induced anti-apoptosis by rescuing Kv1.5 channels in human pulmonary arterial

smooth muscle cells. *Yonsei Medical Journal*, *53*(4), 842–848. https://doi.org/10.3349/ymj.2012.53.4.842

Delcroix, M., & Howard, L. (2015). Pulmonary arterial hypertension: the burden of disease and impact on quality of life. *European Respiratory Review*, *24*(138), 621–629. https://doi.org/10.1183/16000617.0063-2015

Dhoble, S., Patravale, V., Weaver, E., Lamprou, D. A., & Patravale, T. (2022). Comprehensive review on novel targets and emerging therapeutic modalities for pulmonary arterial Hypertension. *International Journal of Pharmaceutics*, *621*, 121792. https://doi.org/10.1016/j.ijpharm.2022.121792

Di Rosso, M. E., Palumbo, M. L., & Genaro, A. M. (2016). Immunomodulatory effects of fluoxetine: A new potential pharmacological action for a classic antidepressant drug? *Pharmacological Research*, *109*, 101–107. https://doi.org/10.1016/j.phrs.2015.11.021

Dolmetsch, R. E., Lewis, R. S., Goodnow, C. C., & Healy, J. I. (1997). Differential activation of transcription factors induced by Ca2+ response amplitude and duration. *Nature*, *386*(6627), 855–858. https://doi.org/10.1038/386855a0

England, S. K., Uebele, V. N., Shear, H., Kodali, J., Bennett, P. B., & Tamkun, M. M. (1995). Characterization of a voltage-gated K+ channel beta subunit expressed in human heart. *Proceedings of the National Academy of Sciences*, *92*(14), 6309–6313. https://doi.org/10.1073/pnas.92.14.6309

Galiè, N., Channick, R. N., Frantz, R. P., Grünig, E., Jing, Z. C., Moiseeva, O., Preston, I. R., Pulido, T., Safdar, Z., Tamura, Y., & McLaughlin, V. V. (2019). Risk stratification and medical therapy of pulmonary arterial hypertension. *European Respiratory Journal*, *53*(1 1801889). https://doi.org/10.1183/13993003.01889-2018

Galiè, N., Humbert, M., Vachiery, J.-L., Gibbs, S., Lang, I., Torbicki, A., Simonneau, G., Peacock, A., Vonk Noordegraaf, A., Beghetti, M., Ghofrani, A., Gomez Sanchez, M. A., Hansmann, G., Klepetko, W., Lancellotti, P., Matucci, M., McDonagh, T., Pierard, L. A., Trindade, P. T., … Hoeper, M. (2016). 2015 ESC/ERS Guidelines for the diagnosis and treatment of pulmonary hypertension. *European Heart Journal*, *37*(1), 67–119. https://doi.org/10.1093/eurheartj/ehv317

Gao, Q.-J., Yang, B., Chen, J., Shi, S.-B., Yang, H.-J., & Liu, X. (2018). Sigma-1 Receptor Stimulation with PRE-084 Ameliorates Myocardial Ischemia-Reperfusion Injury in Rats. *Chinese Medical Journal*, *131*(5), 539–543. https://doi.org/10.4103/0366-6999.226076

González, C., Baez-Nieto, D., Valencia, I., Oyarzún, I., Rojas, P., Naranjo, D., & Latorre, R. (2012). K+ Channels: Function-Structural Overview. In *Comprehensive Physiology* (pp. 2087–2149). Wiley. https://doi.org/10.1002/cphy.c110047

Guignabert, C., Aman, J., Bonnet, S., Dorfmüller, P., Olschewski, A. J., Pullamsetti, S., Rabinovitch, M., Schermuly, R. T., Humbert, M., & Stenmark, K. R. (2024). Pathology and pathobiology of pulmonary hypertension: current insights and future directions. *European Respiratory Journal*, *64*(4), 2401095. https://doi.org/10.1183/13993003.01095-2024

Guignabert, C., Raffestin, B., Benferhat, R., Raoul, W., Zadigue, P., Rideau, D., Hamon, M., Adnot, S., & Eddahibi, S. (2005). Serotonin transporter inhibition prevents and reverses

monocrotaline-induced pulmonary hypertension in rats. *Circulation*, *111*(21), 2812–2819. https://doi.org/10.1161/CIRCULATIONAHA.104.524926

Guignabert, C., Tu, L., Izikki, M., Dewachter, L., Zadigue, P., Humbert, M., Adnot, S., Fadel, E., & Eddahibi, S. (2009). Dichloroacetate treatment partially regresses established pulmonary hypertension in mice with SM22alpha-targeted overexpression of the serotonin transporter. *FASEB Journal : Official Publication of the Federation of American Societies for Experimental Biology*, *23*(12), 4135–4147. https://doi.org/10.1096/fj.09-131664

Gulbins, E., Palmada, M., Reichel, M., Lüth, A., Böhmer, C., Amato, D., Müller, C. P., Tischbirek, C. H., Groemer, T. W., Tabatabai, G., Becker, K. A., Tripal, P., Staedtler, S., Ackermann, T. F., van Brederode, J., Alzheimer, C., Weller, M., Lang, U. E., Kleuser, B., … Kornhuber, J. (2013). Acid sphingomyelinase-ceramide system mediates effects of antidepressant drugs. *Nature Medicine*, *19*(7), 934–938. https://doi.org/10.1038/nm.3214

Gurney, A. M., Osipenko, O. N., MacMillan, D., McFarlane, K. M., Tate, R. J., & Kempsill, F. E. J. (2003). Two-Pore Domain K Channel, TASK-1, in Pulmonary Artery Smooth Muscle Cells. *Circulation Research*, *93*(10), 957–964. https://doi.org/10.1161/01.RES.0000099883.68414.61

Haick, J. M., & Byron, K. L. (2016). Novel treatment strategies for smooth muscle disorders: Targeting Kv7 potassium channels. *Pharmacology & Therapeutics*, *165*, 14–25. https://doi.org/10.1016/j.pharmthera.2016.05.002

Hashimoto, K. (2013). Potential Role of the Sigma-1 Receptor Chaperone in the Beneficial Effects of Donepezil in Dementia with Lewy Bodies. *Clinical Psychopharmacology and Neuroscience*, *11*(1), 43–44. https://doi.org/10.9758/cpn.2013.11.1.43

Hashimoto, K. (2015). Activation of sigma-1 receptor chaperone in the treatment of neuropsychiatric diseases and its clinical implication. *Journal of Pharmacological Sciences*, *127*(1), 6–9. https://doi.org/10.1016/j.jphs.2014.11.010

Hayashi, T., & Su, T.-P. (2001). Regulating ankyrin dynamics: Roles of sigma-1 receptors. *Proceedings of the National Academy of Sciences*, *98*(2), 491–496. https://doi.org/10.1073/pnas.98.2.491

Hayashi, T., & Su, T.-P. (2007). Sigma-1 Receptor Chaperones at the ER- Mitochondrion Interface Regulate Ca2+ Signaling and Cell Survival. *Cell*, *131*(3), 596–610. https://doi.org/10.1016/j.cell.2007.08.036

Hendriks, P. M., Staal, D. P., van de Groep, L. D., van den Toorn, L. M., Chandoesing, P. P., Kauling, R. M., Mager, H.-J., van den Bosch, A. E., Post, M. C., & Boomars, K. A. (2022). The evolution of survival of pulmonary arterial hypertension over 15 years. *Pulmonary Circulation*, *12*(4), e12137. https://doi.org/10.1002/pul2.12137

Hille, B., Armstrong, C. M., & MacKinnon, R. (1999). Ion channels: From idea to reality. *Nature Medicine*, *5*(10), 1105–1109. https://doi.org/10.1038/13415

Hsu, S., Houston, B. A., Tampakakis, E., Bacher, A. C., Rhodes, P. S., Mathai, S. C., Damico, R. L., Kolb, T. M., Hummers, L. K., Shah, A. A., McMahan, Z., Corona-Villalobos, C. P., Zimmerman, S. L., Wigley, F. M., Hassoun, P. M., Kass, D. A., & Tedford, R. J. (2016). Right

Ventricular Functional Reserve in Pulmonary Arterial Hypertension. *Circulation*, *133*(24), 2413–2422. https://doi.org/10.1161/CIRCULATIONAHA.116.022082

Huang, Y., Ma, D., Yang, Z., Zhao, Y., & Guo, J. (2023). Voltage-gated potassium channels KCNQs: Structures, mechanisms, and modulations. *Biochemical and Biophysical Research Communications*, *689*, 149218. https://doi.org/10.1016/j.bbrc.2023.149218

Huh, J. W., Kim, S.-Y., Lee, J. H., & Lee, Y.-S. (2011). YC-1 attenuates hypoxia-induced pulmonary arterial hypertension in mice. *Pulmonary Pharmacology & Therapeutics*, *24*(6), 638–646. https://doi.org/10.1016/j.pupt.2011.09.003

Humbert, M., Guignabert, C., Bonnet, S., Dorfmüller, P., Klinger, J. R., Nicolls, M. R., Olschewski, A. J., Pullamsetti, S. S., Schermuly, R. T., Stenmark, K. R., & Rabinovitch, M. (2019). Pathology and pathobiology of pulmonary hypertension: state of the art and research perspectives. *European Respiratory Journal*, *53*((1) 1801887). https://doi.org/10.1183/13993003.01887-2018

Ishima, T., Fujita, Y., & Hashimoto, K. (2014). Interaction of new antidepressants with sigma-1 receptor chaperones and their potentiation of neurite outgrowth in PC12 cells. *European Journal of Pharmacology*, *727*, 167–173. https://doi.org/10.1016/j.ejphar.2014.01.064

Ito, K., Hirooka, Y., & Sunagawa, K. (2013). Brain Sigma-1 Receptor Stimulation Improves Mental Disorder and Cardiac Function in Mice With Myocardial Infarction. *Journal of Cardiovascular Pharmacology*, *62*(2), 222–228. https://doi.org/10.1097/FJC.0b013e3182970b15

Jensen, M. Ø., Jogini, V., Borhani, D. W., Leffler, A. E., Dror, R. O., & Shaw, D. E. (2012). Mechanism of Voltage Gating in Potassium Channels. *Science*, *336*(6078), 229–233. https://doi.org/10.1126/science.1216533

Jepps, T. A., Carr, G., Lundegaard, P. R., Olesen, S., & Greenwood, I. A. (2015). Fundamental role for the KCNE4 ancillary subunit in Kv7.4 regulation of arterial tone. *The Journal of Physiology*, *593*(24), 5325–5340. https://doi.org/10.1113/JP271286

Jepps, T., Olesen, S., & Greenwood, I. (2013). One man's side effect is another man's therapeutic opportunity: targeting Kv7 channels in smooth muscle disorders. *British Journal of Pharmacology*, *168*(1), 19–27. https://doi.org/10.1111/j.1476-5381.2012.02133.x

Kim, D. M., & Nimigean, C. M. (2016). Voltage-Gated Potassium Channels: A Structural Examination of Selectivity and Gating. *Cold Spring Harbor Perspectives in Biology*, *8*(5), a029231. https://doi.org/10.1101/cshperspect.a029231

Kim, R. Y., Yau, M. C., Galpin, J. D., Seebohm, G., Ahern, C. A., Pless, S. A., & Kurata, H. T. (2015). Atomic basis for therapeutic activation of neuronal potassium channels. *Nature Communications*, *6*(1), 8116. https://doi.org/10.1038/ncomms9116

Kinoshita, M., Matsuoka, Y., Suzuki, T., Mirrielees, J., & Yang, J. (2012). Sigma-1 receptor alters the kinetics of Kv1.3 voltage gated potassium channels but not the sensitivity to receptor ligands. *Brain Research*, *1452*, 1–9. https://doi.org/10.1016/j.brainres.2012.02.070

Klinger, J. R., & Kadowitz, P. J. (2017). The Nitric Oxide Pathway in Pulmonary Vascular Disease. *The American Journal of Cardiology*, *120*(8), S71–S79. https://doi.org/10.1016/j.amjcard.2017.06.012

Kourrich, S., Hayashi, T., Chuang, J.-Y., Tsai, S.-Y., Su, T.-P., & Bonci, A. (2013). Dynamic Interaction between Sigma-1 Receptor and Kv1.2 Shapes Neuronal and Behavioral Responses to Cocaine. *Cell*, *152*(1–2), 236–247. https://doi.org/10.1016/j.cell.2012.12.004

Kovacs, G., Bartolome, S., Denton, C. P., Gatzoulis, M. A., Gu, S., Khanna, D., Badesch, D., & Montani, D. (2024). Definition, classification and diagnosis of pulmonary hypertension. *European Respiratory Journal*, *64*(4), 2401324. https://doi.org/10.1183/13993003.01324-2024

Kovacs, G., Berghold, A., Scheidl, S., & Olschewski, H. (2009). Pulmonary arterial pressure during rest and exercise in healthy subjects: a systematic review. *European Respiratory Journal*, *34*(4), 888–894. https://doi.org/10.1183/09031936.00145608

Kwak, Y.-G., Navarro-Polanco, R. A., Grobaski, T., Gallagher, D. J., & Tamkun, M. M. (1999). Phosphorylation Is Required for Alteration of Kv1.5 Channel Function by the Kvβ1.3 Subunit. *Journal of Biological Chemistry*, *274*(36), 25355–25361. https://doi.org/10.1074/jbc.274.36.25355

L'Abbate, S., Nicolini, G., Forini, F., Lepore, E., Marchetti, S., Unfer, V., Forte, G., & Kusmic, C. (2024). Oral supplementation of inositols effectively recovered lithium-induced cardiac dysfunctions in mice. *Biomedicine & Pharmacotherapy = Biomedecine & Pharmacotherapie*, *178*, 117287. https://doi.org/10.1016/j.biopha.2024.117287

L'Abbate, S., Nicolini, G., Forini, F., Marchetti, S., Di Lascio, N., Faita, F., & Kusmic, C. (2020). Myo-inositol and d-chiro-inositol oral supplementation ameliorate cardiac dysfunction and remodeling in a mouse model of diet-induced obesity. *Pharmacological Research*, *159*, 105047. https://doi.org/10.1016/j.phrs.2020.105047

Lambert, M., Boet, A., Rucker-Martin, C., Mendes-Ferreira, P., Capuano, V., Hatem, S., Adão, R., Brás-Silva, C., Hautefort, A., Michel, J.-B., Dorfmuller, P., Fadel, E., Kotsimbos, T., Price, L., Jourdon, P., Montani, D., Humbert, M., Perros, F., & Antigny, F. (2018). Loss of KCNK3 is a hallmark of RV hypertrophy/dysfunction associated with pulmonary hypertension. *Cardiovascular Research*, *114*(6), 880–893. https://doi.org/10.1093/cvr/cvy016

Lambert, M., Capuano, V., Olschewski, A., Sabourin, J., Nagaraj, C., Girerd, B., Weatherald, J., Humbert, M., & Antigny, F. (2018). Ion channels in pulmonary hypertension: A therapeutic interest? *International Journal of Molecular Sciences*, *19*(10, 3162). https://doi.org/10.3390/ijms19103162

Lange, W., Geißendörfer, J., Schenzer, A., Grötzinger, J., Seebohm, G., Friedrich, T., & Schwake, M. (2009). Refinement of the Binding Site and Mode of Action of the Anticonvulsant Retigabine on KCNQ K+ Channels. *Molecular Pharmacology*, *75*(2), 272–280. https://doi.org/10.1124/mol.108.052282

Lau, E. M. T., Giannoulatou, E., Celermajer, D. S., & Humbert, M. (2017). Epidemiology and treatment of pulmonary arterial hypertension. *Nature Reviews Cardiology*, *14*(10), 603–614. https://doi.org/10.1038/nrcardio.2017.84

Lee, J. E., Park, C. H., Kang, H., Ko, J., Cho, S., Woo, J., Chae, M. R., Lee, S. W., Kim, S. J., Kim, J., & So, I. (2020). The agonistic action of URO-K10 on Kv7.4 and 7.5 channels is attenuated by co-expression of KCNE4 ancillary subunit. *The Korean Journal of Physiology & Pharmacology*, *24*(6), 503–516. https://doi.org/10.4196/kjpp.2020.24.6.503

Lewis, R., Li, J., McCormick, P. J., L-H Huang, C., & Jeevaratnam, K. (2020). Is the sigma-1 receptor a potential pharmacological target for cardiac pathologies? A systematic review. *International Journal of Cardiology. Heart & Vasculature*, *26*, 100449. https://doi.org/10.1016/j.ijcha.2019.100449

Li, Z., Zhou, J., Cui, S., Hu, S., Li, B., Liu, X., Zhang, C., Zou, Y., Hu, Y., Yu, Y., Shen, B., & Yang, B. (2024). Activation of sigma-1 receptor ameliorates sepsis-induced myocardial injury by mediating the Nrf2/HO1 signaling pathway to attenuate mitochondrial oxidative stress. *International Immunopharmacology*, *127*, 111382. https://doi.org/10.1016/j.intimp.2023.111382

Ma, L., Roman-Campos, D., Austin, E. D., Eyries, M., Sampson, K. S., Soubrier, F., Germain, M., Trégouët, D.-A., Borczuk, A., Rosenzweig, E. B., Girerd, B., Montani, D., Humbert, M., Loyd, J. E., Kass, R. S., & Chung, W. K. (2013). A Novel Channelopathy in Pulmonary Arterial Hypertension. *New England Journal of Medicine*, *369*(4), 351–361. https://doi.org/10.1056/NEJMoa1211097

Mackie, A. R., & Byron, K. L. (2008). Cardiovascular KCNQ (Kv7) Potassium Channels: Physiological Regulators and New Targets for Therapeutic Intervention. *Molecular Pharmacology*, *74*(5), 1171–1179. https://doi.org/10.1124/mol.108.049825

Maeno, E., Ishizaki, Y., Kanaseki, T., Hazama, A., & Okada, Y. (2000). Normotonic cell shrinkage because of disordered volume regulation is an early prerequisite to apoptosis. *Proceedings of the National Academy of Sciences of the United States of America*, *97*(17), 9487–9492. https://doi.org/10.1073/pnas.140216197

Mahamed, Z., Shadab, M., Najar, R. A., Millar, M. W., Bal, J., Pressley, T., & Fazal, F. (2023). The Protective Role of Mitochondria-Associated Endoplasmic Reticulum Membrane (MAM) Protein Sigma-1 Receptor in Regulating Endothelial Inflammation and Permeability Associated with Acute Lung Injury. *Cells*, *13*(1). https://doi.org/10.3390/cells13010005

Malar, D. S., Thitilertdecha, P., Ruckvongacheep, K. S., Brimson, S., Tencomnao, T., & Brimson, J. M. (2023). Targeting Sigma Receptors for the Treatment of Neurodegenerative and Neurodevelopmental Disorders. *CNS Drugs*, *37*(5), 399–440. https://doi.org/10.1007/s40263-023-01007-6

Mam, V., Tanbe, A. F., Vitali, S. H., Arons, E., Christou, H. A., & Khalil, R. A. (2010). Impaired Vasoconstriction and Nitric Oxide-Mediated Relaxation in Pulmonary Arteries of Hypoxia- and Monocrotaline-Induced Pulmonary Hypertensive Rats. *The Journal of Pharmacology and Experimental Therapeutics*, *332*(2), 455–462. https://doi.org/10.1124/jpet.109.160119

Manoury, B., Etheridge, S. L., Reid, J., & Gurney, A. M. (2009). Organ culture mimics the effects of hypoxia on membrane potential, K(+) channels and vessel tone in pulmonary artery. *British Journal of Pharmacology*, *158*(3), 848–861. https://doi.org/10.1111/j.1476-5381.2009.00353.x

McKirnan, M. D., Ichikawa, Y., Zhang, Z., Zemljic-Harpf, A. E., Fan, S., Barupal, D. K., Patel, H. H., Hammond, H. K., & Roth, D. M. (2019). Metabolomic analysis of serum and myocardium in compensated heart failure after myocardial infarction. *Life Sciences*, *221*, 212–223. https://doi.org/10.1016/j.lfs.2019.01.040

Michel, M. C., Radziszewski, P., Falconer, C., Marschall-Kehrel, D., & Blot, K. (2012). Unexpected frequent hepatotoxicity of a prescription drug, flupirtine, marketed for about 30 years. *British Journal of Clinical Pharmacology*, *73*(5), 821–825. https://doi.org/10.1111/j.1365-2125.2011.04138.x

Milano, G., Reinero, M., Puyal, J., Tozzi, P., Samaja, M., Porte-Thomé, F., & Beghetti, M. (2025). Inhibition of Sodium/Hydrogen Exchanger-1 in the Right Ventricle and Lung Dysfunction Induced by Experimental Pulmonary Arterial Hypertension in Rats. *Journal of the American Heart Association*, *14*(6), e036859. https://doi.org/10.1161/JAHA.124.036859

Milara, J., Escrivá, J., Ortiz, J. L., Juan, G., Artigues, E., Morcillo, E., & Cortijo, J. (2016). Vascular effects of sildenafil in patients with pulmonary fibrosis and pulmonary hypertension: an ex vivo/in vitro study. *European Respiratory Journal*, *47*(6), 1737–1749. https://doi.org/10.1183/13993003.01259-2015

Mirani, B., Dauz, J. D., Yazaki, K., Latifi, N., Santerre, J. P., Bendeck, M. P., Simmons, C. A., & Friedberg, M. K. (2025). Right Ventricular Stiffening and Function Are Associated With Main Pulmonary Artery Remodeling in a Rat Model of Pulmonary Hypertension. *Arteriosclerosis, Thrombosis, and Vascular Biology*, *45*(6), 945–964. https://doi.org/10.1161/ATVBAHA.124.321354

Mondéjar-Parreño, G., Barreira, B., Callejo, M., Morales-Cano, D., Barrese, V., Esquivel-Ruiz, S., Olivencia, M. A., Macías, M., Moreno, L., Greenwood, I. A., Perez-Vizcaino, F., & Cogolludo, A. (2020). Uncovered Contribution of Kv7 Channels to Pulmonary Vascular Tone in Pulmonary Arterial Hypertension. *Hypertension*, *76*(4), 1134–1146. https://doi.org/10.1161/HYPERTENSIONAHA.120.15221

Mondejar-Parreño, G., Callejo, M., Barreira, B., Morales-Cano, D., Esquivel-Ruiz, S., Moreno, L., Cogolludo, A., & Perez-Vizcaino, F. (2019). miR-1 is increased in pulmonary hypertension and downregulates Kv1.5 channels in rat pulmonary arteries. *The Journal of Physiology*, *597*(4), 1185–1197. https://doi.org/10.1113/JP276054

Mondéjar-Parreño, G., Cogolludo, A., & Perez-Vizcaino, F. (2021). Potassium (K+) channels in the pulmonary vasculature: Implications in pulmonary hypertension Physiological, pathophysiological and pharmacological regulation. *Pharmacology & Therapeutics*, *225*, 107835. https://doi.org/10.1016/j.pharmthera.2021.107835

Mondéjar-Parreño, G., Moral-Sanz, J., Barreira, B., De la Cruz, A., Gonzalez, T., Callejo, M., Esquivel-Ruiz, S., Morales-Cano, D., Moreno, L., Valenzuela, C., Perez-Vizcaino, F., & Cogolludo, A. (2019). Activation of Kv7 channels as a novel mechanism for NO/cGMP-induced pulmonary vasodilation. *British Journal of Pharmacology*, *176*(13), 2131–2145. https://doi.org/10.1111/bph.14662

Mondejar-Parreño, G., Perez-Vizcaino, F., & Cogolludo, A. (2020). Kv7 Channels in Lung Diseases. *Frontiers in Physiology*, *11*. https://doi.org/10.3389/fphys.2020.00634

Montani, D., Chaumais, M.-C., Guignabert, C., Günther, S., Girerd, B., Jaïs, X., Algalarrondo, V., Price, L. C., Savale, L., Sitbon, O., Simonneau, G., & Humbert, M. (2014). Targeted therapies in pulmonary arterial hypertension. *Pharmacology & Therapeutics*, *141*(2), 172–191. https://doi.org/10.1016/j.pharmthera.2013.10.002

Morales-Cano, D., Barreira, B., De Olaiz Navarro, B., Callejo, M., Mondejar-Parreño, G., Esquivel-Ruiz, S., Lorente, J. A., Moreno, L., Barberá, J. A., Cogolludo, Á., & Perez-Vizcaino, F. (2021). Oxygen-Sensitivity and Pulmonary Selectivity of Vasodilators as Potential Drugs for Pulmonary Hypertension. *Antioxidants*, *10*(2), 155. https://doi.org/10.3390/antiox10020155

Morales-Cano, D., Menendez, C., Moreno, E., Moral-Sanz, J., Barreira, B., Galindo, P., Pandolfi, R., Jimenez, R., Moreno, L., Cogolludo, A., Duarte, J., & Perez-Vizcaino, F. (2014). The Flavonoid Quercetin Reverses Pulmonary Hypertension in Rats. *PLoS ONE*, *9*(12), e114492. https://doi.org/10.1371/journal.pone.0114492

Morales-Cano, D., Moreno, L., Barreira, B., Briones, A. M., Pandolfi, R., Moral-Sanz, J., Callejo, M., Mondejar-Parreño, G., Cortijo, J., Salaices, M., Duarte, J., Perez-Vizcaino, F., & Cogolludo, A. (2016). Activation of PPARβ/δ prevents hyperglycaemia-induced impairment of Kv7 channels and cAMP-mediated relaxation in rat coronary arteries. *Clinical Science*, *130*(20), 1823–1836. https://doi.org/10.1042/CS20160141

Morecroft, I., Murray, A., Nilsen, M., Gurney, A., & MacLean, M. (2009). Treatment with the Kv 7 potassium channel activator flupirtine is beneficial in two independent mouse models of pulmonary hypertension. *British Journal of Pharmacology*, *157*(7), 1241–1249. https://doi.org/10.1111/j.1476-5381.2009.00283.x

Morrell, N. W., Aldred, M. A., Chung, W. K., Elliott, C. G., Nichols, W. C., Soubrier, F., Trembath, R. C., & Loyd, J. E. (2019). Genetics and genomics of pulmonary arterial hypertension. *European Respiratory Journal*, *53*(1), 1801899. https://doi.org/10.1183/13993003.01899-2018

Munguia-Galaviz, F. J., Miranda-Diaz, A. G., Cardenas-Sosa, M. A., & Echavarria, R. (2023). Sigma-1 Receptor Signaling: In Search of New Therapeutic Alternatives for Cardiovascular and Renal Diseases. *International Journal of Molecular Sciences*, *24*(3), 1997. https://doi.org/10.3390/ijms24031997

Nelson, M. T., & Quayle, J. M. (1995). Physiological roles and properties of potassium channels in arterial smooth muscle. *The American Journal of Physiology*, *268*(4 Pt 1), C799–C822. https://doi.org/10.1152/ajpcell.1995.268.4.C799

Nguyen, L., Robson, M. J., Healy, J. R., Scandinaro, A. L., & Matsumoto, R. R. (2014). Involvement of sigma-1 receptors in the antidepressant-like effects of dextromethorphan. *PloS One*, *9*(2), e89985. https://doi.org/10.1371/journal.pone.0089985

Okada, Y., Maeno, E., Shimizu, T., Dezaki, K., Wang, J., & Morishima, S. (2001). Receptor-mediated control of regulatory volume decrease (RVD) and apoptotic volume decrease

(AVD). *Journal of Physiology*, *532*(pt 1), 3–16. https://doi.org/10.1111/j.1469-7793.2001.0003g.x

Olschewski, A., Veale, E. L., Nagy, B. M., Nagaraj, C., Kwapiszewska, G., Antigny, F., Lambert, M., Humbert, M., Czirják, G., Enyedi, P., & Mathie, A. (2017). TASK-1 (KCNK3) channels in the lung: from cell biology to clinical implications. *The European Respiratory Journal*, *50*(5). https://doi.org/10.1183/13993003.00754-2017

Orcholski, M. E., Yuan, K., Rajasingh, C., Tsai, H., Shamskhou, E. A., Dhillon, N. K., Voelkel, N. F., Zamanian, R. T., & de Jesus Perez, V. A. (2018). Drug-induced pulmonary arterial hypertension: a primer for clinicians and scientists. *American Journal of Physiology-Lung Cellular and Molecular Physiology*, *314*(6), L967–L983. https://doi.org/10.1152/ajplung.00553.2017

Ozaki, M., Marshall, C., Amaki, Y., & Marshall, B. E. (1998). Role of wall tension in hypoxic responses of isolated rat pulmonary arteries. *The American Journal of Physiology*, *275*(6), L1069-77. https://doi.org/10.1152/ajplung.1998.275.6.L1069

Perez-Vizcaino, F., Cogolludo, A., & Mondejar-Parreño, G. (2021). Transcriptomic profile of cationic channels in human pulmonary arterial hypertension. *Scientific Reports*, *11*(1), 15829. https://doi.org/10.1038/s41598-021-95196-z

Pozeg, Z. I., Michelakis, E. D., McMurtry, M. S., Thébaud, B., Wu, X.-C., Dyck, J. R. B., Hashimoto, K., Wang, S., Moudgil, R., Harry, G., Sultanian, R., Koshal, A., & Archer, S. L. (2003). In Vivo Gene Transfer of the O2 -Sensitive Potassium Channel Kv1.5 Reduces Pulmonary Hypertension and Restores Hypoxic Pulmonary Vasoconstriction in Chronically Hypoxic Rats. *Circulation*, *107*(15), 2037–2044. https://doi.org/10.1161/01.CIR.0000062688.76508.B3

Puls, F., Agne, C., Klein, F., Koch, M., Rifai, K., Manns, M. P., Borlak, J., & Kreipe, H. H. (2011). Pathology of flupirtine-induced liver injury:a histological and clinical study of six cases. *Virchows Archiv*, *458*(6), 709–716. https://doi.org/10.1007/s00428-011-1087-9

Qiu, H., Zhang, Y., Li, Z., Jiang, P., Guo, S., He, Y., & Guo, Y. (2021). Donepezil Ameliorates Pulmonary Arterial Hypertension by Inhibiting M2-Macrophage Activation. *Frontiers in Cardiovascular Medicine*, *8*. https://doi.org/10.3389/fcvm.2021.639541

Rabinovitch, M., Guignabert, C., Humbert, M., & Nicolls, M. R. (2014). Inflammation and Immunity in the Pathogenesis of Pulmonary Arterial Hypertension. *Circulation Research*, *115*(1), 165–175. https://doi.org/10.1161/CIRCRESAHA.113.301141

Recino, A., Rayner, M. L. D., Rohn, J. L., Della Pasqua, O., & UCL Repurposing TIN Committee. (2025). Therapeutic innovation in drug repurposing: Challenges and opportunities. *Drug Discovery Today*, *30*(7), 104390. https://doi.org/10.1016/j.drudis.2025.104390

Remillard, C. V., Tigno, D. D., Platoshyn, O., Burg, E. D., Brevnova, E. E., Conger, D., Nicholson, A., Rana, B. K., Channick, R. N., Rubin, L. J., O'Connor, D. T., & Yuan, J. X.-J. (2007). Function of Kv1.5 channels and genetic variations of KCNA5 in patients with idiopathic pulmonary arterial hypertension. *American Journal of Physiology-Cell Physiology*, *292*(5), C1837–C1853. https://doi.org/10.1152/ajpcell.00405.2006

Roden, D. M., & George, A. L. (1997). Structure and function of cardiac sodium and potassium channels. *American Journal of Physiology-Heart and Circulatory Physiology*, *273*(2), H511–H525. https://doi.org/10.1152/ajpheart.1997.273.2.H511

Schenzer, A., Friedrich, T., Pusch, M., Saftig, P., Jentsch, T. J., Grötzinger, J., & Schwake, M. (2005). Molecular Determinants of KCNQ (Kv 7) K + Channel Sensitivity to the Anticonvulsant Retigabine. *The Journal of Neuroscience*, *25*(20), 5051–5060. https://doi.org/10.1523/JNEUROSCI.0128-05.2005

Schermuly, R. T., Ghofrani, H. A., Wilkins, M. R., & Grimminger, F. (2011). Mechanisms of disease: pulmonary arterial hypertension. *Nature Reviews Cardiology*, *8*(8), 443–455. https://doi.org/10.1038/nrcardio.2011.87

Schmidt, H. R., & Kruse, A. C. (2019). The Molecular Function of σ Receptors: Past, Present, and Future. *Trends in Pharmacological Sciences*, *40*(9), 636–654. https://doi.org/10.1016/j.tips.2019.07.006

Schmidt, H. R., Zheng, S., Gurpinar, E., Koehl, A., Manglik, A., & Kruse, A. C. (2016). Crystal structure of the human σ1 receptor. *Nature*, *532*(7600), 527–530. https://doi.org/10.1038/nature17391

Sedivy, V., Joshi, S., Ghaly, Y., Mizera, R., Zaloudikova, M., Brennan, S., Novotna, J., Herget, J., & Gurney, A. M. (2015). Role of Kv7 channels in responses of the pulmonary circulation to hypoxia. *American Journal of Physiology-Lung Cellular and Molecular Physiology*, *308*(1), L48–L57. https://doi.org/10.1152/ajplung.00362.2013

Seefeld, M. A., Lin, H., Holenz, J., Downie, D., Donovan, B., Fu, T., Pasikanti, K., Zhen, W., Cato, M., Chaudhary, K. W., Brady, P., Bakshi, T., Morrow, D., Rajagopal, S., Samanta, S. K., Madhyastha, N., Kuppusamy, B. M., Dougherty, R. W., Bhamidipati, R., … Matsuoka, Y. (2018). Novel KV7 ion channel openers for the treatment of epilepsy and implications for detrusor tissue contraction. *Bioorganic & Medicinal Chemistry Letters*, *28*(23–24), 3793–3797. https://doi.org/10.1016/j.bmcl.2018.09.036

Serdjebi, C., Chandes, F., Biernat, M., Lepoivre, B., Salvail, D., & Laurent, C.-E. (2024). *Unraveling the lung vascular remodeling in pulmonary hypertension using a quantitative digital pathology software*. https://doi.org/10.1101/2024.07.01.601469

Sevilla-Montero, J., Labrousse-Arias, D., Fernández-Pérez, C., Fernández-Blanco, L., Barreira, B., Mondéjar-Parreño, G., Alfaro-Arnedo, E., López, I. P., Pérez-Rial, S., Peces-Barba, G., Pichel, J. G., Peinado, V. I., Cogolludo, Á., & Calzada, M. J. (2021). Cigarette Smoke Directly Promotes Pulmonary Arterial Remodeling and Kv7.4 Channel Dysfunction. *American Journal of Respiratory and Critical Care Medicine*, *203*(10), 1290–1305. https://doi.org/10.1164/rccm.201911-2238OC

Sewing, S., Roeper, J., & Pongs, O. (1996). Kvβ1 Subunit Binding Specific for Shaker-Related Potassium Channel α Subunits. *Neuron*, *16*(2), 455–463. https://doi.org/10.1016/S0896-6273(00)80063-X

Shen, N. V, Chen, X., Boyer, M. M., & Pfaffinger, P. J. (1993). Deletion analysis of K+ channel assembly. *Neuron*, *11*(1), 67–76. https://doi.org/10.1016/0896-6273(93)90271-r

Shen, Y., Wang, Y., Chou, Y., Liou, K., Yen, J., Wang, W., & Liao, J. (2008). Dimemorfan protects rats against ischemic stroke through activation of sigma-1 receptor-mediated

mechanisms by decreasing glutamate accumulation. *Journal of Neurochemistry*, *104*(2), 558–572. https://doi.org/10.1111/j.1471-4159.2007.05058.x

Sikarwar, A. S., Hinton, M., Santhosh, K. T., Dhanaraj, P., Talabis, M., Chelikani, P., & Dakshinamurti, S. (2018). Hypoxia inhibits adenylyl cyclase catalytic activity in a porcine model of persistent pulmonary hypertension of the newborn. *American Journal of Physiology-Lung Cellular and Molecular Physiology*, *315*(6), L933–L944. https://doi.org/10.1152/ajplung.00130.2018

Simonneau, G., Montani, D., Celermajer, D. S., Denton, C. P., Gatzoulis, M. A., Krowka, M., Williams, P. G., & Souza, R. (2019). Haemodynamic definitions and updated clinical classification of pulmonary hypertension. *European Respiratory Journal*, *53*((1) 1801913). https://doi.org/10.1183/13993003.01913-2018

Sitbon, O., Channick, R., Chin, K. M., Frey, A., Gaine, S., Galiè, N., Ghofrani, H.-A., Hoeper, M. M., Lang, I. M., Preiss, R., Rubin, L. J., Di Scala, L., Tapson, V., Adzerikho, I., Liu, J., Moiseeva, O., Zeng, X., Simonneau, G., & McLaughlin, V. V. (2015). Selexipag for the Treatment of Pulmonary Arterial Hypertension. *New England Journal of Medicine*, *373*(26), 2522–2533. https://doi.org/10.1056/NEJMoa1503184

Soon, E., Holmes, A. M., Treacy, C. M., Doughty, N. J., Southgate, L., Machado, R. D., Trembath, R. C., Jennings, S., Barker, L., Nicklin, P., Walker, C., Budd, D. C., Pepke-Zaba, J., & Morrell, N. W. (2010). Elevated Levels of Inflammatory Cytokines Predict Survival in Idiopathic and Familial Pulmonary Arterial Hypertension. *Circulation*, *122*(9), 920–927. https://doi.org/10.1161/CIRCULATIONAHA.109.933762

Stott, J. B., Jepps, T. A., & Greenwood, I. A. (2014). KV7 potassium channels: a new therapeutic target in smooth muscle disorders. *Drug Discovery Today*, *19*(4), 413–424. https://doi.org/10.1016/j.drudis.2013.12.003

Strutz-Seebohm, N., Seebohm, G., Fedorenko, O., Baltaev, R., Engel, J., Knirsch, M., & Lang, F. (2006). Functional Coassembly of KCNQ4 with KCNE-ß- Subunits in Xenopus Oocytes. *Cellular Physiology and Biochemistry*, *18*(1–3), 57–66. https://doi.org/10.1159/000095158

Summerton, J. (1999). Morpholino antisense oligomers: the case for an RNase H-independent structural type. *Biochimica et Biophysica Acta (BBA) - Gene Structure and Expression*, *1489*(1), 141–158. https://doi.org/10.1016/S0167-4781(99)00150-5

Summerton, J. (2007). Morpholino, siRNA, and S-DNA Compared: Impact of Structure and Mechanism of Action on Off-Target Effects and Sequence Specificity. *Current Topics in Medicinal Chemistry*, *7*(7), 651–660. https://doi.org/10.2174/156802607780487740

Sun, Y., Wan, W., Zhao, X., Han, X., Ye, T., Chen, X., Ran, Q., Wang, X., Liu, X., Qu, C., Shi, S., Zhang, C., & Yang, B. (2022). Chronic Sigma 1 receptor activation alleviates right ventricular dysfunction secondary to pulmonary arterial hypertension. *Bioengineered*, *13*(4), 10843–10856. https://doi.org/10.1080/21655979.2022.2065953

Sztuka, K., Orszulak-Michalak, D., & Jasińska-Stroschein, M. (2018). Systematic review and meta-analysis of interventions tested in animal models of pulmonary hypertension. *Vascular Pharmacology*, *110*, 55–63. https://doi.org/10.1016/j.vph.2018.08.004

Tagashira, H., Bhuiyan, S., Shioda, N., Hasegawa, H., Kanai, H., & Fukunaga, K. (2010). σ1 - Receptor stimulation with fluvoxamine ameliorates transverse aortic constriction-induced myocardial hypertrophy and dysfunction in mice. *American Journal of Physiology-Heart and Circulatory Physiology*, *299*(5), H1535–H1545. https://doi.org/10.1152/ajpheart.00198.2010

Tajsic, T., & Morrell, N. W. (2010). Smooth Muscle Cell Hypertrophy, Proliferation, Migration and Apoptosis in Pulmonary Hypertension. In *Comprehensive Physiology* (pp. 295–317). Wiley. https://doi.org/10.1002/cphy.c100026

Tang, H., Chen, J., Fraidenburg, D. R., Song, S., Sysol, J. R., Drennan, A. R., Offermanns, S., Ye, R. D., Bonini, M. G., Minshall, R. D., Garcia, J. G. N., Machado, R. F., Makino, A., & Yuan, J. X.-J. (2015). Deficiency of Akt1, but not Akt2, attenuates the development of pulmonary hypertension. *American Journal of Physiology. Lung Cellular and Molecular Physiology*, *308*(2), L208-20. https://doi.org/10.1152/ajplung.00242.2014

Tchedre, K. T., Huang, R.-Q., Dibas, A., Krishnamoorthy, R. R., Dillon, G. H., & Yorio, T. (2008). Sigma-1 Receptor Regulation of Voltage-Gated Calcium Channels Involves a Direct Interaction. *Investigative Opthalmology & Visual Science*, *49*(11), 4993. https://doi.org/10.1167/iovs.08-1867

Townsley, M. I. (2012). Structure and composition of pulmonary arteries, capillaries, and veins. *Comprehensive Physiology*, *2*(1), 675–709. https://doi.org/10.1002/cphy.c100081

Vera-Zambrano, A., Baena-Nuevo, M., Rinné, S., Villegas-Esguevillas, M., Barreira, B., Telli, G., de Benito-Bueno, A., Blázquez, J. A., Climent, B., Pérez-Vizcaino, F., Valenzuela, C., Decher, N., Gonzalez, T., & Cogolludo, A. (2023). Sigma-1 receptor modulation fine-tunes KV1.5 channels and impacts pulmonary vascular function. *Pharmacological Research*, *189*, 106684. https://doi.org/10.1016/j.phrs.2023.106684

Vera-Zambrano, A., Lago-Docampo, M., Gallego, N., Franco-Gonzalez, J. F., Morales-Cano, D., Cruz-Utrilla, A., Villegas-Esguevillas, M., Fernández-Malavé, E., Escribano-Subías, P., Tenorio-Castaño, J. A., Perez-Vizcaino, F., Valverde, D., González, T., & Cogolludo, A. (2023). Novel Loss-of-Function KCNA5 Variants in Pulmonary Arterial Hypertension. *American Journal of Respiratory Cell and Molecular Biology*, *69*(2), 147–158. https://doi.org/10.1165/rcmb.2022-0245OC

Vonk-Noordegraaf, A., Haddad, F., Chin, K. M., Forfia, P. R., Kawut, S. M., Lumens, J., Naeije, R., Newman, J., Oudiz, R. J., Provencher, S., Torbicki, A., Voelkel, N. F., & Hassoun, P. M. (2013). Right heart adaptation to pulmonary arterial hypertension: physiology and pathobiology. *Journal of the American College of Cardiology*, *62*(25 Suppl), D22-33. https://doi.org/10.1016/j.jacc.2013.10.027

Wang, J., Juhaszova, M., Rubin, L. J., & Yuan, X. J. (1997). Hypoxia inhibits gene expression of voltage-gated K+ channel alpha subunits in pulmonary artery smooth muscle cells. *Journal of Clinical Investigation*, *100*(9), 2347–2353. https://doi.org/10.1172/JCI119774

Wang, J., Weigand, L., Wang, W., Sylvester, J. T., & Shimoda, L. A. (2005). Chronic hypoxia inhibits Kv channel gene expression in rat distal pulmonary artery. *American Journal of Physiology-Lung Cellular and Molecular Physiology*, *288*(6), L1049–L1058. https://doi.org/10.1152/ajplung.00379.2004

Webb, R. C. (2003). Smooth muscle contraction and relaxation. *American Journal of Physiology - Advances in Physiology Education*, *27*(1–4), 201–206. https://doi.org/10.1152/advan.00025.2003

Weng, T.-Y., Tsai, S.-Y. A., & Su, T.-P. (2017). Roles of sigma-1 receptors on mitochondrial functions relevant to neurodegenerative diseases. *Journal of Biomedical Science*, *24*(1), 74. https://doi.org/10.1186/s12929-017-0380-6

Wulff, H., Castle, N. A., & Pardo, L. A. (2009). Voltage-gated potassium channels as therapeutic targets. *Nature Reviews Drug Discovery*, *8*(12), 982–1001. https://doi.org/10.1038/nrd2983

Wuttke, T. V., Seebohm, G., Bail, S., Maljevic, S., & Lerche, H. (2005). The New Anticonvulsant Retigabine Favors Voltage-Dependent Opening of the Kv7.2 (KCNQ2) Channel by Binding to Its Activation Gate. *Molecular Pharmacology*, *67*(4), 1009–1017. https://doi.org/10.1124/mol.104.010793

Xiao, N., Yin, L., Teopiz, K. M., Kwan, A. T. H., Le, G. H., Wong, S., Valentino, K., Choi, H., Rosenblat, J. D., Ho, R., Lee, S., & McIntyre, R. S. (2025). The sigma-1 receptor: a mechanistically-informed therapeutic target for antidepressants. *Expert Opinion on Therapeutic Targets*, *29*(6), 345–359. https://doi.org/10.1080/14728222.2025.2500424

Xu, Z.-Z., Zhou, J., Duan, K., Li, X.-T., Chang, S., Huang, W., Lu, Q., Tao, J., & Xie, W.-B. (2024). Blocking Sigmar1 exacerbates methamphetamine-induced hypertension. *Biochimica et Biophysica Acta (BBA) - Molecular Basis of Disease*, *1870*(7), 167284. https://doi.org/10.1016/j.bbadis.2024.167284

Yang, L., Yu, D., Fan, H.-H., Feng, Y., Hu, L., Zhang, W.-Y., Zhou, K., & Mo, X.-M. (2014). Triggering the succinate receptor GPR91 enhances pressure overload-induced right ventricular hypertrophy. *International Journal of Clinical and Experimental Pathology*, *7*(9), 5415–5428.

Yuan, J. X.-J., Aldinger, A. M., Juhaszova, M., Wang, J., Conte, J. V., Gaine, S. P., Orens, J. B., & Rubin, L. J. (1998). Dysfunctional Voltage-Gated K+ Channels in Pulmonary Artery Smooth Muscle Cells of Patients With Primary Pulmonary Hypertension. *Circulation*, *98*(14), 1400–1406. https://doi.org/10.1161/01.CIR.98.14.1400

Yuan, X. J., Wang, J., Juhaszova, M., Gaine, S. P., & Rubin, L. J. (1998). Attenuated K+ channel gene transcription in primary pulmonary hypertension. *Lancet (London, England)*, *351*(9104), 726–727. https://doi.org/10.1016/S0140-6736(05)78495-6

Yuan, X.-J., Wang, J., Juhaszova, M., Golovina, V. A., & Rubin, L. J. (1998). Molecular basis and function of voltage-gated K+ channels in pulmonary arterial smooth muscle cells. *American Journal of Physiology-Lung Cellular and Molecular Physiology*, *274*(4), L621–L635. https://doi.org/10.1152/ajplung.1998.274.4.L621

Zhai, F., Zhang, X., & Wang, H. (2009). Fluoxetine protects against monocrotaline-induced pulmonary arterial hypertension: potential roles of induction of apoptosis and upregulation of kv1.5 channels in rats. *Clinical and Experimental Pharmacology and Physiology*, *36*(8), 850–856. https://doi.org/10.1111/j.1440-1681.2009.05168.x

Zhang, K., Zhao, Z., Lan, L., Wei, X., Wang, L., Liu, X., Yan, H., & Zheng, J. (2017). Sigma-1 Receptor Plays a Negative Modulation on N-type Calcium Channel. *Frontiers in Pharmacology*, *8*. https://doi.org/10.3389/fphar.2017.00302

Zhang, L., Foster, K., Li, Q., & Martens, J. R. (2007). S-acylation regulates Kv1.5 channel surface expression. *American Journal of Physiology-Cell Physiology*, *293*(1), C152–C161. https://doi.org/10.1152/ajpcell.00480.2006

Zhang, Y.-T., Xue, J.-J., Wang, Q., Cheng, S.-Y., Chen, Z.-C., Li, H.-Y., Shan, J.-J., Cheng, K.-L., & Zeng, W.-J. (2019). Dehydroepiandrosterone attenuates pulmonary artery and right ventricular remodeling in a rat model of pulmonary hypertension due to left heart failure. *Life Sciences*, *219*, 82–89. https://doi.org/10.1016/j.lfs.2018.12.056

Zhao, X., Liu, X., Chen, X., Han, X., Sun, Y., Fo, Y., Wang, X., Qu, C., & Yang, B. (2022). Activation of the sigma-1 receptor exerts cardioprotection in a rodent model of chronic heart failure by stimulation of angiogenesis. *Molecular Medicine*, *28*(1), 87. https://doi.org/10.1186/s10020-022-00517-1

Zhu, R., Bi, L.-Q., Wu, S.-L., LI, L., KONG, H., XIE, W.-P., WANG, H., & MENG, Z.-L. (2015). Iptakalim attenuates hypoxia-induced pulmonary arterial hypertension in rats by endothelial function protection. *Molecular Medicine Reports*, *12*(2), 2945–2952. https://doi.org/10.3892/mmr.2015.3695